NASA CR- 1 3 2 4 5 1

The Pennsylvania State University
The Graduate School

ABSORPTION CHARACTERISTICS OF GLASS FIBER MATERIALS AT NORMAL AND OBLIQUE INCIDENCE

A Thesis in

Engineering Acoustics

by

Barry R. Wyerman

Submitted in Partial Fulfillment
of the Requirements
for the Degree of

Master of Science

June 1974

The Pennsylvania State University

The Graduate School

Absorption Characteristics of Glass Fiber Materials at

Normal and Oblique Incidence

A Thesis in

Engineering Acoustics

by

Barry R. Wyerman

Submitted in Partial Fulfillment
of the Requirements
for the Degree of

Master of Science

June 1974

Date of Signature: Signatories:

_____   _____

                           Gerhard Reethof
                           Alcoa Professor of Mechanical Engineering
                           Thesis Advisor

_____   _____

                           Jiri Tichy
                           Chairman of the Committee on Engineering
                           Acoustics

ACKNOWLEDGEMENT

TABLE OF CONTENTS

LIST OF FIGURES

Figure   Page

Figure   Page

LIST OF TABLES

NOMENCLATURE

a = length of a side of the square sample

c = phase velocity of sound

d = thickness of material

f = frequency

F = temperature in degrees Fahrenheit

j = $(-1)^{\frac{1}{2}}$

K = compressibility of medium

K' = modulus of elasticity of medium

m = integer number

n = integer number

p = pressure

p_{ref} = acoustic reference pressure

Q = flow rate

r = reflection coefficient

R_f = flow resistance

R_s = flow resistance per unit thickness

S = area

SWR = standing wave ratio

t = time

u = particle velocity

v = particle velocity

x = coordinate axis

y = coordinate axis

z = coordinate axis

Z = specific normal acoustic impedance

NOMENCLATURE CONTINUED

α = absorption coefficient

β = phase constant

γ = ratio of specific heats at constant pressure and at constant volume

δ = change in density

ς = propagation constant

θ = angle designation

λ = wavelength

η = angle designation

ξ = normalized specific acoustic impedance

ρ = density

σ = attenuation constant

ϕ = velocity potential

ψ = phase angle

Ω = porosity

ABSTRACT

A free field method for measuring the specific normal impedance
and absorption coefficient of a material at oblique incidence has
been investigated. The surface pressure method, developed by Ingard
and Bolt, compares the pressure and phase of an incident wave at a
point on the surface of an absorbent material to a similar measure-
ment at the surface of a perfectly reflecting boundary. A contin-
uous recording of these quantities as a function of angle of inci-
dence yields the impedance and absorption coefficient for oblique
angles. Measurements were taken with a six foot square sample
mounted in an anechoic chamber. Due to the finite size of the
sample, the measurements are limited both with respect to frequency
and angle of incidence because of diffraction effects. Without
having analyzed the diffraction problem, the limitations of this
method are determined from experimental results. The low frequency
limit for measurements is inversely proportional to the sample size
which must be large enough relative to the wavelength so that it
behaves as an infinite surface. The upper frequency limit is de-
termined by the accuracy in measuring the phase angle, upon which
the results depend strongly. Further limitations including diffrac-
tion effects, sample geometry, and temperature problems are also con-
sidered with recommendations included for improvement of the surface
pressure method.

The absorption characteristics of several fibrous materials of
the Owens Corning 700 Fiberglas Series were measured to determine the
variation in impedance as a function of incident angle of the sound

wave. The results indicate that the fibrous absorbents behave as extended reacting materials. The poor agreement between measurement and theory for sound absorption based on the parameters of flow resistance and porosity indicates that this theory does not adequately predict the acoustic behavior of fibrous materials. A much better agreement with measured results is obtained for values calculated from the bulk acoustic parameters of the material.

CHAPTER I

INTRODUCTION

1.1 Sound Absorbing Materials

Several types of sound absorbing materials are currently available for noise control applications. These materials are generally of a porous nature, constructed either from plastic foams or from organic or glass fibers held together with a binder, and are available in the form of flexible blankets or semi-rigid and rigid sheets. Materials of woven and sintered metals or perforated sheet metals are also used for special noise control applications under adverse environmental conditions.

There are four factors to be considered in choosing a sound absorbing material for a particular noise control problem - acoustic performance, environment, appearance, and price. Since the primary purpose of these materials is to control the sound reflection from a surface and thus reduce the overall noise level, the most important factor is the acoustic behavior of the material. Secondly, the environment in which the material will be used must be considered so that it will not interfere with its acoustic performance. As a minor factor, the appearance of the material becomes important in certain architectural applications. Finally, the cost of the material must be considered so that a material which meets the desired acoustic standards is an economically feasible solution to the problem.

The sound absorbing properties of a material are most often described by two parameters - the absorption coefficient and the specific normal impedance. When a sound wave impinges on the surface of an

absorbing material, part of it is reflected and part of it is absorbed and dissipated. The amount of sound energy dissipated is called the absorption coefficient, which ranges in value from zero for a perfectly reflecting surface to 1.0 for a totally absorbing surface. If the material is placed in a diffuse field where sound waves are incident at all angles, the random incidence or statistical absorption coefficient is used to describe the amount of sound energy absorbed by the material. The specific normal impedance is the ratio of the acoustic pressure to the normal particle velocity at the surface of the material. These two properties are a function of the surface characteristics, internal structure and thickness of a material, the mounting conditions, the frequency, the sound intensity, and the angle of incidence for the sound wave.

1.2 Methods for Measuring the Sound Absorption of Materials

The absorption characteristics of a material are commonly measured using two standard techniques.

1. Standing Wave Tube Method

If a sample of material is placed at one end of a rigid-walled tube and a sound source at the other, an incident wave will be reflected from the surface of the material and, for preferred modes of propagation, will generate a standing wave between the source and the material. The properties of the standing wave can be measured to yield the absorption coefficient and impedance of the sample for a plane wave at normal incidence to its surface (1).

2. Reverberation Room Method

The reverberation time - the time for the sound pressure to

decay to a value one thousandth of its original value - is measured for a room with acoustically highly reflecting surfaces. When a large sample of material is placed in this room, the statistical absorption coefficient of the sample can be determined from the change in reverberation time (2).

Several relationships and graphs (3) are available for calculating the statistical absorption coefficient from data obtained with the standing wave tube method.

The majority of work with sound absorbing materials has been restricted to absorption at normal incidence. This is because experimental procedures become much more difficult when considering sound absorption at oblique incidence. A few of the more common measurement techniques for determining the acoustic behavior of a material at oblique incidence are listed.

1. Interference Pattern Method

A large sample is mounted in an anechoic chamber in the presence of an obliquely incident sound wave. An interference pattern similar to the pattern generated in a standing wave tube is investigated to determine the absorption characteristics of the material at oblique incidence (4).

2. Pulse Method

If a sound source located a distance from a material at an angle to the normal to the surface emits a short sound pulse, a microphone can be positioned to measure two pulses - the direct pulse from the source and the reflected pulse from the sample surface. A consideration of the geometrical configuration and the measured intensities reveals the absorption coefficient of

the material for a particular angle of incidence. A large sample
and free field conditions are required for this method (5).

3. Standing Waves in a Rectangular Room

The natural modes of a rectangular room determine the angles
of incidence for plane waves reflected at the walls. By covering
certain walls of the room with a sound absorbing material, the
absorption coefficient can be determined for specific angles of
incidence and frequencies (6).

4. Acoustic Waveguide

Similar to an electromagnetic waveguide, an acoustic wave-
guide is a rigid walled duct which limits wave propagation
within it to its principal and transverse modes. If a sample
of material is placed at one end of the tube and a sound source
at the other, the oblique incidence behavior of a material can
be measured by employing the transverse modes of the duct
(7, 8, and 9).

5. Surface Pressure Method

A sample is mounted in an anechoic chamber in the presence
of obliquely incident sound. The pressure and phase of the
incident wave at the surface of the absorbing material are
compared with similar measurements at the surface of a perfectly
reflecting boundary. From this data, the absorption character-
istics can be determined as a function of incident angle (10).

In all of these measurement techniques, it is important to first
determine the limitations inherent with each method before the absorp-
tion characteristics of a material can be measured. The surface
pressure method will be the subject of further study and is discussed

in detail in Section 4.3.

1.3 Statement of the Problem

Of all the sound absorbing materials commercially available,
glass fiber absorbents are one of the most economical products in
terms of noise reduction per cost of material. These materials are
fairly inexpensive and possess high absorption characteristics over
a very broad frequency range. Although the absorption characteristics
of these materials at normal incidence are fairly well known, their
oblique incidence acoustic behavior has not been completely investi-
gated. This is because measurements at oblique incidence are much
more difficult to perform than measurements at normal incidence.
Therefore, a suitable oblique incidence measurement technique should
be investigated for determining the acoustic properties of these
materials at oblique angles of incidence.

It would also be helpful to be able to predict the acoustic
absorption of a fibrous material from a knowledge of its physical
properties and parameters. Although several theories for sound
absorption by a porous material have been developed, these theories
cannot be universally applied to all materials because the mathematic
models characterize some absorbents better than others. Therefore,
the limitations of these theories with respect to fibrous materials
must be determined.

1.4 Purpose of the Research

The purpose of this study is to determine the validity of the
surface pressure method as a technique for measuring the specific
normal impedance and absorption coefficient of a material at oblique

incidence. It is hoped to determine under what conditions and over what frequencies this technique provides reasonable measurements of the acoustic characteristics of a material. The behavior of fibrous absorbents of the Owens Corning 700 Fiberglas Series is investigated to determine the variation in specific normal impedance as a function of incident angle. Furthermore, measured values of absorption are compared with calculated values to determine if theories for porous absorbents adequately predict the acoustic behavior of glass fiber materials.

CHAPTER II

MATERIALS AND THEIR PROPERTIES

Because of the low cost and the high acoustic absorption of glass
fiber materials, the acoustic properties of several samples of this
type material were investigated. These samples are marketed by Owens
Corning as the Fiberglas 700 Series of Industrial Insulation and are
used for insulating duct work and equipment operating at high tempera-
tures. The Fiberglas 700 Series products are constructed of inorganic
glass fibers held together with a binder and pre-formed into semirigid
and rigid rectangular boards of varying densities. These materials
are available in 24" x 48" boards and in thicknesses of 1" to 4" with
1/2" increments. Although these products have been designed as insu-
lation materials, they also possess highly desirable sound absorbing
properties. However, the acoustical properties of each material are
quite variable, both within manufacturing tolerance specifications
and from one position to another in the same board or in different
boards. The acoustical properties of greatest importance will be
described.

The porosity of a sample is defined as the ratio of the volume
of voids within the sample to the total volume of the sample. The
porosity of a fibrous material can be calculated if the densities of
the material and the glass fibers which comprise it are known. For
a fibrous material, the weight and volume of the binder which cements
together the densely packed fibers must also be included. For a
material with negligible binder by weight, the porosity Ω is

$$\Omega = \frac{V_a}{V_m} = 1 - \frac{V_f}{V_m} \tag{2.1}$$

$$\Omega = 1 - \frac{\rho_m \, m_f}{\rho_f \, m_m} \tag{2.2}$$

where

V = volume

m = mass

ρ = density

The subscripts a, m, and f refer to the voids within the material (therefore air), the material, and the fibers respectively. Since the density of the material is much greater than the density of air, we will assume that the mass of the material is approximately equal to the mass of the fibers.

$$m_m \approx m_f \tag{2.3}$$

This is a reasonable assumption as can be seen by considering the error for the extreme cases of a porosity of .90 and .99 for the materials. The relationship between the mass of the material and the mass of the fibers is

$$\frac{m_m}{m_f} = 1 + \frac{\rho_a V_a}{\rho_f V_f} \tag{2.4}$$

For a porosity of .90 we have

$$\frac{m_m}{m_f} = 1 + 0.004 \approx 1$$

where the density of air was taken as 1.18 kg/m^3 and the density of the fibers as 2.5 x 10^3 kg/m^3. Similarly, for a porosity of .99

$$\frac{m_m}{m_f} = 1 + 0.047 \approx 1$$

Therefore, the expression for porosity (11) can be written as

$$\Omega = 1 - \frac{\rho_m}{\rho_f} \qquad (2.5)$$

where

ρ_m = density of material

ρ_f = density of glass fibers (2.5×10^3 kg/m^3)

The specific flow resistance of a layer of material is defined as the pressure drop across the specimen divided by the particle velocity of air through and perpendicular to the two faces of the layer. Thus,

$$R_f = \frac{\Delta p}{u}$$

where

Δp = pressure drop across the sample (dynes/cm^2)

u = particle velocity (cm/sec)

The units of R_f are dyne-sec/cm^3 or CGS rayls. For bulk materials, the flow resistivity or specific flow resistance per unit thickness of material is commonly used. Thus,

$$R_s = \frac{R_f}{d}$$

where d is the thickness of the material. In all future work, the term "flow resistance" as applied to a sound absorbing material will mean the specific flow resistance per unit thickness. The flow resistance is essentially constant for values of u from 0 to some small value and increases rapidly with increasing values of u above this linear range.

Table 1 lists the performance characteristics of the Owens Corning 700 Fiberglas Series including flow resistance values (12, 13). Due to the manufacturing tolerances in both density and fiber diameter for these materials, a corresponding range of flow resistance values would be expected. The discontinuity in the flow resistance versus density curve for the 704 and 705 samples is due to a coarser fiber for these two products. The statistical absorption coefficients determined by the reverberation chamber method for these materials mounted with a rigid backing are listed in Table 2 for data furnished by Owens Corning (14).

TABLE 1

Performance Characteristics of Owens Corning 700 Series Fiberglas

Type	Density (lb/ft^3)	Porosity	Specific Flow Resistance — (cgs rayls/inch thickness)	
			Average Density and Fiber Diameter	Range Within Manufacturing Specifications
701	1.58	.990	26	19-35
702	2.25	.986	38	27-56
703	3.00	.981	60	42-87
704	4.20	.973	45	35-57
705	6.00	.961	78	60-99

TABLE 2

Statistical Absorption Coefficient for Owens Corning 700
Series Fiberglas Materials Mounted with a Rigid Backing

		Statistical Absorption Coefficient				
Type	Thickness	250 Hz	500 Hz	1000 Hz	2000 Hz	4000 Hz
701	1"	.20	.57	.88	.86	.79
	2"	.58	.92	.93	.86	.79
702	1"	.19	.50	.85	.85	.76
	2"	.54	.91	.97	.87	.77
703	1"	.22	.62	.95	.90	.82
	2"	.59	.93	.98	.87	.78
704	1"	.18	.51	.89	.88	.80
	2"	.47	.90	.97	.86	.78
705	1"	.19	.57	.93	.90	.83
	2"	.55	.91	.97	.87	.78

CHAPTER III

THEORETICAL BACKGROUND

3.1 Introductory Theory

We begin the theoretical analysis of sound waves and acoustic absorption by considering the simplest case of a plane wave at normal incidence to the surface of an absorbing material as in Figure 1. The wave equation for the pressure p

$$\frac{\partial^2 p}{\partial x^2} = \frac{1}{c^2}\frac{\partial^2 p}{\partial t^2} \tag{3.1}$$

has a solution of the form

$$p = P_i\, e^{j(\omega t - kx)} + P_r\, e^{j(\omega t + kx)} \tag{3.2}$$

The first term represents an incident wave propagating in the positive x direction p_i and the second term represents a reflected wave p_r so that

$$p_i = P_i\, e^{j(\omega t - kx)} \tag{3.3}$$

$$p_r = P_r\, e^{j(\omega t + kx)} \tag{3.4}$$

The particle velocity for a plane wave in terms of the pressure is

$$v = \frac{j}{k\rho c}\frac{\partial p}{\partial x} \tag{3.5}$$

Since the velocity is also a solution to the wave equation, we have

$$v = \frac{P_i}{\rho c}\, e^{j(\omega t - kx)} - \frac{P_r}{\rho c}\, e^{j(\omega t + kx)} \tag{3.6}$$

where the incident particle velocity is V_i and the reflected particle velocity is V_r.

$$V_i = V_i\, e^{j(\omega t - kx)} \tag{3.7}$$

$$V_r = V_r e^{j(\omega t + kx)} \tag{3.8}$$

The minus sign in Equation 3.6 occurs because the velocities are vector quantities traveling in opposite directions. The acoustic properties of a material are defined by the specific normal impedance Z which is the ratio of the pressure to the normal particle velocity at the surface. Unless otherwise noted, the term "impedance" as used in this study will refer to the specific normal impedance defined above and will have the dimensions of Nt sec/m^3 or MKS rayls. If the pressure and velocity are out of phase, the impedance will be complex, having a real and imaginary component.

$$Z = R + jX \tag{3.9}$$

R is called the resistance and X is called the reactance. Thus, we have

$$Z = \left. \frac{P}{V} \right|_{x=0} \tag{3.10}$$

$$Z = \frac{P_i + P_r}{\frac{P_i}{\rho c} - \frac{P_r}{\rho c}} \tag{3.11}$$

Rearranging Equation 3.11 yields the reflection coefficient r

$$r = \frac{P_r}{P_i} = \frac{Z - \rho c}{Z + \rho c} \tag{3.12}$$

The absorption coefficient is a measure of the energy absorbed by the material and is defined by

$$\alpha = 1 - |r|^2 \tag{3.13}$$

In terms of the impedance of the material and Equations 3.12 and 3.13, the absorption coefficient is

$$\alpha = \frac{4R\rho c}{(R + \rho c)^2 + X^2} \qquad (3.14)$$

The impedance and absorption coefficient for plane waves at normal incidence to a material are not constant but are a function of several factors including frequency, material properties and thickness, and mounting conditions.

For some materials, the impedance and absorption coefficients are also a function of the incident angle of sound (15). A material is termed locally reacting if the impedance is independent of the angle of incidence, while extended reaction occurs for materials whose impedance varies with angle of incidence. For a plane wave incident at an angle θ to the normal to the surface in Figure 2, the impedance is

$$Z_\theta = \left. \frac{P_i + P_r}{V_{i_n} + V_{r_n}} \right|_{x = 0}$$

$$Z_\theta = \frac{P_i + P_r}{\dfrac{P_i}{\rho c} \cos\theta - \dfrac{P_r}{\rho c} \cos\theta} \qquad (3.15)$$

From the diagram, V_{i_n} and V_{r_n} are the normal components of the incident and reflected particle velocities so that

$$V_{i_n} = \frac{P_i}{\rho c} \cos\theta \qquad (3.16)$$

$$V_{r_n} = -\frac{P_r}{\rho c} \cos\theta \qquad (3.17)$$

Therefore, the impedance is

$$\frac{Z_\theta}{\rho c} \cos\theta = \frac{P_i + P_r}{P_i - P_r} \qquad (3.18)$$

and the reflection coefficient r is
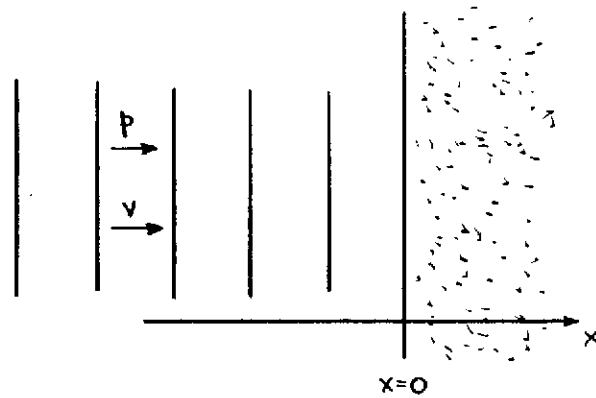
Figure 1 Plane Wave Propagating Normal to the Surface of Material
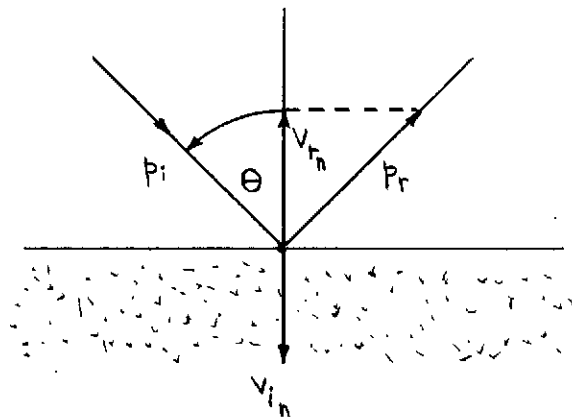
Figure 2 Plane Wave Propagating at Oblique Incidence
to the Surface of Material

$$r = \frac{P_r}{P_i} = \frac{Z_\theta \cos \theta - \rho c}{Z_\theta \cos \theta + \rho c} \qquad (3.19)$$

If the material is locally reacting, then for all angles of incidence, we have

$$Z_\theta = Z \qquad (3.20)$$

If the impedance for any angle θ is known, the absorption coefficient can also be determined. From Equation 3.13, the absorption coefficient for oblique angles is

$$\alpha_\theta = 1 - |r|^2 \qquad (3.21)$$

where the plane wave reflection coefficient r is defined by Equation 3.19.

It would be highly desirable to be able to predict the acoustic behavior of material from knowledge of its physical properties. Several theories for sound absorption based on the acoustic properties of a porous material have been developed. The theories of both Beranek and Ford have used the parameters of flow resistance and porosity to predict normal and oblique incidence behavior of a material. Using normal impedance measurements, Pyett has determined the bulk acoustic parameters of a material which are used in predicting the acoustic behavior at oblique incidence. Each of these theories will be presented in the following sections.

3.2 Beranek's Theory for Porous Materials

Beranek (16) has developed an expression for the specific normal impedance of a porous material in terms of three constants - the flow resistance, porosity, and the density of the enclosed air. The

continuity equation and force equation are derived and then combined to give the wave equation for propagation within the material. We begin by considering the incremental volume of material in Figure 3. This volume $S\Delta x$ contains a volume of solid matter $S_2\Delta x_2$ and a volume of air $S\Delta x_1 + S_1\Delta x_2$ such that the porosity is

$$\Omega = 1 - \frac{\Delta x_2}{\Delta x} \frac{1}{1 + (S_1/S_2)} \qquad (3.22)$$

where $S = S_1 + S_2$.

The continuity equation for the air passing through the material is

$$\frac{\partial}{\partial x}(\rho u) = -\Omega \frac{\partial \rho}{\partial t} \qquad (3.23)$$

which becomes

$$\rho \frac{\partial u}{\partial x} + \Omega \frac{\partial \rho}{\partial t} = 0 \qquad (3.24)$$

Beranek assumes that the cycles of condensation and rarefaction of the enclosed air in the material occur isothermally, which he states is valid for many acoustic materials and especially for frequencies below 2000 Hz. Therefore, for an isothermal process at atmospheric pressure P_0

$$\frac{\Delta P_0}{P_0} = -\frac{\Delta V}{V} \qquad (3.25)$$

and

$$\frac{\Delta P_0}{P_0} = \frac{\Delta \rho}{\rho} \qquad (3.26)$$

If ΔP_0 is the acoustic pressure p, the continuity equation becomes

$$\frac{\partial u}{\partial x} + \frac{\Omega}{P_0} \frac{\partial p}{\partial t} = 0 \qquad (3.27)$$

which for steady state conditions is

$$\frac{\partial u}{\partial x} + \frac{j\omega \Omega p}{P_0} = 0 \qquad (3.28)$$

The net force applied to the incremental volume of Figure 3 is
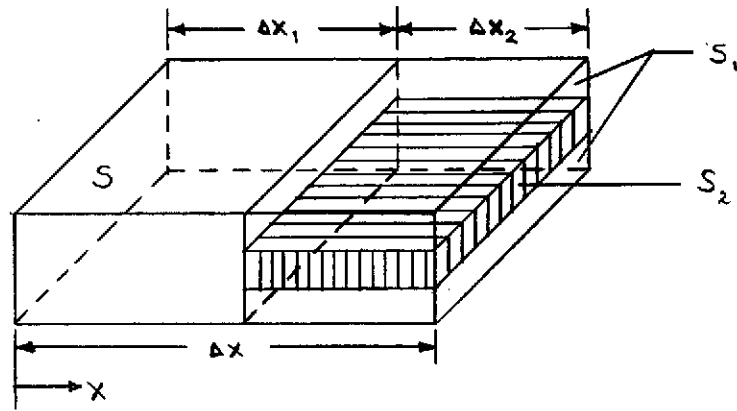
Figure 3   Incremental Volume of Material

$$pS - \left(p + \frac{\partial p}{\partial x} \Delta x \right) S = - \frac{\partial p}{\partial x} S \Delta x \qquad (3.29)$$

This force will be opposed by the sum of the mass times the acceleration of the air and solid particles in the incremental volume and by a force dependent on friction - therefore the flow resistance. If u is the average velocity of particle motion through the face S, then the following continuity equation holds

$$S u = S_1 u_1 + S_2 u_2 \qquad (3.30)$$

where u_1 is the velocity of particle motion through S_1 and u_2 is the velocity of the solid matter of area S_2. The flow resistance of the material introduces a force that will oppose the air flow through the material. This force due to friction F_f is then

$$F_f = R_s \Delta x \, S \, u \qquad (3.31)$$

where R_s is the specific flow resistance per unit thickness. Since u_2 will be zero for non-moving solid, we have

$$F_f = R_s \Delta x \, u = R_2 \Delta x_2 \, S_1 u_1 \qquad (3.32)$$

and

$$R_2 = \frac{R_s \Delta x}{\Delta x_2} \qquad (3.33)$$

The forces on the areas S_1 and S_2 are

$$p S_1 = \rho S_1 \Delta x_2 \frac{\partial u_1}{\partial t} + R_2 S_1 \Delta x_2 \left(u_1 - u_2 \right) \qquad (3.34)$$

$$p S_2 = \rho_2 S_2 \Delta x_2 \frac{\partial u_2}{\partial t} + R_2 S_1 \Delta x_2 \left(u_2 - u_1 \right) \qquad (3.35)$$

where ρ_2 is the density of the solid matter. Therefore, the force

equation becomes

$$-\frac{\partial p}{\partial x} S \Delta x = \rho S \Delta x_1 \frac{\partial u}{\partial t} + \rho S_1 \Delta x_2 \frac{\partial u_1}{\partial t} + \rho_2 S_2 \Delta x_2 \frac{\partial u_2}{\partial t} \qquad (3.36)$$

Using Equations 3.30, 3.34, and 3.35, u_1 and u_2 can be eliminated and

for steady state conditions we have

$$-\frac{\partial p}{\partial x} = j\omega\rho u \left[1 + \frac{S_2 \Delta x_2}{S_1 \Delta x} \left(\frac{\rho_2}{\rho} - 1 \right) \frac{1}{(1 + S_2/S_1) + j(1-\Omega)(\omega\rho_2/R_s)} \right] \quad (3.37)$$

If $\rho_2 \gg \rho$ and $(1-\Omega)^2 (\omega\rho_2/R_s)^2 \gg 1$, the equation yields

$$-\frac{\partial p}{\partial x} = R_s \left(1 + \frac{S_2}{S_1} \right) u + j\omega\rho u \left[1 + \frac{R_s^2 \left(1 + \frac{S_2}{S_1} \right)^2}{(1-\Omega)\omega^2\rho\rho_2} \right] \qquad (3.38)$$

or

$$-\frac{\partial p}{\partial x} = R_1 u + j\omega\rho_1 u \qquad (3.39)$$

where

$$R_1 = R_s \left(1 + \frac{S_2}{S_1} \right) \qquad (3.40)$$

$$\rho_1 = \rho \left[1 + \frac{R_s^2 \left(1 + \frac{S_2}{S_1} \right)^2}{(1-\Omega)\omega^2\rho\rho_2} \right] \qquad (3.41)$$

It can be shown that the approximations $R_1 = R_s$ and $\rho_1 = \rho$ are valid

for the materials we are interested in. Combining the force equation

and continuity equation, we obtain a wave equation

$$\frac{\partial^2 p}{\partial x^2} = \frac{(j\omega R_1 - \omega^2\rho_1)}{\rho_1 c_1^2} \Omega p \qquad (3.42)$$

with

$$c_1^2 = \frac{P_0}{\rho_1} \tag{3.43}$$

This is of the form of the wave equation in free air

$$\frac{\partial^2 P}{\partial x^2} = -\bar{K}^2 P \tag{3.44}$$

with K now being a complex quantity $\bar{K}$ to account for losses as the wave propagates in the material

$$\bar{K} = \frac{\omega}{c_2} = \frac{\omega}{c_1}\left(1 - \frac{jR_1}{\rho_1\omega}\right)^{\frac{1}{2}}\Omega^{\frac{1}{2}} \tag{3.45}$$

and

$$c_2 = \frac{c_1}{\Omega^{\frac{1}{2}}\left(1 - \frac{jR_1}{\rho_1\omega}\right)^{\frac{1}{2}}} \tag{3.46}$$

The solution to the wave equation can be written in the form

$$P = A_+ e^{j(\omega t - \bar{K}x)} + A_- e^{j(\omega t + \bar{K}x)}$$

$$P = 2A_+ e^{j(\omega t + \psi)}\cosh\left(j\bar{K}x + \psi\right) \tag{3.47}$$

where

$$\psi = -\frac{1}{2}\ln\left(\frac{A_+}{A_-}\right) \tag{3.48}$$

A_+ and A_- are the amplitudes of the forward and backward traveling waves respectively. The normal component of velocity is obtained from the force Equation 3.39, and the ratio of P to u at the surface of the material gives the impedance

$$Z_d = \frac{\rho_1 c_1}{\Omega^{\frac{1}{2}}}\left(1 - \frac{jR_1}{\rho_1\omega}\right)^{\frac{1}{2}}\coth\left[j\frac{\omega}{c_1}\left(1 - \frac{jR_1}{\rho_1\omega}\right)^{\frac{1}{2}}\Omega^{\frac{1}{2}}d + \psi\right] \tag{3.49}$$

The value of ψ is obtained by boundary conditions for the material as determined by its mounting procedure. For the rigid wall backing

of Figure 4, $u = 0$ at $x = 0$, so that $Z_0 = \infty$ at $x = 0$. Therefore, the impedance with a rigid wall backing is

$$Z_d = \frac{\rho_1 c_1}{\Omega^{\frac{1}{2}}} \left(1 - \frac{jR_1}{\rho_1 \omega}\right)^{\frac{1}{2}} \coth\left[j \frac{\omega}{c_1}\left(1 - \frac{jR_1}{\rho_1 \omega}\right)^{\frac{1}{2}}\Omega^{\frac{1}{2}} d\right] \qquad (3.50)$$

For a plane wave incident at an arbitrary angle Θ as in Figure 5, we assume that Snell's law holds

$$\frac{\sin\Theta}{c} = \frac{\sin\Theta_2}{c_2} \qquad (3.51)$$

and derive the impedance for any angle of incidence. By applying the boundary conditions for a rigid wall backing, the impedance is

$$Z_d = \frac{\rho_1 c_1 \left(1 - \frac{jR_1}{\rho_1 \omega}\right)^{\frac{1}{2}}}{\Omega^{\frac{1}{2}} \cos\Theta_2} \coth\left[j \frac{\omega}{c_2} \cos\Theta_2\ d\right] \qquad (3.52)$$

and from Equation 3.51

$$\cos\Theta_2 = \left(1 - \frac{c_2^2}{c_1^2} \sin^2\Theta\right)^{\frac{1}{2}} \qquad (3.53)$$

3.3 Ford's Theory for Porous Materials

Ford, Landau, and West (17) derive an expression for the reflection coefficient and impedance of a hard porous absorbent in terms of the porosity and flow resistance of the material. An air wave incident at the surface of the absorbent propagates through and within the pores of the rigid material. It is assumed that the pores are interconnected in a random manner and are of variable diameter and also that the porosity is constant over an area which is small compared to a wavelength.

We begin by examining the force equation and continuity equation for the porous material. Introducing a coefficient of viscous friction R_s (or flow resistance per unit length), the force equation for an
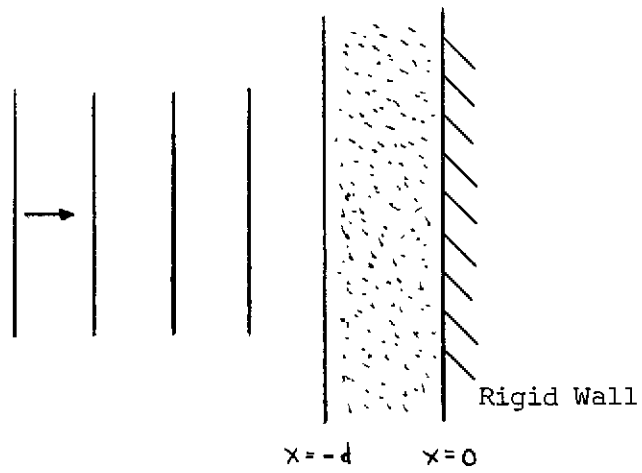
Figure 4   Plane Waves at Normal Incidence to a
Material with Rigid Wall Backing
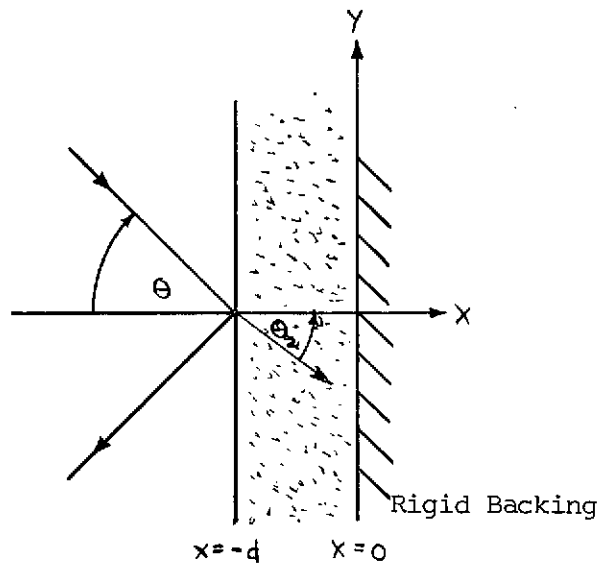
Figure 5   Plane Wave at Oblique Incidence to a
Material with Rigid Wall Backing

incremental volume of material is

$$- \text{grad } p_t = \rho \frac{\partial v_t}{\partial t} + R_s v_t = - \rho \text{ grad} \left(\frac{\partial \phi_t}{\partial t} \right)$$

$$- \text{grad } p_t = j \omega \rho v_t + R_s v_t = - j \omega \rho \text{ grad } \phi_t \qquad (3.54)$$

where ϕ_t is the velocity potential in the material.

Therefore

$$v_t = - \frac{1}{\left(1 - \frac{j R_s}{\rho \omega} \right)} \text{ grad } \phi_t = - D \text{ grad } \phi_t \qquad (3.55)$$

where

$$D = \frac{1}{\left(1 - \frac{j R_s}{\rho \omega} \right)} \qquad (3.56)$$

The equation of continuity for propagation within the material is

$$\text{div } v_t = - \frac{1}{\rho} \frac{\partial \rho}{\partial t} \qquad (3.57)$$

From Morse and Ingard (18), the following expressions are developed

$$\delta = \rho K p \qquad (3.58)$$

$$c^2 = \frac{1}{\rho K} \qquad (3.59)$$

where K is the compressibility of the medium, ρ is the density, δ is

the change in density, and C is the speed of sound in the medium.

From Equation 3.57, we have

$$\frac{1}{K} \text{ div } v_t = - \frac{\partial p_t}{\partial t} \qquad (3.60)$$

Using Ford's notation, this becomes

$$K' \text{ div } v_t = - \frac{\partial p_t}{\partial t} \qquad (3.61)$$

where K' is the modulus of elasticity of the air in the pores. Sub-

stituting Equations 3.54 and 3.55 in Equation 3.61 results in the

wave equation

$$\nabla^2 \Phi_t + \frac{\omega^2 \rho}{K'D} \Phi_t = 0 \tag{3.62}$$

Now, we let

$$c_z = \left(\frac{K'D}{\rho}\right)^{\frac{1}{2}} = \left(\frac{K'/\rho}{1 - \frac{jR_s}{\rho\omega}}\right)^{\frac{1}{2}} \tag{3.63}$$

The speed of sound for isothermal ($\gamma = 1.0$) and adiabatic ($\gamma = 1.4$) conditions is C_T and C_S respectively so that

$$c_T^2 = \frac{1}{\rho K_T} \tag{3.64}$$

$$c_S^2 = \frac{1}{\rho K_S} \tag{3.65}$$

where K_T and K_S are the isothermal and adiabatic compressibility of the medium. Since $K_T = \gamma K_S$, the speed of sound for either condition or for a value of γ between these two extremes is

$$c^2 = \frac{\gamma}{1.4} c_S^2 = q^2 c_S^2 \tag{3.66}$$

where the speed of sound for adiabatic conditions C_S is the same as the speed of sound in air. The speed of sound in the material becomes

$$c_z = \frac{cq}{\left(1 - \frac{jR_s}{\rho\omega}\right)^{\frac{1}{2}}} \tag{3.67}$$

where

$$q = \left(\frac{\gamma}{1.4}\right)^{\frac{1}{2}} \tag{3.68}$$

The field in air is described by a velocity potential Φ such that the pressure and velocity are given by

$$p = \rho \frac{\partial \Phi}{\partial t} \tag{3.69}$$

$$v = - \text{grad } \phi \tag{3.70}$$

Similarly, the field in the absorbent is characterized by a potential ϕ_t so that the resulting pressure and velocity are given by

$$p = \rho_t \frac{\partial \phi_t}{\partial t} \tag{3.71}$$

$$v_t = - D \text{ grad } \phi_t \tag{3.72}$$

where D is the coefficient derived from the force equation. Considering the absorbent with a rigid backing in Figure 6, the fields can be described by the following potentials.

$$\phi = A \left(e^{jk(z-d)\cos\theta} + r e^{-jk(z-d)\cos\theta} \right) e^{-jkx\sin\theta} \tag{3.73}$$

$$\phi_t = B \left(e^{jk_t(z-d)\cos\theta_t} + e^{-jk_t(z-3d)\cos\theta_t} \right) e^{-jk_t x \sin\theta_t} \tag{3.74}$$

We now apply the boundary conditions and introduce Snell's law

$$\frac{\sin\theta}{c} = \frac{\sin\theta_t}{c_t} \tag{3.75}$$

$$k \sin\theta = k_t \sin\theta_t \tag{3.76}$$

Continuity of pressure from Equations 3.69 and 3.71 requires that at $z = d$

$$\phi = \phi_t \tag{3.77}$$

$$(1+r) = T \left(1 + e^{jk_t 2d \cos\theta_t} \right) \tag{3.78}$$

where $T = \dfrac{B}{A}$

Continuity of normal flow from Equations 3.70 and 3.72 requires that at $z = d$

$$-\frac{\partial \Phi}{\partial z} = -D\Omega \frac{\partial \Phi_t}{\partial z} \qquad (3.79)$$

$$jk\cos\Theta(1-r) = D\Omega\, jK_t \cos\Theta_t\left(1 - e^{jK_t 2d\cos\Theta_t}\right) T \qquad (3.80)$$

From Equations 3.78 and 3.80, we solve for r to obtain

$$r = \frac{\rho c_t \cos\Theta \coth\left(jK_t d \cos\Theta_t\right) + D\Omega\rho c \cos\Theta_t}{\rho c_t \cos\Theta \coth\left(jK_t d \cos\Theta_t\right) - D\Omega\rho c \cos\Theta_t} \qquad (3.81)$$

Using the potential Φ, the impedance at the surface for a plane wave incident at an angle Θ is

$$Z_d = \left.\frac{P}{V}\right|_{z=d} = \left.\frac{\rho\frac{\partial \Phi}{\partial t}}{-\frac{\partial \Phi}{\partial z}}\right|_{z=d}$$

$$Z_d = \frac{j\omega\rho\,(1+r)}{-jk\cos\Theta\,(1-r)} \qquad (3.82)$$

From equation 3.81, we obtain

$$Z_d = \frac{\rho c_z \coth\left(jK_t d \cos\Theta_t\right)}{D\Omega \cos\Theta_t} \qquad (3.83)$$

For normal incidence, $\Theta = 0$, this becomes

$$Z_d = \frac{\rho c_z \coth\left(jK_t d\right)}{D\Omega} \qquad (3.84)$$

3.4 Pyett's Theory for Non-isotropic Porous Materials

Pyett (7) has derived an expression for the specific normal impedance in terms of two experimentally determined propagation parameters of a homogeneous porous material. A treatment of wave

propagation in an isotropic medium is first presented and then general-
ized to the case of propagation in a non-isotropic medium using tensor
notation.

The force equation for propagation of an acoustic wave in an
isotropic medium such as air is

$$- \operatorname{grad} p = \rho \, \frac{\partial u}{\partial t} \tag{3.85}$$

where p and u are the acoustic pressure and velocity respectively.
The equation of continuity is

$$\operatorname{div} u = - \frac{1}{\rho} \, \frac{\partial \rho}{\partial t} \tag{3.86}$$

$$\frac{1}{K} \operatorname{div} u = - \frac{\partial p}{\partial t} \tag{3.87}$$

$$K' \operatorname{div} u = - \frac{\partial p}{\partial t} \tag{3.88}$$

where K is the compressibility of the medium. Now, taking the diver-
gence of Equation 3.85 and the derivative with respect to time of
Equation 3.88 and combining, we obtain the wave equation

$$\nabla^2 p = \frac{\rho}{K'} \, \frac{\partial^2 p}{\partial t^2} \tag{3.89}$$

Assuming a time dependence $e^{j\omega t}$ this becomes

$$\nabla^2 p = \gamma^2 p \tag{3.90}$$

where

$$\gamma = j\omega \left(\frac{\rho}{K'} \right)^{\frac{1}{2}} \tag{3.91}$$

The characteristic impedance Z of the medium will be defined as

$$Z = \left(\rho K' \right)^{\frac{1}{2}} \tag{3.92}$$

From the force equation

$$- \text{grad } p = j\omega\rho u = (\rho K')^{\frac{1}{2}} \mathcal{S} u$$

$$- \text{grad } p = Z \mathcal{S} u \qquad (3.93)$$

we obtain the velocity

$$u = - \frac{1}{\mathcal{S} Z} \text{grad } p \qquad (3.94)$$

The quantity $\mathcal{S}$ has a real and imaginary component

$$\mathcal{S} = \sigma + j\beta \qquad (3.95)$$

where σ is the attenuation constant and β is the phase constant which corresponds to k in air. For a plane wave propagating in the positive x direction, the pressure and velocity are

$$p = P e^{j\omega t - \mathcal{S} x} \qquad (3.96)$$

$$u = \frac{p}{Z} \qquad (3.97)$$

For an anisotropic medium, ρ and K' may depend on the direction of u so it is necessary to use tensor notation for Equations 3.85 and 3.88. These relations in tensor form become

$$\frac{\partial}{\partial t}\left(\rho_{ij} u_j \right) = - \frac{\partial p}{\partial x_i} \qquad (3.98)$$

$$\frac{\partial}{\partial x_i}\left(K'_{ij} u_j \right) = - \frac{\partial p}{\partial t} \qquad (3.99)$$

If the ρ and K' tensors are both symmetric and have the same principal axes, then, referred to these axes, both matrices are diagonal. The wave equation becomes

$$\frac{\partial^2 p}{\partial x_i^2} = \frac{\rho_{ii}}{K'_{ii}} \frac{\partial^2 p}{\partial t^2} = \mathcal{S}_i^2 p \qquad (3.100)$$

with

$$\mathcal{J}_i = j\omega \left(\frac{\rho_{ii}}{K'_{ii}}\right)^{\frac{1}{2}} \tag{3.101}$$

and

$$Z_i = \left(\rho_{ii} K'_{ii}\right)^{\frac{1}{2}} \tag{3.102}$$

The velocity is now given by

$$u_i = -\frac{1}{\mathcal{J}_i Z_i}\frac{\partial p}{\partial x_i} \tag{3.103}$$

The specific normal impedance of a thickness d of a homogeneous porous material can now be calculated for a plane wave incident at angle Θ to the normal. The layer is assumed to be backed by a rigid wall having an infinite impedance as shown in Figure 7. If the plane of the incident acoustic ray makes an angle η with the y axis, then the sum of the sound pressures of the incident and reflected waves is

$$P_i = \left(A_i e^{-jkx\cos\Theta} + B_i e^{jkx\cos\Theta}\right) e^{jk(y\sin\eta + z\sin\eta)\sin\Theta} \tag{3.104}$$

where the time factor $e^{j\omega t}$ will be omitted. The transmitted pressure, including the component reflected from the rigid backing is

$$P = \left(A e^{-qx} + B e^{qx}\right) e^{ry + sz} \tag{3.105}$$

where

$$r = jK\cos\eta \sin\Theta \tag{3.106}$$

$$s = jK\sin\eta \sin\Theta \tag{3.107}$$

Substituting the pressure in Equation 3.100, we obtain

$$\frac{q^2}{\mathcal{J}_x^2} + \frac{r^2}{\mathcal{J}_y^2} + \frac{s^2}{\mathcal{J}_z^2} = 1 \tag{3.108}$$
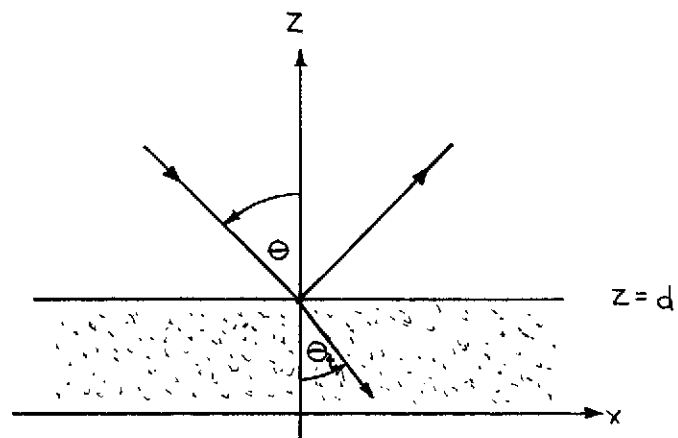
Figure 6   Plane Wave at Oblique Incidence to a
Material with Rigid Wall Backing
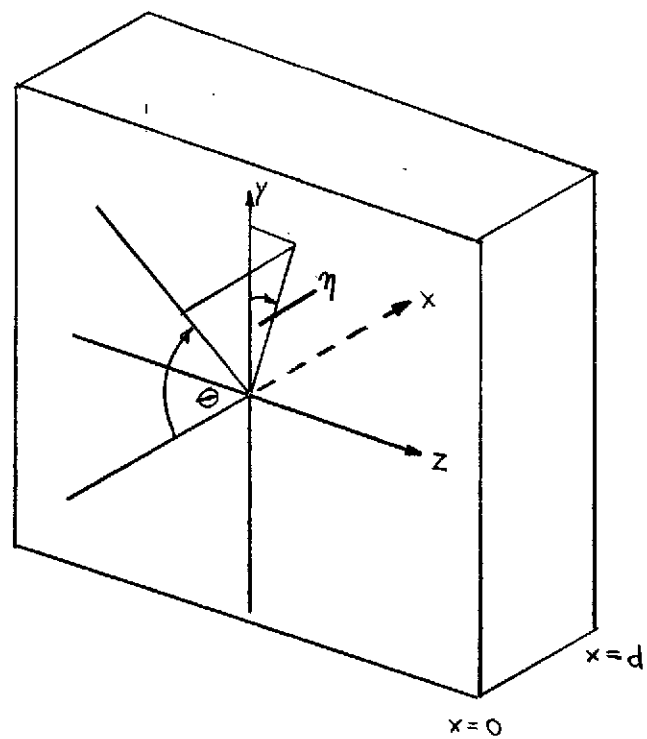
Figure 7   Wave Propagating at Oblique Incidence to Material

The velocity in the x direction is

$$u_x = -\frac{1}{\rho_x Z_x}\frac{\partial P}{\partial x}$$

$$u_x = -\frac{q}{\rho_x Z_x}\left(A e^{-qx} - B e^{qx}\right) e^{ry+sz} \tag{3.109}$$

We now apply the boundary conditions at the surface and backing of

the material. Continuity of pressure across the surface $x = 0$ requires

$$A + B = A_o + B_o \tag{3.110}$$

Because of the rigid backing, $u_x = 0$ at $x = d$ and

$$A e^{-qd} - B e^{qd} = 0 \tag{3.111}$$

Therefore, the specific normal impedance at $x = 0$ is

$$Z(d,\theta) = \frac{\rho_x Z_x}{q}\coth(qd) \tag{3.112}$$

The value of q from Equation 3.108 is

$$q = \rho_x\left[1 + k^2\sin^2\theta\left(\frac{\cos^2\eta}{\rho_y^2} + \frac{\sin^2\eta}{\rho_z^2}\right)\right]^{\frac{1}{2}} \tag{3.113}$$

The expression for q can be simplified if either $\eta = 0$ or $\rho_y = \rho_z$

$$q = \rho_x\left(1 + \frac{k^2\sin^2\theta}{\rho_y^2}\right)^{\frac{1}{2}} \tag{3.114}$$

We define an arbitrary angle ϕ by

$$k\sin\theta = \beta_y\sin\phi \tag{3.115}$$

The angle ϕ has no meaning beyond the above definition except for the

case of zero attenuation $\sigma = 0$, when it is identical with the angle of

refraction given by Snell's law

$$jk\sin\theta = \rho_y\sin\phi_r \tag{3.116}$$

When σ_x and σ_y are small compared with β_x and β_y, Equation 3.114 becomes

$$q = \frac{\sigma_x}{\cos\phi}\left[\cos^2\phi + \sin^2\phi \frac{\sigma_y \beta_x}{\sigma_x \beta_y}\right] + j\beta_x \cos\phi \qquad (3.117)$$

Furthermore, when $\sigma_y/\beta_y = \sigma_x/\beta_x$ Equation 3.117 is simplified to

$$q = \frac{\sigma_x}{\cos\phi} + j\beta_x \cos\phi \qquad (3.118)$$

The two propagation parameters for the material are q, the propagation constant, and Z_x, the characteristic impedance. For normal incidence $\theta = 0$ and $q = \mathcal{J}_x$, and Equation 3.112 becomes

$$Z(d,o) = Z_x \coth(\mathcal{J}_x d) \qquad (3.119)$$

The two propagation parameters can be determined from normal impedance measurements for samples of different thickness. If the thickness of the samples are in the ratio of 1 to 2, and the samples are backed by a rigid wall, the impedance will be

$$Z(d,o) = Z_x \coth(\mathcal{J}_x d) = R + jX \qquad (3.120)$$

$$Z(2d,o) = Z_x \coth(2\mathcal{J}_x d) = R' + jX' \qquad (3.121)$$

so that

$$\frac{Z(d,o)}{Z(2d,o)} = \frac{1 + \cosh(2\mathcal{J}_x d)}{\cosh(2\mathcal{J}_x d)} \qquad (3.122)$$

Rearranging Equation 3.122, we have

$$\cosh(2\mathcal{J}_x d) = \frac{R' + jX'}{(R-R') + j(X-X')} = U + jV \qquad (3.123)$$

where

$$V = \frac{X(R-R') - R'(X-X')}{(R-R')^2 + (X-X')^2} \qquad (3.124)$$

$$V = \frac{X'(R-R') - R'(X-X')}{(R-R')^2 + (X-X')^2} \qquad (3.125)$$

Using a standing wave tube for normal impedance measurements, the measured values of R, X, R', and X' from Equations 3.120 and 3.121 are inserted in Equations 3.124 and 3.125. The values of $2\mathcal{S}_x d$ in Equation 3.123 may be determined from nomograms for the hyperbolic cosine of a complex argument (19) or, as in this case, determined by an iteration technique (20) for complex numbers using the IBM 370 computer. This iteration technique is discussed in Appendix A. From Equation 3.95, the value of $\mathcal{S}$ is

$$\mathcal{S} = \sigma + j\beta \qquad (3.126)$$

Once $\mathcal{S}_x$ has been determined, Z_x may be calculated from Equation 3.119. Using these values, the impedance can be calculated as a function of incident angle from Equations 3.112 and 3.118. The validity of these theoretical approaches will be discussed in Section 5.4 in connection with the presentation of the experimental results.

CHAPTER IV

PROCEDURE AND TECHNIQUES

4.1 Standing Wave Tube

Measurements of the normal incidence behavior of absorbing

materials can be made using a standing wave tube, also known as an

impedance tube or constant length acoustic interferometer. A Bruel

and Kjaer Type 4002 Standing Wave Apparatus, which meets the specifi-

cations of ASTM Standard C384-58 (1), was used for measuring the

impedance and absorption coefficients at normal incidence. The

apparatus consists of a rigid walled tube with a sound source at one

end and the sample of absorbing material to be tested at the other

end as shown in Figure 8. The sound field in the tube is generated

by the loudspeaker and pressure levels are measured with a moveable

probe microphone. The formation of a reflected wave at the absorbing

material generates a pattern of standing waves. The sound pressure

at a distance x from the sample is the sum of the incident wave p_i

and the reflected wave p_r (21).

$$p = A e^{j(\omega t - \overline{k}x)} + B_1 e^{j(\omega t + \overline{k}x)} \tag{4.1}$$

The wavenumber $\overline{k}$ is complex, to account for attenuation in the tube.

However, if we assume that losses in the tube as the sound wave

propagates are negligible, then the wavenumber $\overline{k}$ has only a real part

k so that $\overline{k} = k = \omega/c$. If we can determine the phase and magnitude

of the reflected pressure amplitude B_1 relative to A, the specific

normal impedance can be determined. If the reflected pressure ampli-

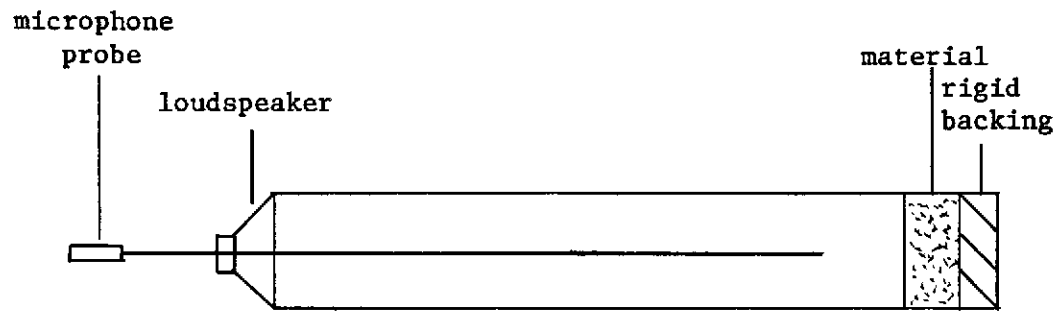tude is complex, it may be written as

Figure 8   Standing Wave Tube

$$B_1 = B e^{j\phi} = |r| A e^{j\phi} \qquad (4.2)$$

so that

$$P = \left(A e^{-jK_1} + B e^{jK_1} \right) e^{jT_1} \qquad (4.3)$$

where $K_1 = kx + \dfrac{\phi}{2}$ and $T_1 = \omega t + \dfrac{\phi}{2}$.

The acoustic pressure is the real part of Equation 4.3

$$P = \left[(A+B)^2 \cos^2 K_1 + (A-B)^2 \sin^2 K_1 \right]^{\frac{1}{2}} \cos(T_1 + \epsilon) \qquad (4.4)$$

and the amplitude of the standing wave pattern is

$$P = \left[(A+B)^2 \cos^2 \left(kx + \dfrac{\phi}{2} \right) + (A-B)^2 \sin^2 \left(kx + \dfrac{\phi}{2} \right) \right]^{\frac{1}{2}} \qquad (4.5)$$

From Equation 4.5 pressure maximum and minimum will be located at

antinodes and nodes respectively such that

$$P_{max} = A + B = A \left(1 + |r| \right) \qquad (4.6)$$

$$P_{min} = A - B = A \left(1 - |r| \right) \qquad (4.7)$$

For the conditions of a minimum at a point x_n, Equation 4.7 indicates

that all nodes will be located at positions such that $\sin\left(kx + \dfrac{\phi}{2} \right)$

will be a maximum. Therefore,

$$kx_n + \dfrac{\phi}{2} = -\dfrac{\pi}{2} \qquad (4.8)$$

and

$$\phi = -\pi - \dfrac{4\pi x_n}{\lambda} \qquad (4.9)$$

The wavelength λ can be measured directly by taking the distance

between successive minimums at x_n and x_{n+1}. The standing wave ratio

SWR is the ratio of maximum and minimum pressures

$$SWR = \frac{P_{max}}{P_{min}} = \frac{1 + |r|}{1 - |r|} \tag{4.10}$$

Thus,

$$r = \frac{B}{A} = \frac{SWR-1}{SWR+1} \tag{4.11}$$

The specific normal impedance at the surface of the material is then

$$\frac{Z}{\rho c} = \frac{1 + |r|e^{j\phi}}{1 - |r|e^{j\phi}} \tag{4.12}$$

Finally, the absorption coefficient can also be determined and is

$$\alpha = 1 - |r|^2 \tag{4.13}$$

A moveable probe microphone is inserted in the tube so that X_n and SWR can be measured.

ASTM Standard C384-58 lists specifications for low and high frequency limits of measurements based on impedance tube dimensions. The lower limiting frequency f_L is determined by the length L of the tube in feet and is given by

$$f_L = \frac{1000}{L} \tag{4.14}$$

Similarly, the upper limiting frequency f_u for measurements is given by

$$f_u = \frac{8000}{b} \tag{4.15}$$

where b is the diameter of the tube in inches. Within this frequency range higher order modes of propagation are restricted, and we have only plane wave propagation in the tube. Because of these limitations, two tubes of different sizes were used to take measurements over the frequency range of interest. These limits, together with the limits for measurements specified by Bruel and Kjaer (22) for each size tube,

are listed in Table 3. The standing wave tube provides a quick and
inexpensive means of determining the relative absorption properties
of many materials in a short period of time. However, the absorption
of most materials is higher at oblique incidence than at normal inci-
dence. Since propagation within the tube is limited to plane waves,
the impedance tube measurement gives an absorption coefficient which
is usually the minimum performance expected for a material.

TABLE 3

Frequency Limits for Standing Wave Tube Measurements

			Frequency Limits			
			Bruel and Kjaer		ASTM Standards	
Tube Size	Length	Diameter	Low	High	Low	High
Large	40"	1 1/8"(3cm)	90 Hz	1800 Hz	99 Hz	2030 Hz
Small	13 3/4"	3 7/8"(10cm)	800 Hz	6500 Hz	288 Hz	6780 Hz

4.2 Flow Resistance

The apparatus used for flow resistance measurements, shown in
Figure 9, follows specifications outlined in ASTM Standard C522-69 (23).
Since the fiberglass samples are not completely rigid, caution must be
used in inserting the material in the sample holder because compressing
the material would yield a high flow resistance. With the flow control
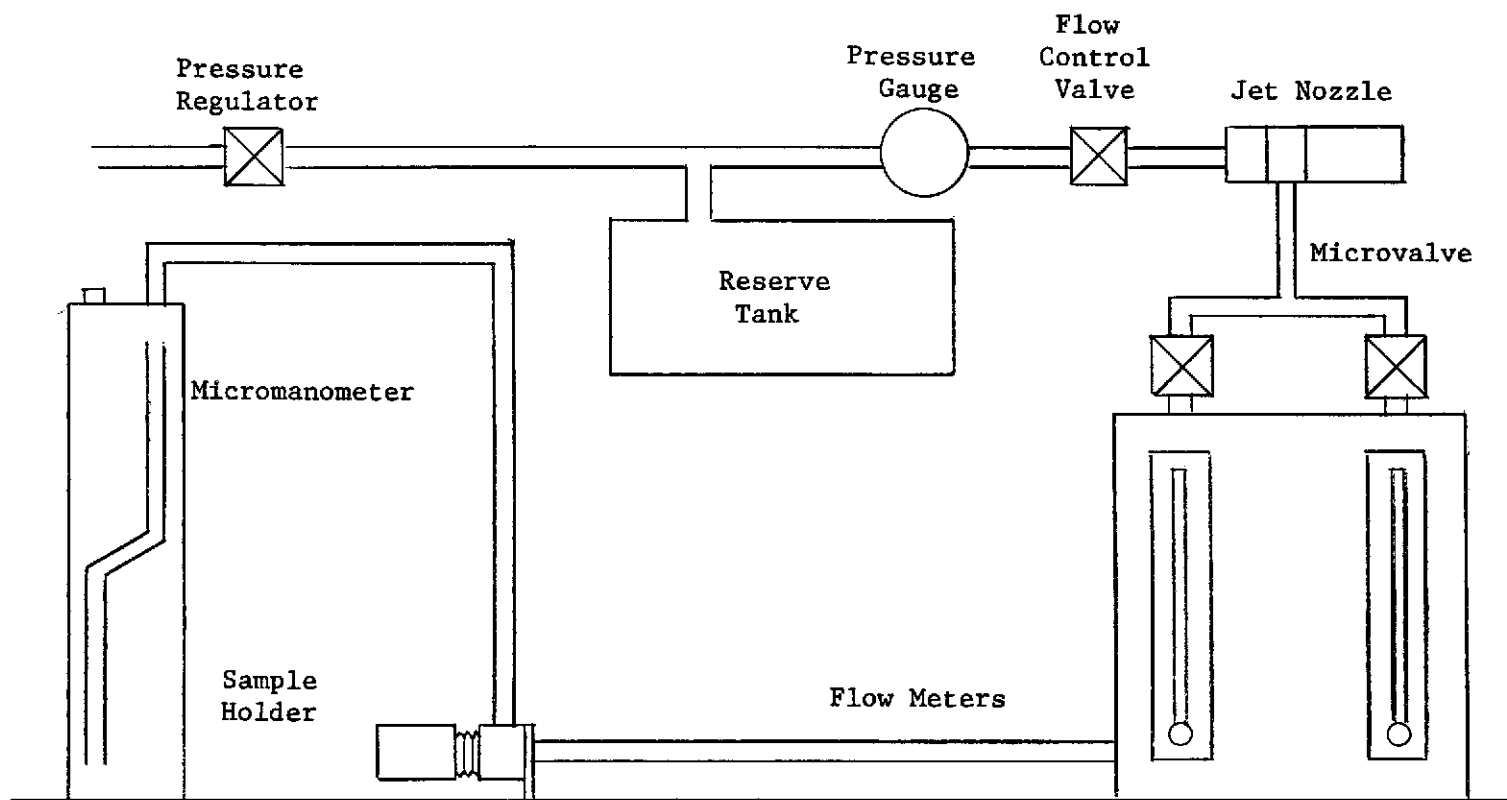
Figure 9   Flow Resistance Apparatus

valve closed and the pressure regulator adjusted, the inlet supply valve is opened to fill the reserve tank. As the flow control valve is opened, flow through the jet nozzle causes a vacuum at its center section which draws air through the sample and the rotameters and then out the jet. With the rotameter valves fully opened, the flow control valve is opened until the maximum flow rate of 1700 cc/min is achieved. The flow can now be regulated from 0 to 1700 cc/min using the micro-valve alone. Since the pressure drop across the specimen for these flow rates is on the order of thousandths of an inch of water, it is measured using a micromanometer. The pressure drop in units of dynes/cm^2 is

$$\Delta p = \rho g h = 2490 \, h \tag{4.16}$$

where h is the pressure drop in inches of water. The particle velocity in cm/sec can be determined from the cross sectional area A of the sample and the flow rate Q in cc/min

$$u = \frac{Q}{60 \, A} \tag{4.17}$$

The specific flow resistance per unit thickness d in cgs rayls/inch is then

$$R_s = \frac{\Delta p}{u d} = \frac{\Delta p A}{Q d} \tag{4.18}$$

For an area of 8.73 cm^2, this becomes

$$R_s = 1.3 \times 10^6 \, \frac{h}{Q} \tag{4.19}$$

where

    h = pressure drop in inches of water

    Q = flow rate in cc/min

Since the flow resistance increases rapidly with u , it is important

that measurements of flow resistance be performed within a range of

values for u corresponding to particle velocities encountered in sound

pressure levels appropriate to noise control problems. The sound

pressure level in decibels, re. 0.002 microbars, which corresponds

to a certain particle valocity can be determined from the following

equation

$$SPL = 20 \log_{10} \frac{p}{p_{ref}} = 20 \log_{10} \frac{\rho c u}{p_{ref}} \qquad (4.20)$$

$$SPL = 20 \log_{10} Q + 51.8 \qquad (4.21)$$

and is listed in Table 4 for the range of flow rates used in testing.

4.3 Surface Pressure Method

Measurements of the absorption characteristics of a material

at oblique incidence were taken using a free field measuring technique

first presented by Ingard and Bolt (10). This method, known as the

surface pressure method, compares the pressure and phase of a plane

wave measured as a function of incident angle at a point on the sur-

face of an absorbent material to a similar measurement at the same

point in space at the surface of a completely reflecting panel. A

sufficiently large sample is assumed so that the theory of reflection

from an infinite plane boundary can be used in the analysis. The

two measurements are illustrated in Figure 10. In future use, the

TABLE 4

Flow Rate Versus dB Level, re. 0.002 Microbars,
for Flow Resistance Measurements

Flow Rate (cc/min)	dB Level
10	71.8
20	77.8
40	83.8
80	89.8
100	91.8
150	95.3
200	97.8
400	103.8
600	107.4
800	109.9
1000	111.8
1200	113.4
1400	114.7
1600	115.9
2000	117.8

pressures p_1 and p_2 will be referred to as the hard wall pressure and the absorbing surface pressure respectively. Assuming the pressure of the incident wave is p_i, the following relationship can be written for p_1 and p_2.

$$P_1 = p_i + p_r = 2 p_i = P_1 e^{j\psi_1} \qquad (4.22)$$

$$P_2 = p_i + p_r = P_2 e^{j\psi_2} \qquad (4.23)$$

The relationship between these expressions can be visualized by the vector diagram in Figure 11, where $\psi = \psi_2 - \psi_1$. From Equation 4.22 and 4.23

$$p_i = \frac{P_1}{2} \qquad (4.24)$$

$$p_r = p_2 - p_i = p_2 - \frac{P_1}{2} \qquad (4.25)$$

and from the vector diagram

$$p_2 = P_2 \left(\cos \psi_2 + j \sin \psi_2 \right) \qquad (4.26)$$

$$p_1 = P_1 \left(\cos \psi_1 + j \sin \psi_1 \right) \qquad (4.27)$$

Now, combining Equations 4.26 and 4.27

$$|p_r|^2 = P_2^2 + \frac{P_1^2}{4} - P_1 P_2 \cos\psi \qquad (4.28)$$

Dividing Equation 4.28 by $|p_i|^2$ we obtain

$$\frac{|p_r|^2}{|p_i|^2} = 4 \left(\frac{P_2^2}{P_1^2} - \frac{P_2}{P_1} \cos\psi + \frac{1}{4} \right) \qquad (4.29)$$
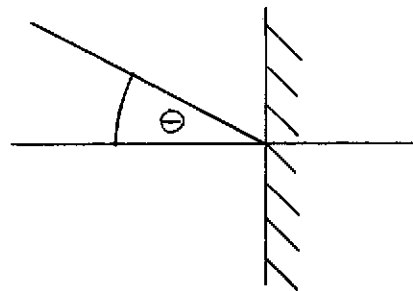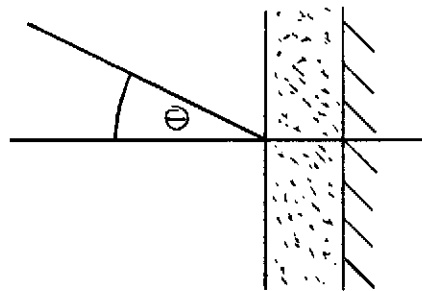
Hard Wall Pressure P_1

Absorbing Surface Pressure P_2

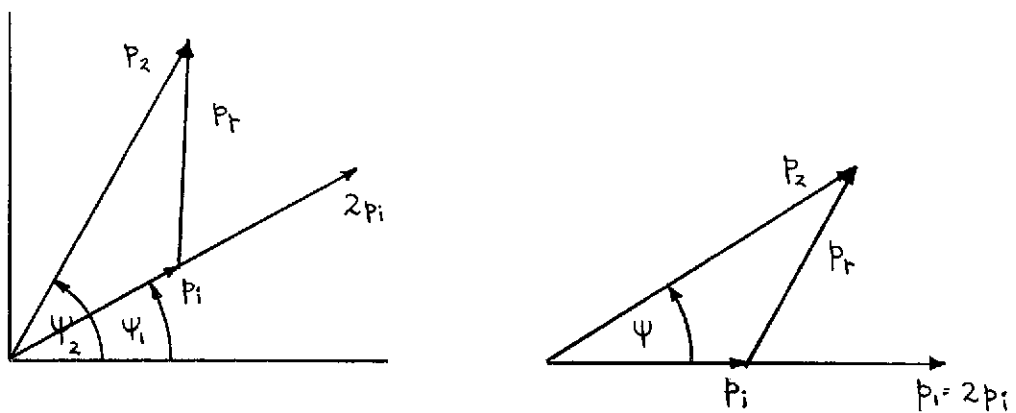Figure 10   Surface Pressure Method Measurements

Figure 11   Phase Relations Between Measurements
with the Surface Pressure Method

The absorption coefficient as a function of incident angle is then

$$\alpha_\theta = 1 - \frac{|p_r|^2}{|p_i|^2}$$

$$\alpha_\theta = 4 \frac{P_2}{P_1} \left(\cos\psi - \frac{P_2}{P_1} \right) \tag{4.30}$$

For an incoming wave at angle Θ, the incident and reflected pressures are related from Equation 3.19 as follows

$$\frac{p_r}{p_i} = \frac{Z_\theta \cos\Theta - \rho c}{Z_\theta \cos\Theta + \rho c} \tag{4.31}$$

where Z_θ is the specific normal impedance of the material at the angle Θ. Letting $\xi = \frac{Z_\theta}{\rho c}$ and $W = \frac{P_2}{P_1} = \frac{P_2}{P_1} e^{j\psi}$ we have

$$W = \frac{\xi \cos\Theta}{\xi \cos\Theta + 1} \tag{4.32}$$

Therefore, for measurements using the hard wall pressure P_2 as a reference, the normalized impedance is given by

$$\xi = \frac{W}{1-W} \frac{1}{\cos\Theta} \tag{4.33}$$

If the reference pressure is measured for free field conditions instead of at the surface of the perfectly reflecting boundary, we then have for the free field pressure P_3

$$P_3 = P_i = \frac{P_1}{2} \tag{4.34}$$

The expressions for absorption and impedance, using a free field pressure as a reference, are now

$$\alpha_\theta = \frac{P_2}{P_3} \left(2\cos\psi - \frac{P_2}{P_3} \right) \tag{4.35}$$

$$\xi = \frac{w}{2-w} \frac{1}{\cos \Theta} \tag{4.36}$$

Therefore, a reference pressure for measurements can be taken either for free field conditions or at the surface of a perfectly reflecting boundary.

The experimental arrangement for the surface pressure method is shown schematically in Figure 12. The material to be tested is mounted on a panel and placed in an anechoic chamber. The measurements at the material surface and at the reflecting surface (or free field position) must be made at the same point in space so that no additional phase shift between the two is introduced. The surface of the material and the surface of the reflecting panel must then occupy the same plane in space. A probe microphone located either at the surface of the material or at the surface of the reflecting boundary measures the pressure. The phase difference between the electrical driving voltage to the loudspeaker and the acoustic pressure at the reflecting surface is ψ_1'. The corresponding phase difference for the measurement at the surface of the material is ψ_2'. Thus,

$$\psi = \psi_2' - \psi_1' = \psi_2 - \psi_1 \tag{4.37}$$

As the sample rotates in the presence of an approximately plane wave, the pressure and phase are recorded continuously as a function of incident angle.

A few differences exist between the surface pressure method as performed by Ingard and Bolt and as performed in this study. The "hard wall" used by Ingard and Bolt was an eight-foot square panel rotated about a vertical axis at a speed of approximately one half
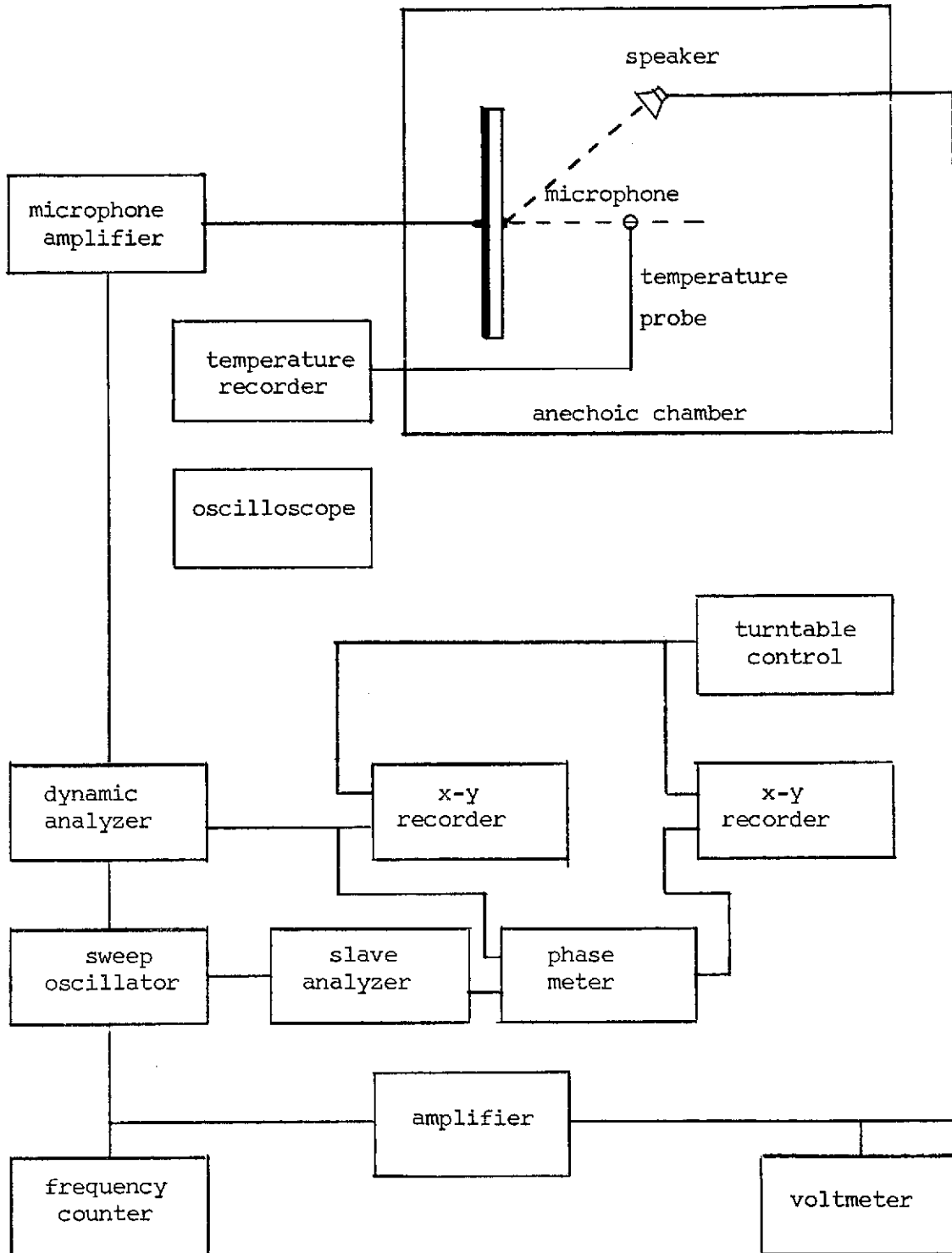
Figure 12   Schematic for Surface Pressure Method Tests

revolution per minute. A large horn speaker was used as a sound source and the pressure at the surface of the material and panel was measured using a probe tube connected to a 640-AA condenser microphone.

The initial attempt to investigate this method was made using a three-foot square panel as the reflecting surface. To satisfy the conditions of a hard walled rigid surface, the panel was constructed of a three quarter inch plywood board with a one-eighth inch thick aluminum sheet bonded to its surface. The panel was mounted on a turntable in the anechoic chamber and rotated about its vertical axis at a speed of approximately 1/3 revolution per minute. The pressure and phase were recorded continuously as a function of incident angle with a Bruel and Kjaer Type 4136 quarter inch condensor microphone mounted at the center of the board. Preliminary tests concluded that the three-foot panel was too small for the assumption of an infinite reflecting surface to be valid for the frequency limits of interest in this study. Limitations regarding sample size will be discussed in Section 5.3. As an alternative, a larger six-foot square panel of similar construction was used as the "infinite" reflecting surface. Due to the size and weight of this board, it was held stationary while the sound source was mounted at the end of a boom and rotated about the vertical axis of the board at a fixed distance of 8'4". The sound source, a CTS 4 1/2" diameter mid-range speaker enclosed in a 4" x 4 1/2" x 7 1/2" wooden box, was suspended from the boom as shown in Figure 13 at the same vertical height as the Bruel and Kjaer Type 4136 quarter inch microphone mounted at the center of the panel.
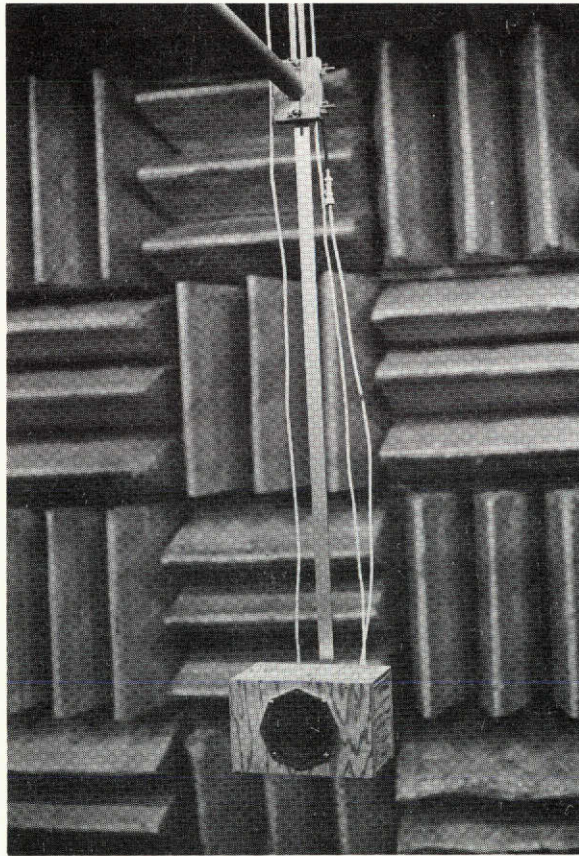
Figure 13   Sound Source for Surface Pressure Method Tests

The distance between the source and microphone must be kept constant for testing samples of varying thicknesses so that no additional phase shift is introduced in the phase angle measurement. The piston-type mounting arrangement shown in Figure 14 allows the panel to be moved horizontally so that the surface of the absorbing material and the reflecting boundary can be placed at the same plane in space for each measurement. The positioning of the surface was facilitated by using a plumb bob suspended from a fixed point above the reflecting panel. The apparatus is shown in Figures 15 and 16 for a hard wall pressure and surface pressure measurement respectively. Since measurements of the pressure and phase for several different samples were recorded and then compared to a reference measurement, it was necessary to monitor temperature variations in the chamber. The effect of temperature changes on phase measurements will be shown in Section 5.3.
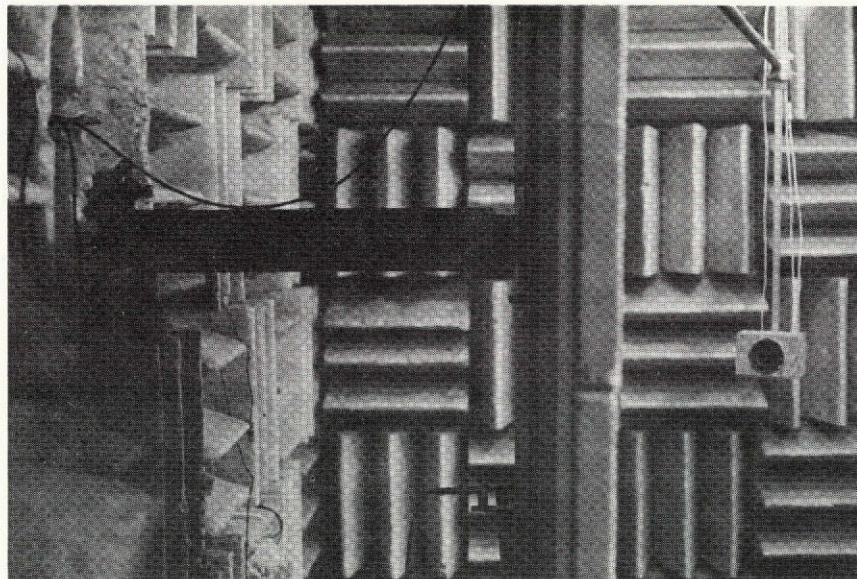
Figure 14 Mounting Arrangement for Reflecting Panel
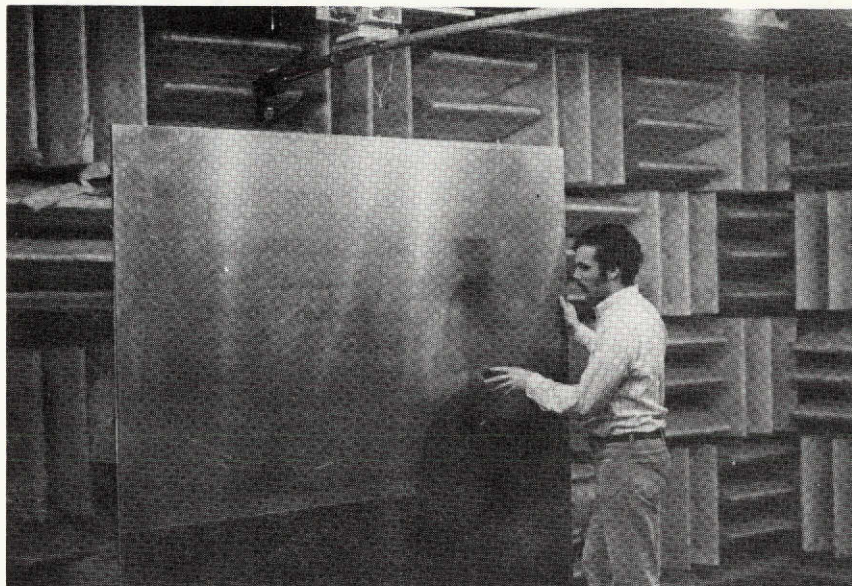
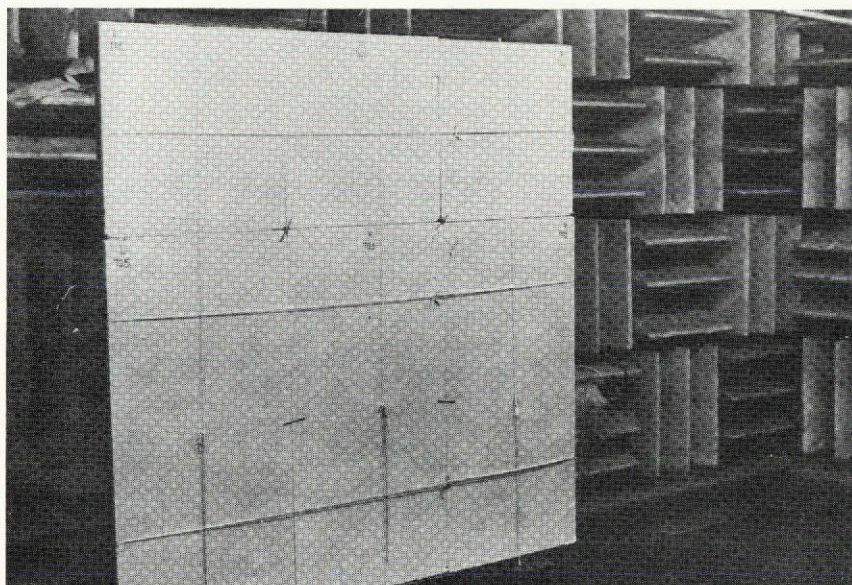Figure 15 Panel with Hard Wall Surface

Figure 16 Panel with Surface of Sound Absorbing Material

CHAPTER V

DISCUSSION OF RESULTS

5.1 Standing Wave Tube

The results of absorption measurements at normal incidence using

the standing wave tube described in Section 4.1 are shown in Figures

17 to 22 for one-inch thick samples of Owens Corning 703, 704, and 705

Fiberglas. These three samples were taken from the materials used in

the surface pressure method tests. According to limits set by both

Bruel and Kjaer, and the ASTM Standards, measurements with our appara-

tus should be possible for frequencies up to 6000 Hz. However,

successive pressure minimums did not repeat at half wavelength inter-

vals for measurements at 6000 Hz. This effect would tend to discredit

absorption measurements at the high frequency limit of the standing

wave tube. There is some question as to whether these limits are

valid for measurements with both locally reacting and extended reacting

materials. For an extended reacting material, the behavior at a point

on the surface of the material is affected by the behavior at an

adjacent point. In this case, then, there is a possibility modes

would be generated that would interfere with plane wave propagation

within the tube.

The agreement between measurements for an overlapping frequency

range using the large tube and the small tube is quite good, indicating

that the absorption of the fibrous materials is independent of sample

size. For each material, the resistive component of the impedance is

positive, being essentially constant over the frequency range from

500 Hz to 3000 Hz, while the reactive component of the impedance has

Figure 17   Specific Normal Impedance Measured by the
            Standing Wave Tube for O.C. 703 Fiberglas -1.0"

Figure 18   Absorption Coefficient Measured by the
            Standing Wave Tube for O.C. 703 Fiberglas -1.0"

Figure 19   Specific Normal Impedance Measured by the Standing
Wave Tube for O.C. 704 Fiberglas -1.0"

Figure 20   Absorption Coefficient Measured by the Standing
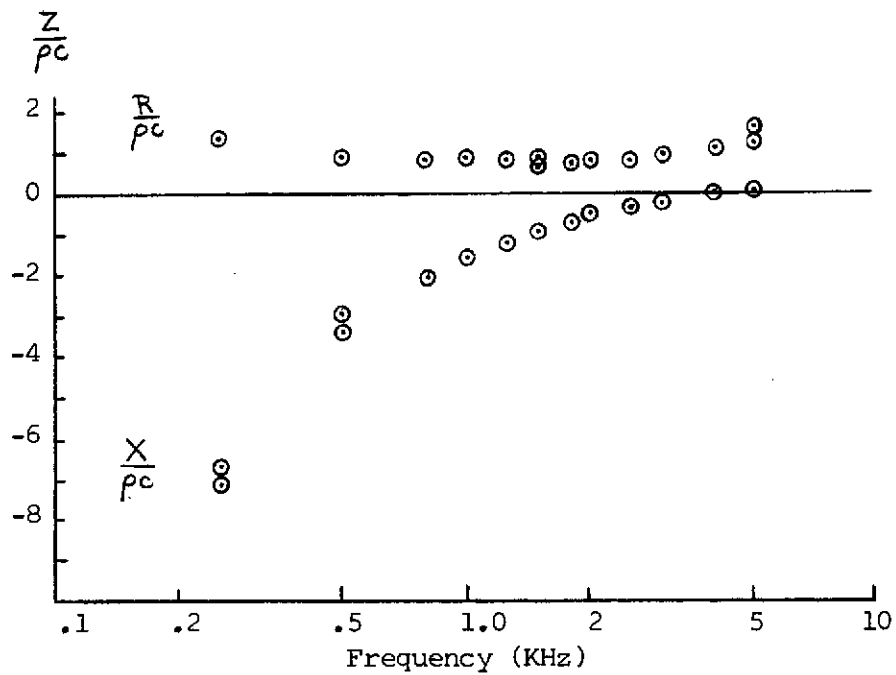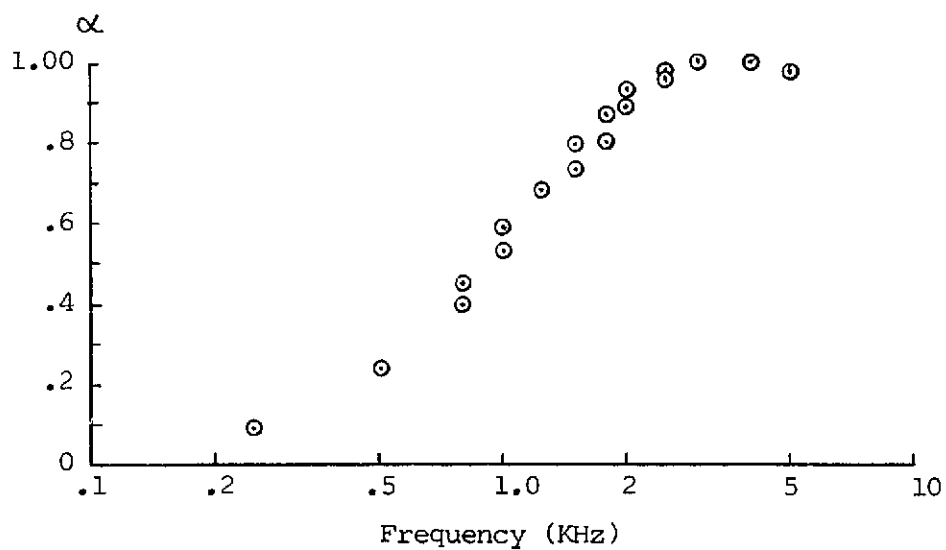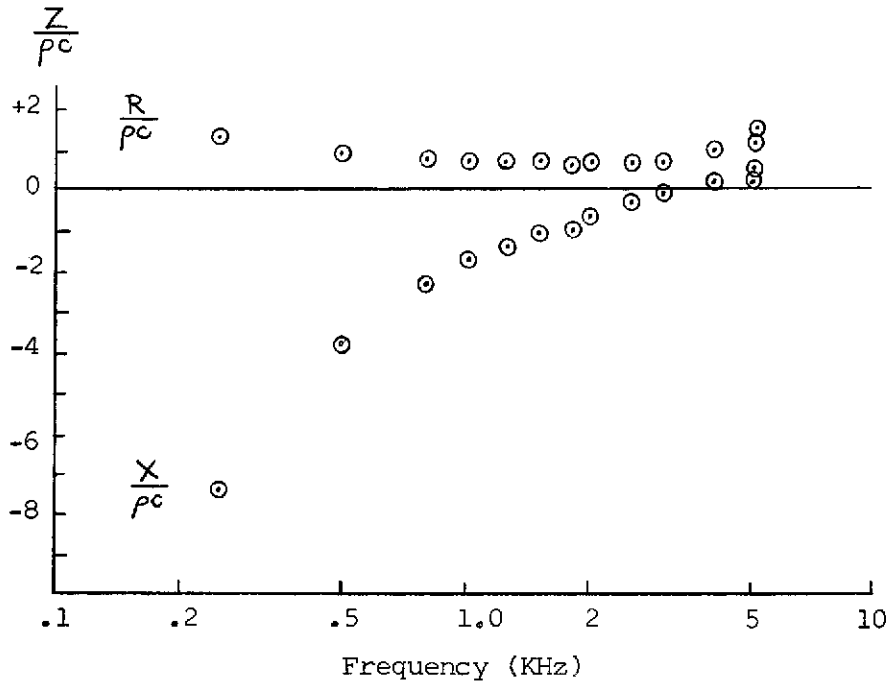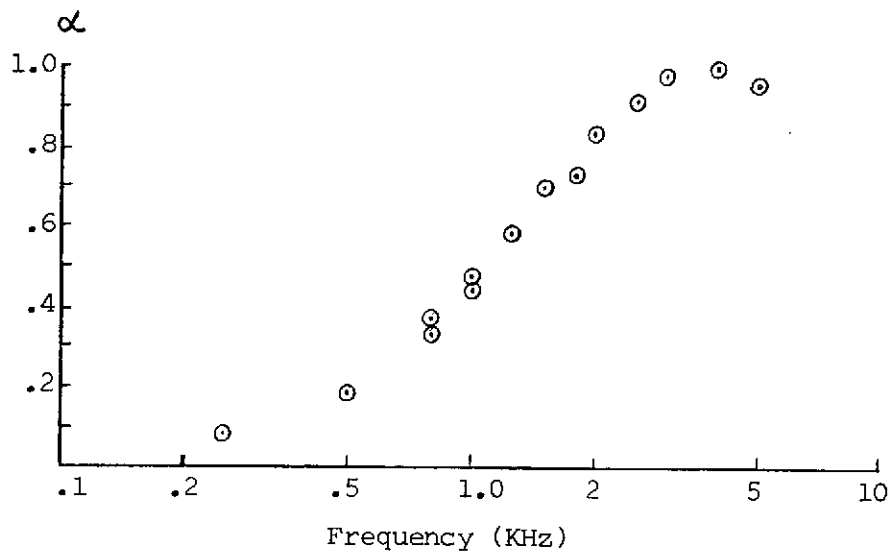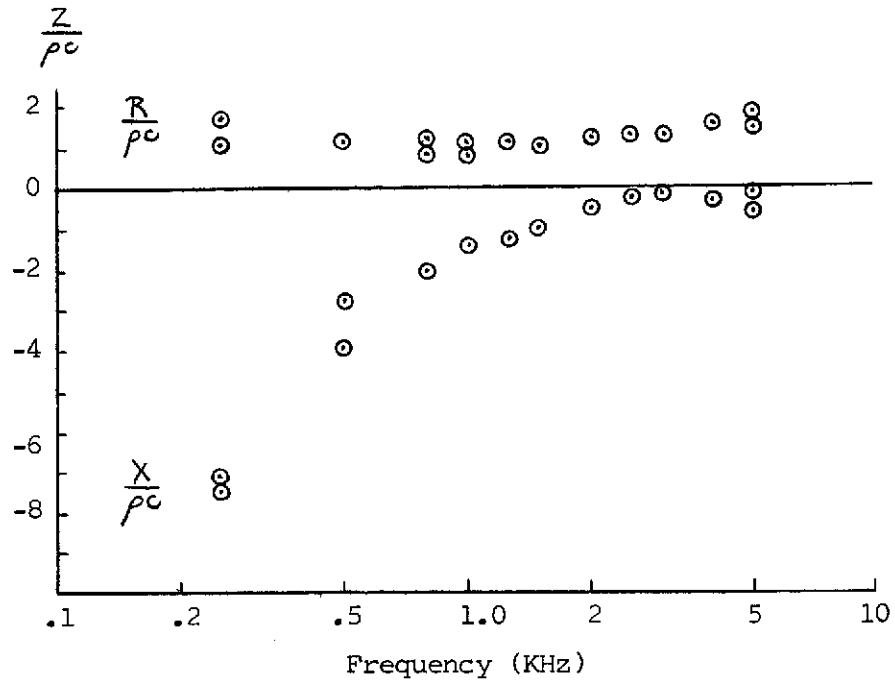Wave Tube for O.C. 704 Fiberglas -1.0"

Figure 21   Specific Normal Impedance Measured by the Standing
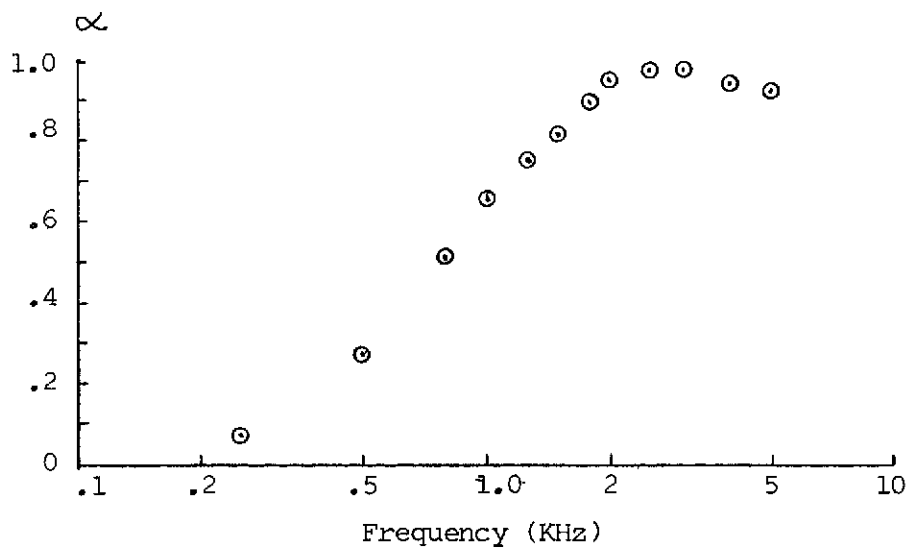Wave Tube for O.C. 705 Fiberglas -1.0"

Figure 22   Absorption Coefficient Measured by the Standing
Wave Tube for O.C. 705 Fiberglas 1.0"

a large negative value at low frequencies which increases as the frequency is increased. Although the reactance is approximately the same for each of the 1" thick samples of Owens Corning 703, 704, and 705 Fiberglas, the resistance for each sample is different. This can be explained by the difference in flow resistance for each material. In Section 5.4, it will be shown that an increase in the flow resistance of a material will raise the value of the real component of the impedance but will not affect the reactance. This result is consistent with the flow resistance measured for each sample and described in Section 5.2.

5.2   Flow Resistance

The specific flow resistance per unit thickness of the material was measured using the apparatus discussed in Section 4.2. Each sample tested was one inch thick and had an area of 8.73 cm^2. The samples were taken from the materials used for the surface pressure method tests and were removed from a position adjacent to the sample used for standing wave tube measurements. In this manner, a smaller variation in acoustic properties between the two samples would be expected. The flow resistance for two samples is shown as a function of the flow rate in Figure 23, and is in general constant for the linear velocity range. The increase in flow resistance for low flow rates is due to the error in measuring pressure drops of only a few thousandths of an inch of water rather than to the properties of the material. The value of flow resistance per unit thickness for each of the fibrous materials was determined by taking the average of several measurements at the maximum flow rate of 1600 cc/min. These values are listed in Table 5, together with the range of values
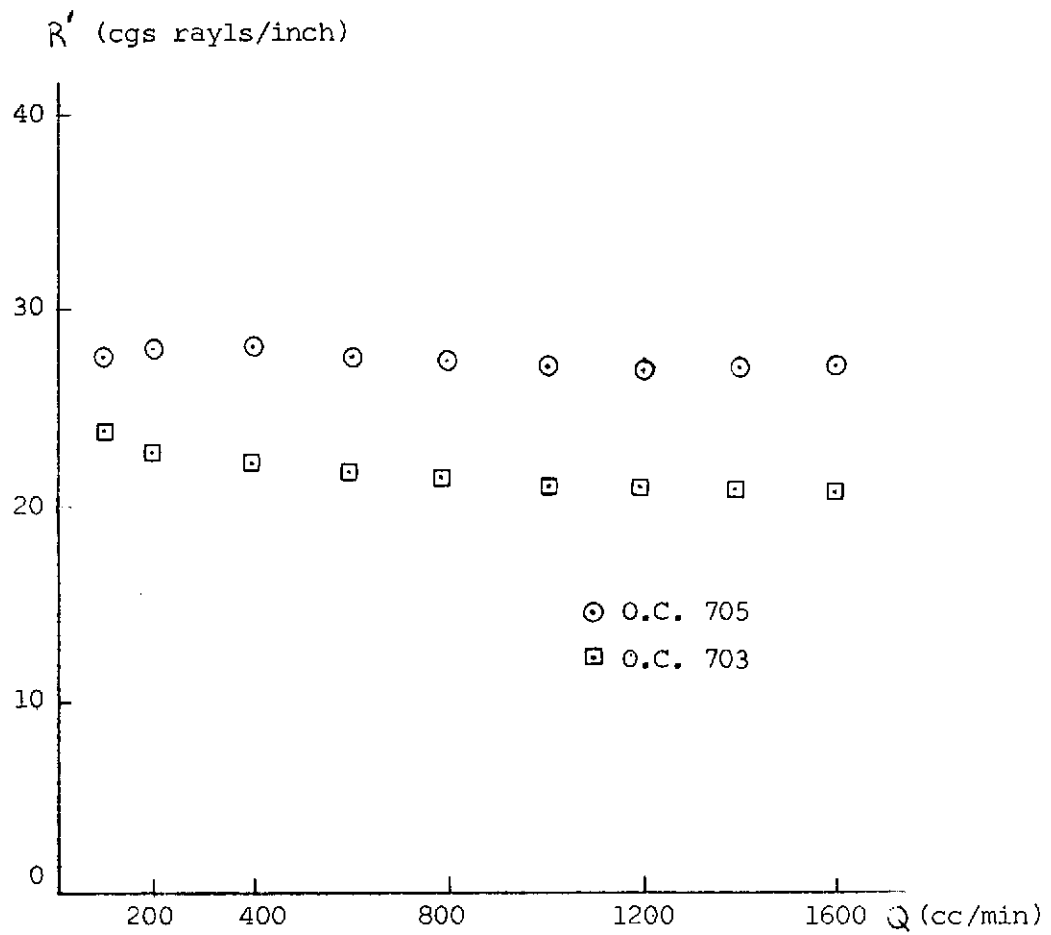
Figure 23 Specific Flow Resistance Vs. Flow Rate
for O.C. 700 Series Fiberglas Samples

specified by Owens Corning for manufacturing tolerances. The measured

values were roughly one third of the flow resistance values for nominal

density and fiber diameter and were below the lower limit of the range

of values for manufacturing specifications. These low values prompted

further testing to determine the validity of these measurements. To

guard against air leaking around the sides of the sample, vaseline

was used as a seal between the material and the sample holder with no

appreciable change in flow resistance measured. These abnormally low

values cannot be explained unless the samples tested all came from

high tolerance production runs. It will be shown later that neither

the measured value or nominal value of flow resistance is high enough

to calculate impedance values from theory that are comparable to

standing wave tube measurements. This indicates that the flow resist-

ance for a fibrous absorbent does not provide a complete means of

specifying its acoustic properties. This limitation will be discussed

in connection with the theoretical results in Section 5.4.

TABLE 5

Flow Resistance Data for Owens Corning 700 Series Fiberglas

Specific Flow Resistance (cgs rayls/inch)

Type	Average Density and Fiber Diameter	Range Within Manufacturing Specifications	Measured
701	26	19-35	--
702	38	27-56	12.83
703	60	42-87	20.77
704	45	35-57	15.55
705	78	60-99	26.30

5.3 Surface Pressure Method

Before considering the impedance and absorption coefficient

measured by the surface pressure method, we will investigate the

pressure and phase measurements. It is obvious that measurements with

this method are limited both in frequency and angle of incidence due

to diffraction effects from the finite size of the sample and the re-

flecting surface. Not having analyzed the problem theoretically,

these limitations will be determined from experimental results.

The surface pressure p_2 measured as a function of incident angle

at the center of a six-foot square sample of one-inch thick Owens

Corning 705 Fiberglass is shown in Figure 24 for several frequencies.

As the incident angle increases from normal incidence, the pressure

decreases slowly until a cut-off angle is reached where the pressure

drops rapidly. Furthermore, as the angle of incidence approaches 90

degrees or grazing incidence, p_2 approaches zero. The pressure p_2

at the surface of an absorbing material with a specific normal imped-

ance ξ is given by Equation 4.32 in terms of the pressure p_1 at the

reflecting surface. Thus,

$$\frac{p_2}{p_1} = \frac{\xi \cos\Theta}{\xi \cos\theta + 1} \tag{4.32}$$

For a finite impedance, p_2 will approach zero as Θ approaches 90

degrees, and for a surface with an infinite impedance, p_2 approaches

p_1. However, since we can never have an infinite impedance, even

for the perfectly reflecting surface, a similar pressure drop will be

observed for the hard wall pressure as Θ approaches 90 degrees. The

angle at which this pressure drop occurs for the hard wall measurement

will limit oblique incidence measurements. The experimentally
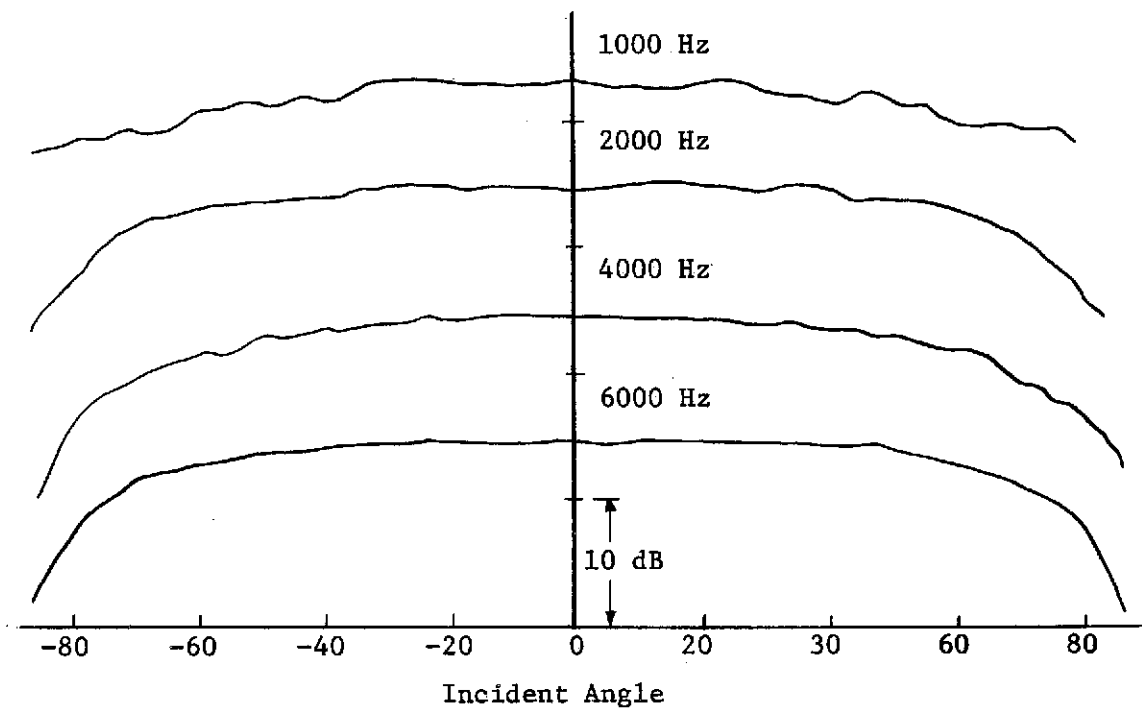
Figure 24   Pressure as a Function of Incident Angle at the Surface of O.C. 705 Fiberglas —1.0"

determined cut off angles for measurements with the six-foot square

reflecting surface are taken at the point where this pressure drop

begins to occur and are listed in Table 6.

TABLE 6

Cut Off Angles For Hard Wall Pressure Measurements

Frequency	Cut Off Angle
1000	68°
2000	75°
3000	78°
4000	80°
5000	82°
6000	82°

The pressure ratio P_1/P_2 in decibels between the surface pressure

for a sample of Owens Corning 705 Fiberglas and the hard wall pressure

is shown in Figure 25. The corresponding phase measurements are

shown in Figure 26. As seen by the curves, the surface pressure

relative to the hard wall pressure approaches zero as Θ approaches

90 degrees.

The hard wall pressure measured as a function of incident angle

at the center of a three-foot square perfectly reflecting panel is

shown in Figure 27 for several different frequencies. As the incident

angle is increased, the pressure alternately passes through a series

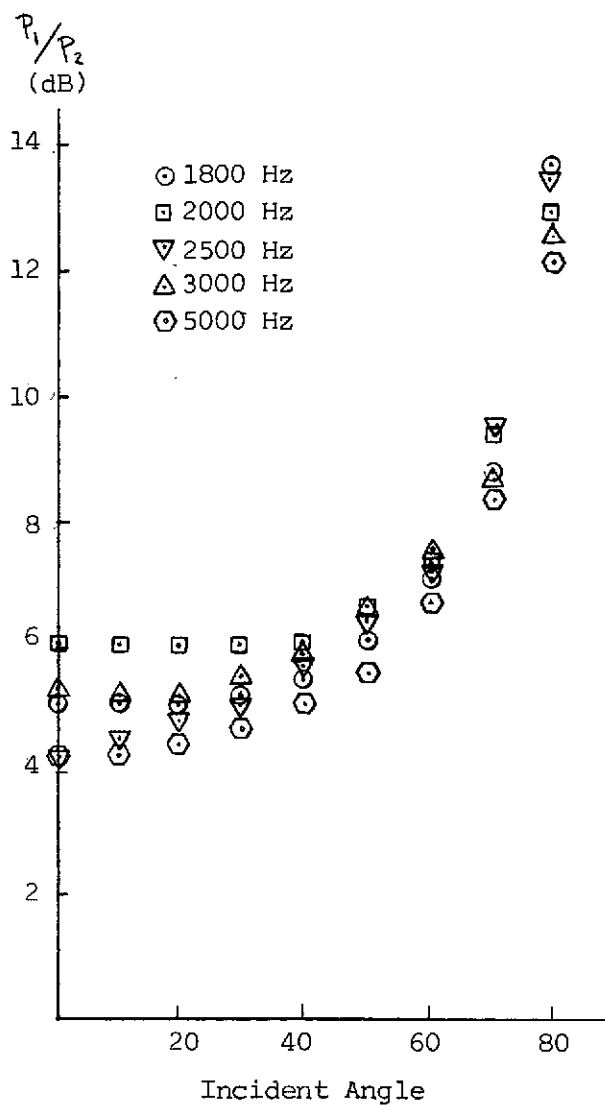of maximum and minimum values. As would be expected, the phase

Figure 25   Measured Surface Pressure P_2 in dB Below Hard
Wall Pressure P_1 for O.C. 705 Fiberglas -1.0
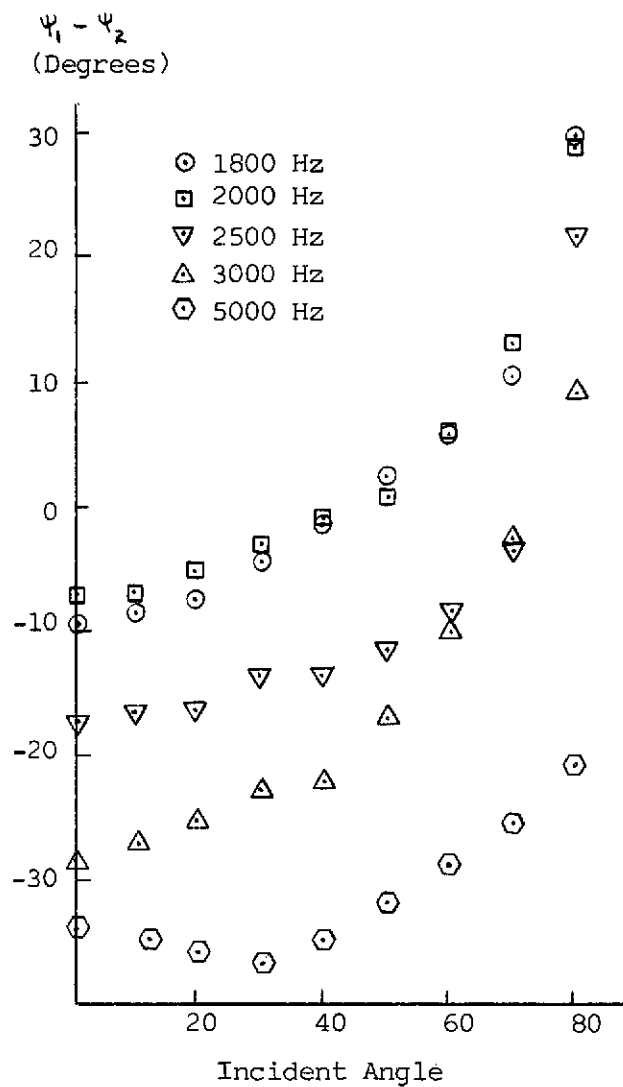
Figure 26   Measured Phase Difference Between the Hard Wall
            Pressure and Surface Pressure for O.C. 705 Fiberglas
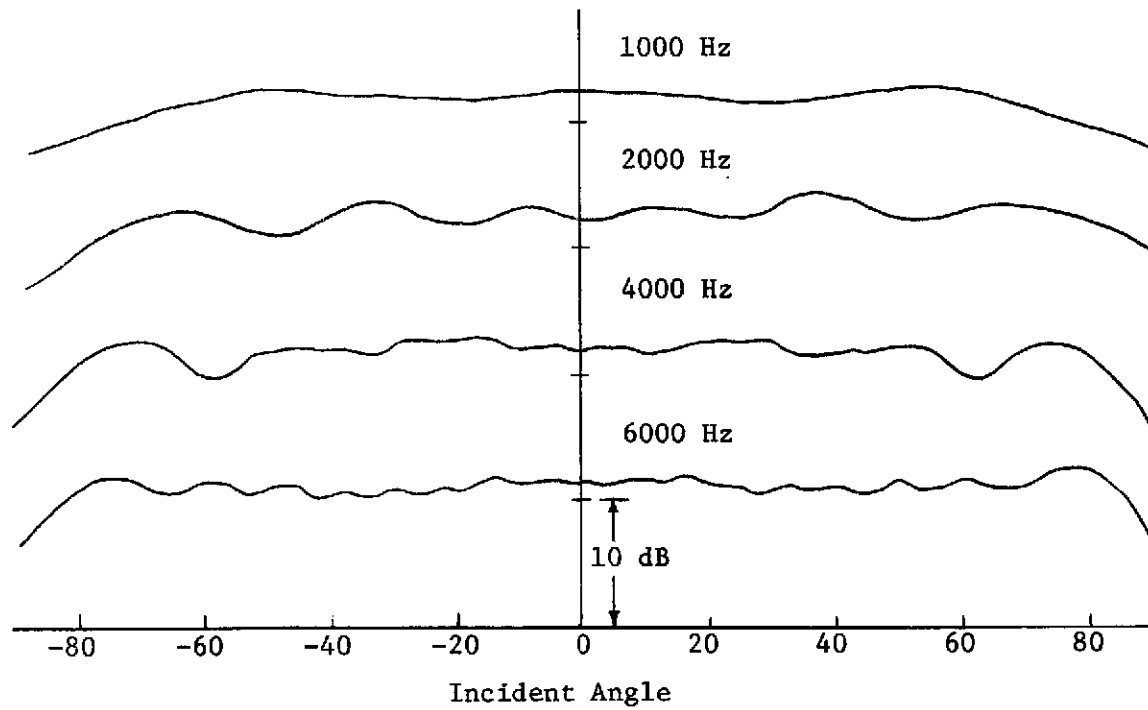   -1.0"

Figure 27   Hard Wall Pressure as a Function of Incident Angle for Three-Foot Square Panel

component exhibits a similar pattern with a peak-to-peak phase varia-
tion of 20 to 30 degrees. The behavior of this pattern indicates
some sort of diffraction effects due to the finite size of the re-
flecting panel. As the frequency is increased, the magnitude of this
pressure fluctuation decreases. Therefore, at high frequencies where
the wavelength is much smaller than the dimensions of the surface,
the reflecting panel better approximates an infinite surface and
diffraction effects are less prominent. Recent work by Hughes (24)
indicates that an incident wave diffracted by the sharp discontinuity
at the edge of a finite size panel produces a significant secondary
source at this edge. The wave from this secondary source travels
along the face of the panel and is measured together with the incident
wave by the microphone at the center. For certain angles of incidence,
these pressures will combine so that the total pressure will have
maximum and minimum values. From Appendix B, these maximums and
minimums will be located at angles Θ such that

1. $\Theta = 90^{\circ}$

2. $\sin \Theta = n \dfrac{\lambda}{a}$ $\qquad n = 0, 1, 2 \ldots$

where

a = the horizontal dimension of the panel

λ = the wavelength

The first condition is satisfied at grazing incidence where the pres-
sure will approach zero as Θ approaches 90 degrees. This result
was previously verified by the hard wall pressure measurements and
by Equation 4.32. The second condition locates the maximum and
minimum pressures as a function of incident angle. For a three-foot
square panel, the angles at which the measured and predicted pressure

variations occur are listed in Tables 7 and 8. Diffraction patterns from perfectly reflecting square baffles in an anechoic tank (24) reveal pressure fluctuations similar to those measured with the reflecting panel in air for equal ratios of the length of a side of the panel to the wavelength. Thus, we would expect similar results for tests at different frequencies and with different board sizes if the ratio between the length of a side of the panel a and the wavelength λ were the same. Therefore, comparing equal values of ka, where k is the wavenumber, similar pressure patterns for measurements with different size reflecting surfaces would be obtained for frequencies related by

$$ ka = k'a' \tag{5.1} $$

$$ f = \frac{a'}{a} f' \tag{5.2} $$

where f and a are the frequency and horizontal dimension of the panel respectively for each measurement. These results are confirmed in Figure 28 for the hard wall pressure measurements at the surface of a two-foot square reflecting panel.

To reduce or eliminate the fluctuations in pressure and phase due to diffraction, several modifications were investigated using the three-foot square panel. Since the secondary pressure waves originate at the edges, it would seem that treating the vertical edges of the panel with sound absorbing material would eliminate the effect of diffraction. When a three-inch thickness of Owens Corning 705 Fiberglas was placed along each vertical edge of the panel, the results of Figure 29 indicate that this treatment has no appreciable

TABLE 7

Pressure Maxima and Minima at 1 KHz, 3-Foot Square Surface

n	$n\frac{\lambda}{a}$	θ_{CALC}	θ_{MEAS}
1	.376	22.1	22
2	.752	48.6	49

TABLE 8

Pressure Maxima and Minima at 2 KHz, 3-Foot Square Surface

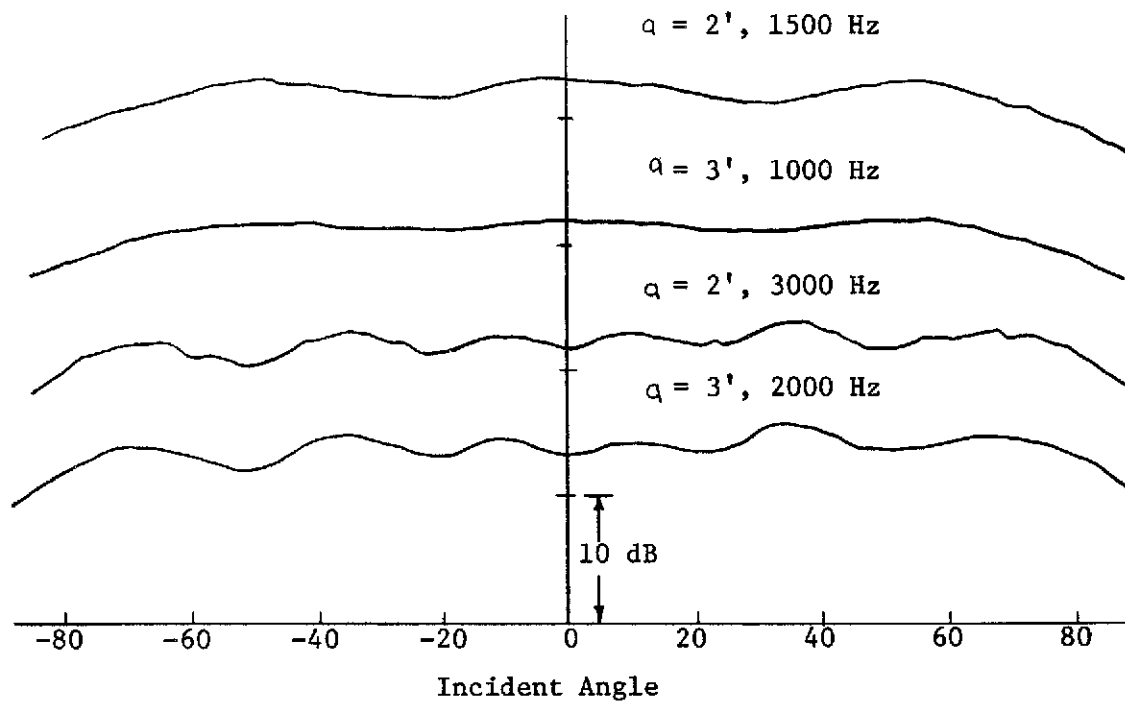| n	$n\frac{\lambda}{a}$	θ_{CALC}	θ_{MEAS}
1	.188	10.8	10
2	.376	22.1	22
3	.564	34.3	35
4	.752	48.6	50
5	.940	70	67

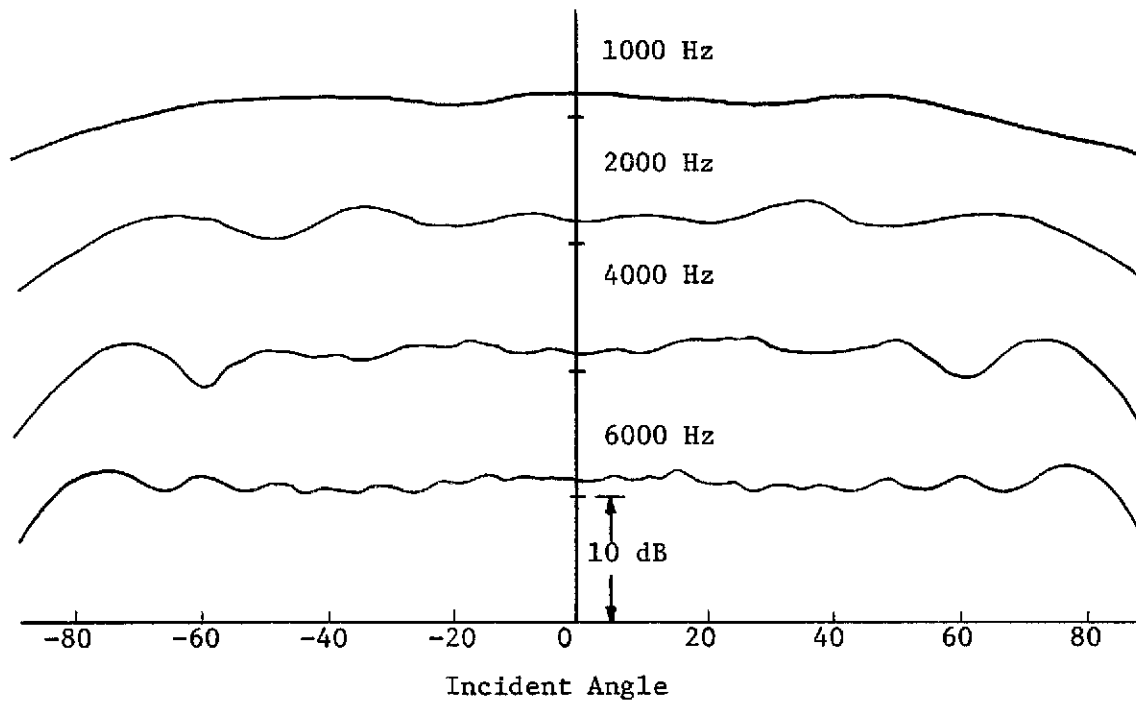Figure 28 Hard Wall Pressure as a Function of Incident Angle for Two Different Panels

Figure 29   Hard Wall Pressure as a Function of Incident Angle with Edges Treated

effect on the hard wall pressure. This is because the discontinuity

at the edge of the rigid panel is still present despite the fact that

the material is highly absorbing. To remove this discontinuity, the

edge must be completely covered by the material. With the edge of the

panel covered, the incident wave is attenuated as it travels through

the material to be diffracted at the edge. Furthermore, the diffracted

wave is also attenuated as it travels outward through the material

and toward the microphone at the center of the panel. The resulting

pressure is shown in Figure 30. Modifications to the edges, such as

rounding the corners, would have no effect on edge diffraction for

the frequencies we are interested in. This would only become effective

when the wavelength is the same size or smaller than the diameter of

the rounded corner. The importance of surface geometry was investi-

gated by measuring the pressure as a function of incident angle at

the center of a perfectly reflecting three-foot diameter circular

board. The results, shown in Figure 31, indicate that the geometry

of the circular panel strongly reinforces the diffraction effects.

In fact, this result would be expected since each secondary source

at the circumference of the panel is the same distance from the

microphone at the center. Since the pressure fluctuations are more

pronounced for this geometry, a square or rectangular panel would be

preferred for the reflecting boundary.

As seen by the curves in Figure 27, the magnitude of the fluctua-

tion in pressure as a function of incident angle decreases as the

frequency is increased. At high frequencies where the dimensions of

the panel are large compared to the wavelength, the effect of

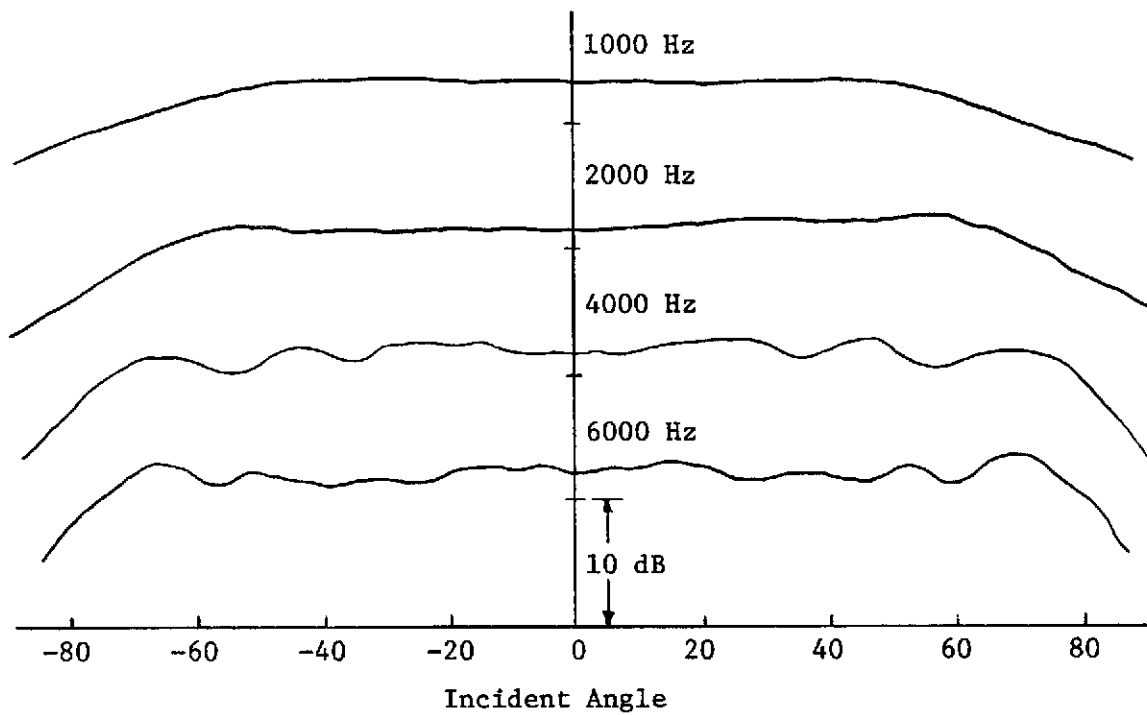diffraction is less pronounced, and the panel is a better approximation

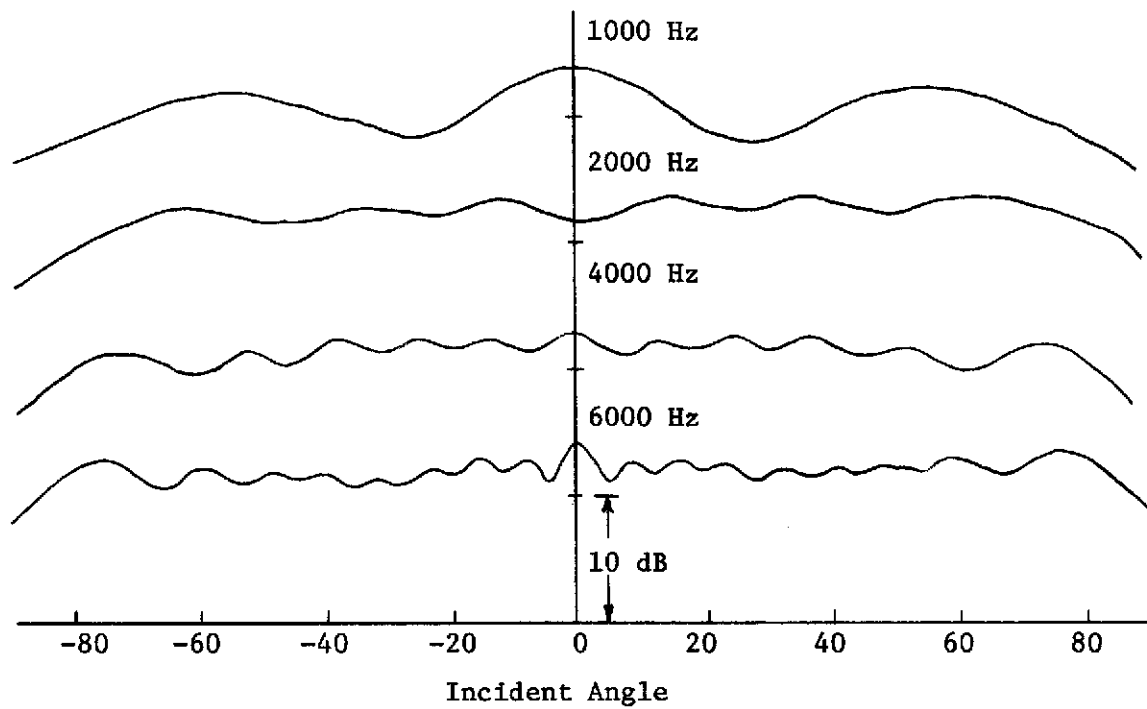Figure 30 Hard Wall Pressure as a Function of Incident Angle with Corners Covered

Figure 31 Hard Wall Pressure as a Function of Incident Angle for a Circular Panel

to an infinite boundary. Therefore, the largest surface possible should be chosen for measurements with the surface pressure method in order that the assumption of an infinite boundary be valid at the lowest frequency of interest. Furthermore, the diffracted wave from the edge will be attenuated by the additional distance it must travel to the microphone at the center of a larger panel. It can be seen then that the use of a larger surface would reduce diffraction effects and also result in a lower limit for measurements. For these reasons, a six-foot square panel was used instead of the three-foot panel for all future measurements with the surface pressure method. The hard wall pressure measured as a function of incident angle is shown in Figure 32 for several frequencies with the larger surface. Despite the fact that the edges have not been treated, the improved performance for the larger surface, especially at high frequencies, can be seen.

The pressure measured at the surface of an absorbing material as a function of incident angle shows little evidence of the diffraction effects that were obtained with hard wall pressure measurements. This is because the material covering the surface of the rigid panel helps to eliminate the discontinuity at the edges and will attenuate a diffracted wave as it travels across its surface to the microphone.

A further limitation and source of error for measurements with the surface pressure method are the temperature variations during testing. Although this variation has a minimal effect on the pressure levels, it has a direct relationship on the measurement of the phase angle. A change in temperature will affect the speed of sound and thus the wavelength. The speed of sound as a function of temperature is
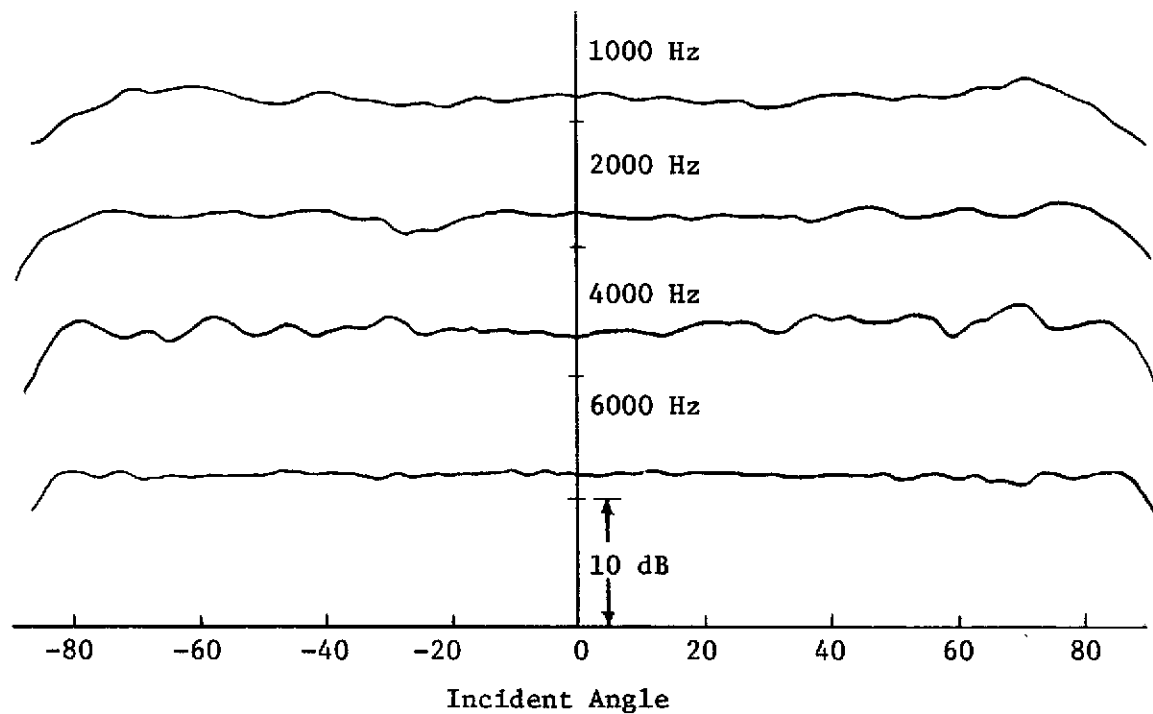
Figure 32   Hard Wall Pressure as a Function of Incident Angle for Six-Food Square Panel

$$c = 49.03 \left(459.6 + °F \right)^{\frac{1}{2}} \tag{5.3}$$

where

c = speed of sound in ft/sec

$°F$ = temperature in degrees Fahrenheit

Since the wavelength λ is related to the speed of sound,

$$\lambda = \frac{c}{f} \tag{5.4}$$

it is also affected by a temperature change and will influence the measurement of the phase angle. If the same phase measurement is made at different temperatures, a phase shift between the two will be noted as shown in Figure 33. Although there is only a very small variation in one wavelength for the temperature change, this variation is accumulated over a distance of several wavelengths. Therefore, over a distance of one wavelength, there is less error in the phase measurement than over a distance of two wavelengths. At high frequencies, where there are several wavelengths between the loudspeaker and microphone, the probability of error in measuring the phase angle becomes very high. The following expression corrects the phase error between similar measurements made at different temperatures T_1 and T_2.

$$\Delta \Psi = x f \left(\frac{1}{c_1} - \frac{1}{c_2} \right) \tag{5.4}$$

where

x = the distance between source and microphone

c_1 = speed of sound at temperature T_1

c_2 = speed of sound at temperature T_2

T_1, c_1, λ_1

$\Delta \psi$

T_2, c_2, λ_2

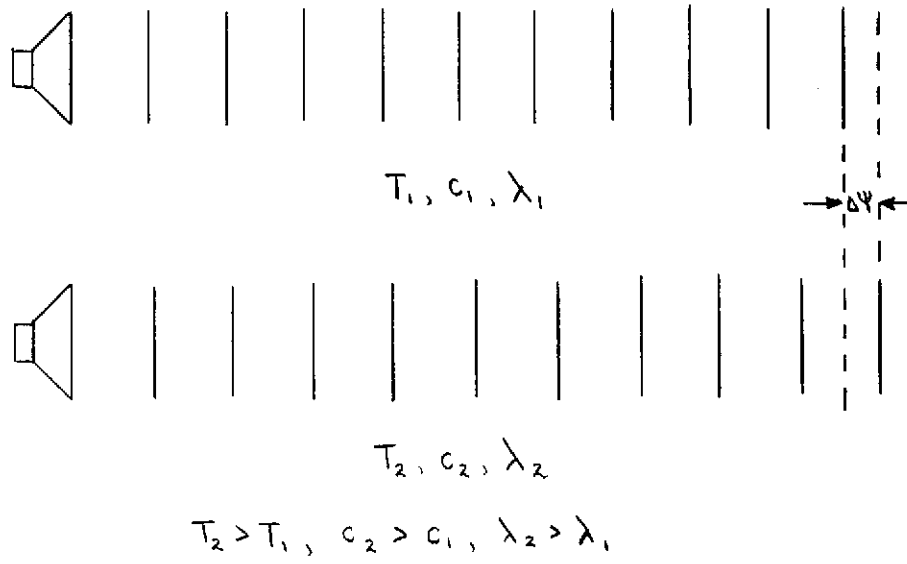$T_2 > T_1, \quad c_2 > c_1, \quad \lambda_2 > \lambda_1$

Figure 33   Phase Variation for Temperature Changes

To control temperature variation in the anechoic chamber, the thermostat of the temperature control system for the room was set at a constant level during all measurements. Although the temperature was constant to within $\pm 0.5^{\circ}$F during each testing period, the actual temperature levels between different tests could vary as much as 0.5°F to 1°F. The phase correction for measurements taken over a distance of 8'4" between the source and microphone and for temperature variations of 0.5° and 1.0°F is listed in Table 9 for several frequencies. In the same manner, a temperature gradient between the source and microphone would further interfere with an accurate measurement of phase angle. Therefore, the phase measurement is especially sensitive to temperature changes.

As mentioned previously, measurements with the surface pressure method can be made using a free field pressure instead of the hard wall pressure as the reference measurement. However, there is some difference between the data obtained using each of these measurements. Since the same surface pressure was used for each measurement, the error must be due to the reference measurements at the perfectly reflecting boundary and for free field conditions. Assuming a pressure doubling effect for the incident pressure at the perfectly reflecting surface, the difference between the hard wall pressure and the free field pressure at the same point in space should be six decibels. For a perfectly reflecting surface with an infinite impedance, the phase component of the hard wall pressure should be the same as the phase components of the free field pressure. Therefore, the difference between the phase components should be zero. The pressure ratio and phase difference between these measurements

TABLE 9

Error in Phase Measurements Due to Temperature Variations

	Wavelength (cm)			Delta Phi (Degrees)	
Freq	$T_1 = 76.0$	$T_2 = 76.5$	$T_3 = 77.0$	T_1, T_2	T_1, T_3
500	69.177	69.210	69.242	0.6	1.2
1000	34.589	34.605	34.621	1.2	2.5
2000	17.294	17.302	17.310	2.5	4.9
3000	11.530	11.535	11.540	3.7	7.4
4000	8.647	8.651	8.655	4.9	9.9
5000	6.918	6.921	6.924	6.2	12.3
6000	5.765	5.768	5.770	7.4	14.8
8000	4.324	4.326	4.328	9.9	19.7

as a function of incident angle are shown in Figures 34 and 35. The
pressure ratios are on the order of six decibels and are relatively
unchanged for angle of incidence. Only at 1000 Hz, where the length
of a side of the six-foot square surface is approximately six times
the wavelength is the pressure ratio much less than six decibels.
This is because the assumption of an infinite surface is not valid at
this frequency. The phase differences, on the other hand, vary
considerably both with frequency and angle of incidence. Therefore,
the phase angle is responsible for the error between measurements
using a reference pressure at the reflecting surface and for free
field conditions. A 3% error in the phase angle will result in a
10 degree phase shift which will clearly alter the absorption proper-
ties of the material. However, the error limits for absorption
measurements cannot be quantitatively stated in terms of the error in
measuring the phase angle. This is because the absorption properties
are also dependent on the difference in pressure levels at the reflect-
ing surface and material surface for each measurement. Nonetheless,
it can be stated that the surface pressure method strongly depends on
an accurate measurement of the phase angle.

It is obvious that by using a finite sample and reflecting sur-
face, the assumption of an infinite boundary is not valid at low
frequencies where the wavelength is on the order of the dimensions of
the sample. Therefore, the low frequency limit for measurements with
this method must be determined. Measurements by Ingard and Bolt using
and eight-foot square panel indicate reasonable data for frequencies
as low as 500 and 700 Hz. Considering Equation 5.2 and comparing our
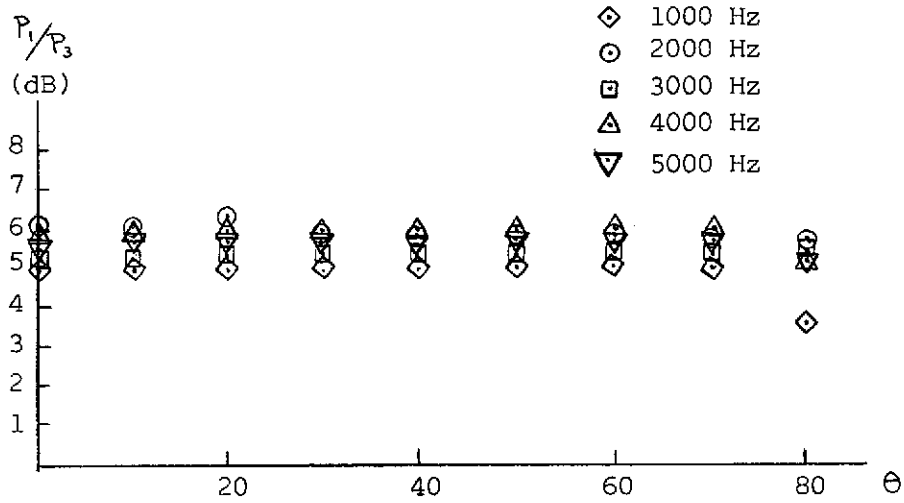results relative to those of Ingard and Bolt, reasonable measurements

83

Figure 34   Pressure Ratio in Decibels as a Function of Incident
            Angle Between the Hard Wall Pressure P_1 and the Free
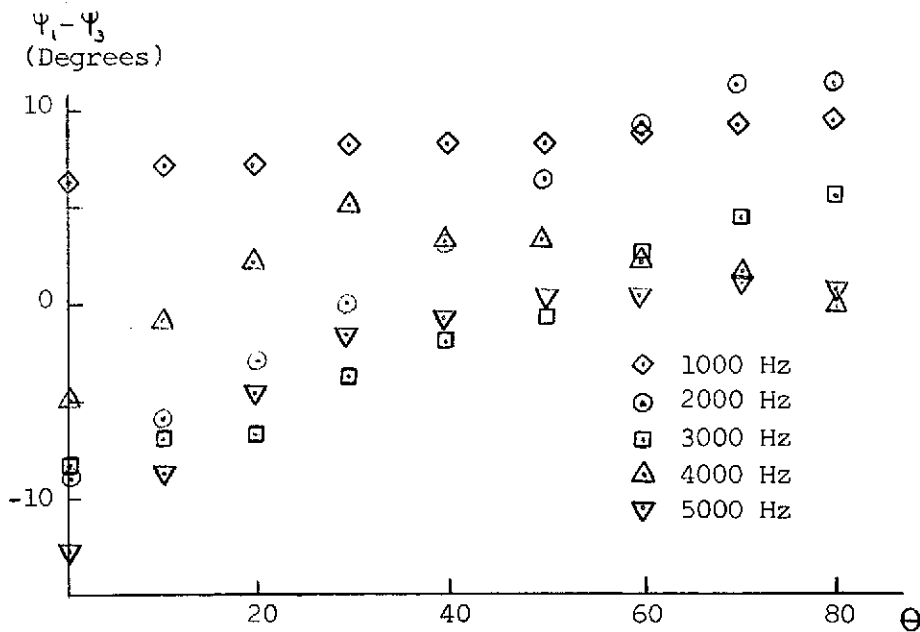   Field Pressure P_3

Figure 35   Phase Difference as a Function of Incident Angle Between
            the Hard Wall Pressure and the Free Field Pressure

with the six-foot panel used in this study should be obtained for
frequencies as low as 700 and 1000 Hz. However, experimental results
indicate that the low frequency limit for measurements occurs for a
much higher frequency. Measurements at normal incidence with the
surface pressure method were compared with measurements using a
standing wave tube to determine the actual limits of this method.
The absorption coefficient and impedance at normal incidence of a
one inch thick sample of Owens Corning 705 Fiberglas measured with
a standing wave tube are shown by the curves in Figures 36 and 37
respectively. The data points in these figures are the values at
normal incidence measured by the surface pressure method for a six-
foot square sample of the same material. The imaginary component of
the impedance does not have a negative value until 3000 Hz for these
measurements. At this frequency the length of the side of the sample
is approximately 15 times the wavelength. It becomes apparent that
for frequencies below this limit, the wavelength becomes comparable
to the dimensions of the sample and the surface does not behave as an
infinite boundary. Therefore, the ratio of the horizontal dimension
of the sample to the wavelength at the lower limiting frequency
should be at least 15 for the assumption of an infinite boundary to
be valid.

Using the surface pressure method and proceeding as outlined in
Chapter 4.3, the specific normal impedance of a one-inch thick sample
of Owens Corning 705 Fiberglas was measured as a function of incident
angle for several frequencies. The results are shown in Figures 36
to 41, where measurements are compared for both the hard wall pressure
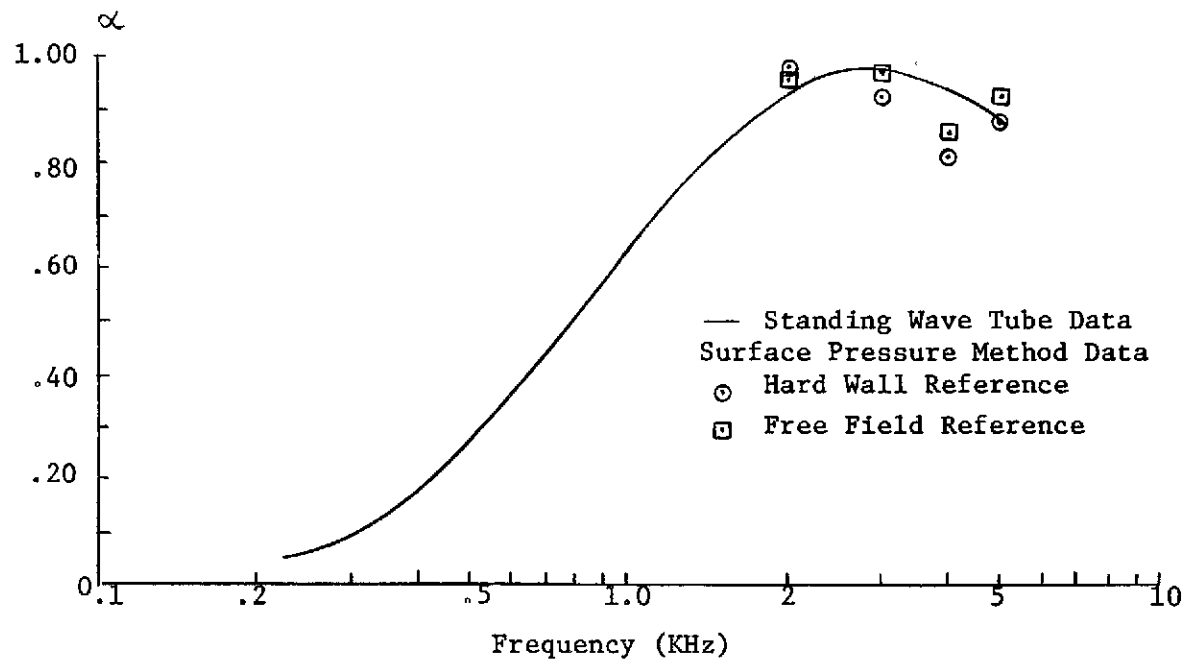and free field pressure used as a reference. The discrepancy between

Figure 36 Absorption Coefficient at Normal Incidence Measured by the Standing Wave Tube
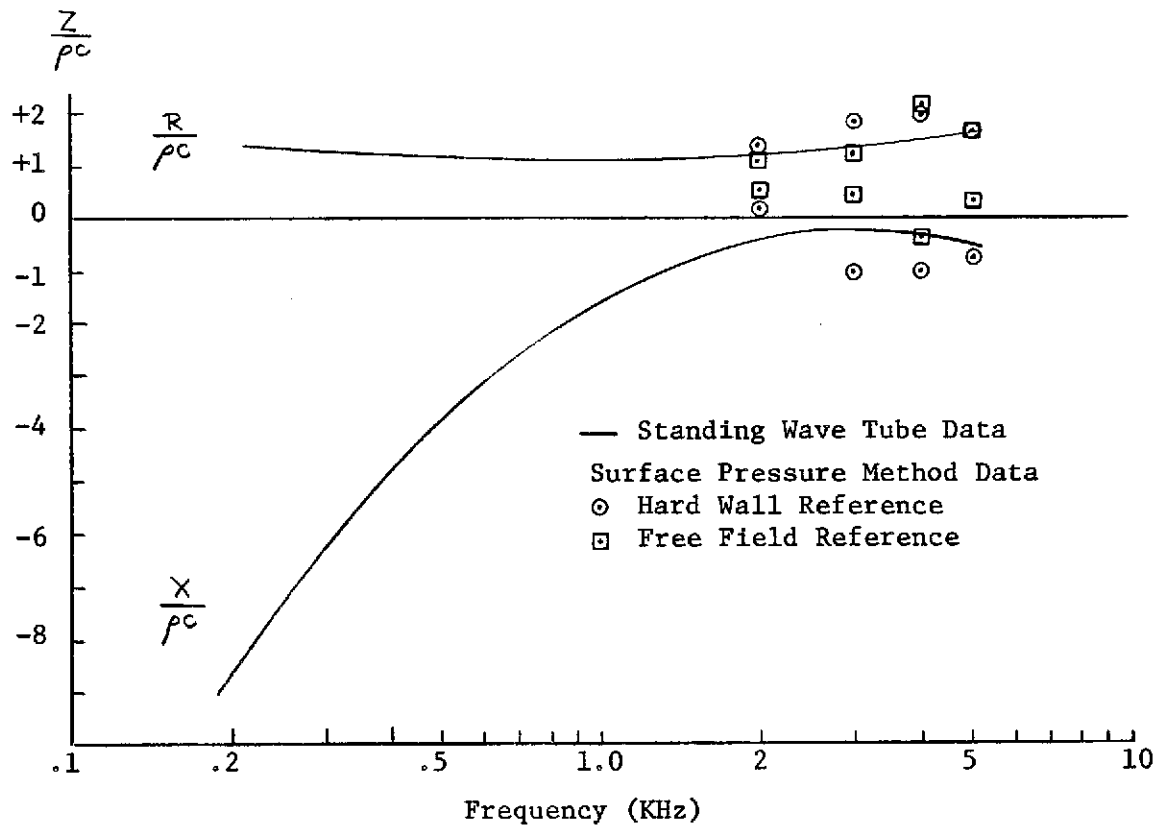and by the Surface Pressure Method for O.C. 705 Fiberglass -1.0"

Figure 37   Specific Normal Impedance Measured by the Standing Wave Tube
and by the Surface Pressure Method for O.C. 705 Fiberglas -1.0"

these measurements is due to the difficulty in measuring the phase angle as stated previously. Both the real and imaginary components of the impedance increase from the values at normal incidence as the incident angle is increased from zero to 90 degrees. Similar results at each frequency indicate that the glass fiber material behaves as an extended reacting material.

The absorption coefficients measured as a function of incident angle for the same sample are shown in Figures 42 to 45. In each of these figures, data is again compared for measurements using both the hard wall pressure and free field pressure as a reference. Despite the difference in impedance values for these two measurements, the variation between absorption coefficient data is small. This is especially obvious at 3000 Hz, where the large discrepancy between impedance measurements in Figure 39 makes itself evident in Figure 43 as only a small difference between the absorption coefficients. As the incident angle increases from zero to 90 degrees, the absorption coefficient increases from its normal incidence value to a maximum value and then decreases as the incident angle approaches grazing incidence. At an oblique angle of approximately 60 degrees, the absorption coefficient has a maximum value and the material is almost totally absorbent. The behavior of the absorption coefficient at grazing incidence is confirmed from our investigation of the pressure at the surface of the material as a function of incident angle. From Equation 4.30, the absorption coefficient as a function of incident angle is

$$\alpha_\theta = 4 \, \frac{P_2}{P_1} \left(\cos \psi - \frac{P_2}{P_1} \right)$$
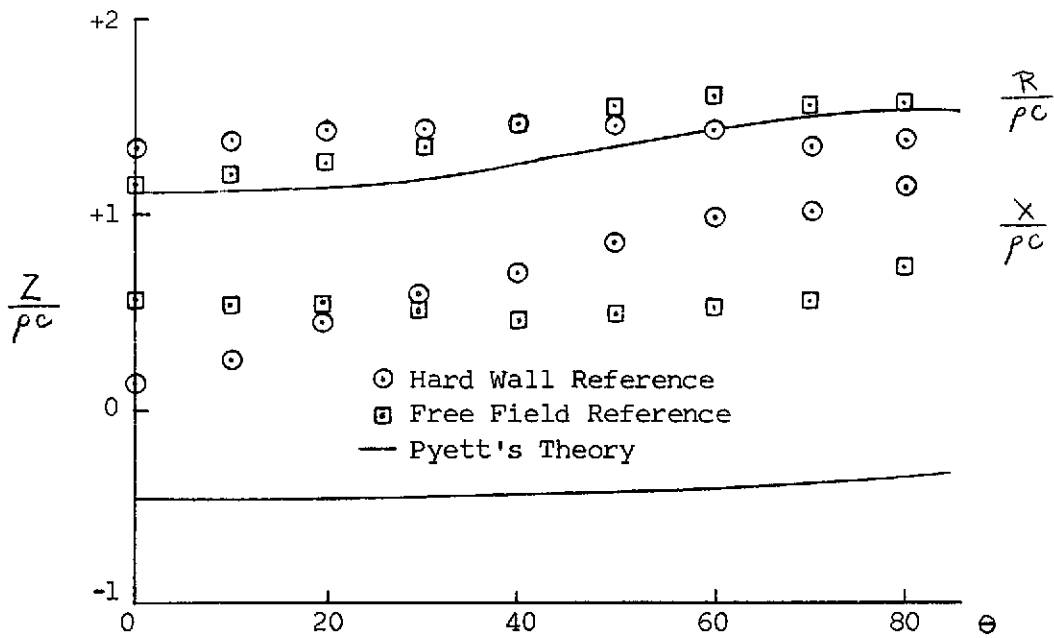
(4.30)

Figure 38   Impedance Vs. Incident Angle for
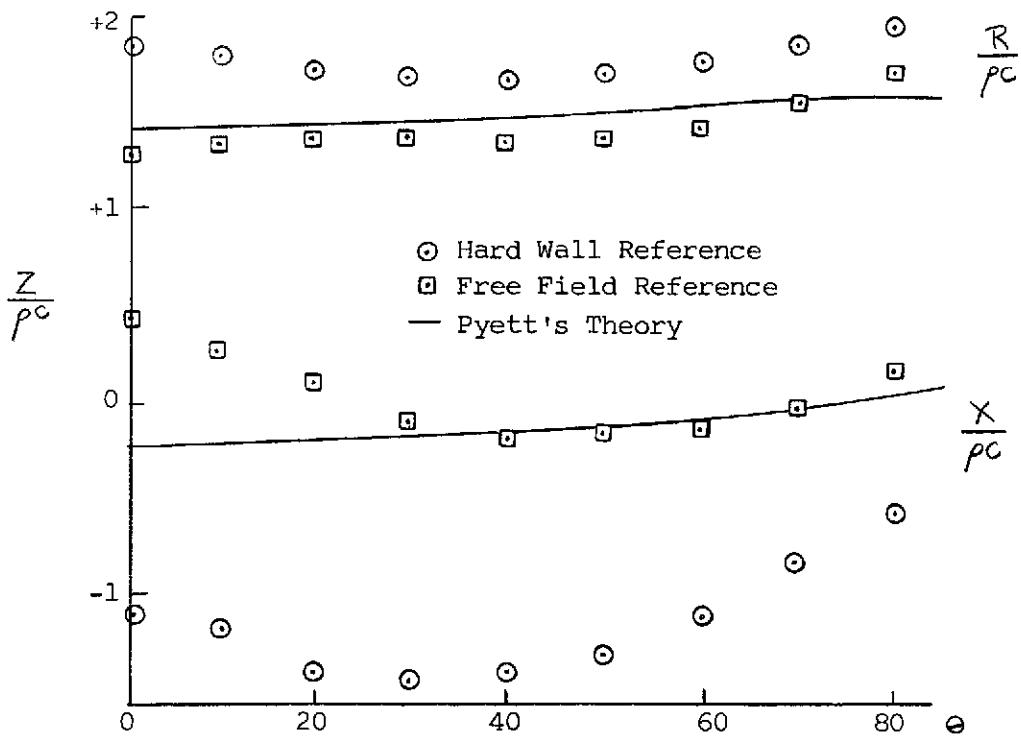O.C. 705 Fiberglas -1.0", 2000 Hz

Figure 39   Impedance Vs. Incident Angle for
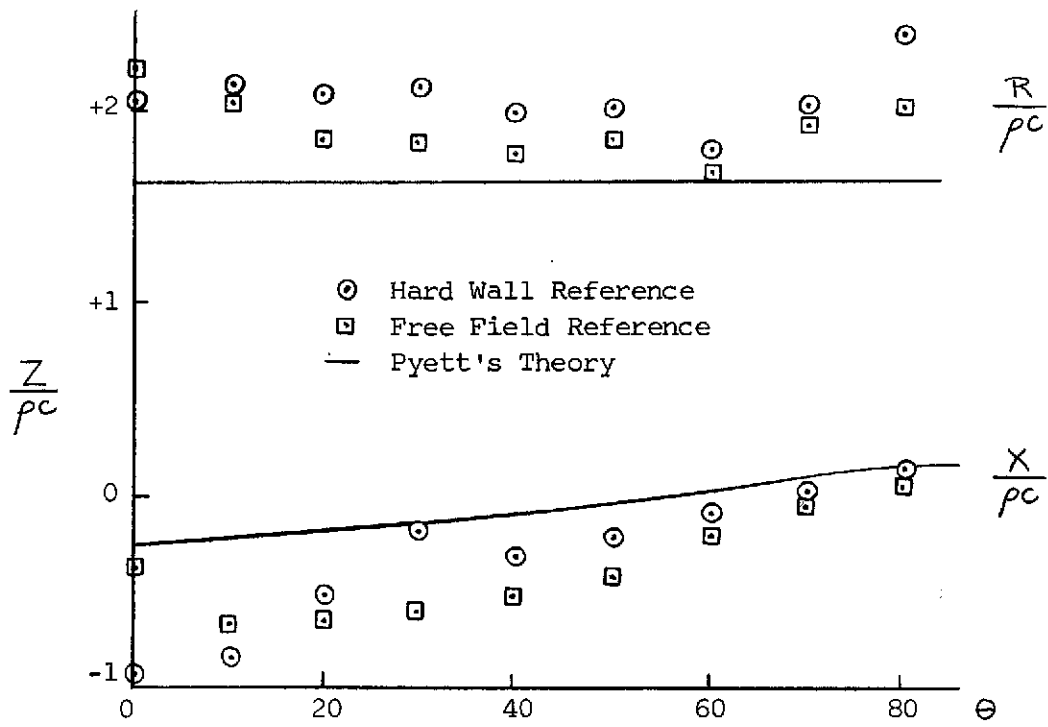O.C. 705 Fiberglas -1.0", 3000 Hz

89

Figure 40   Impedance Vs. Incident Angle for
O.C. 705 Fiberglas -1.0", 4000 Hz

Figure 41   Impedance Vs. Incident Angle for
O.C. 705 Fiberglas -1.0", 5000 Hz

Figure 42   Absorption Coefficient Vs. Incident Angle
for O.C. 705 Fiberglas -1.0", 2000 Hz

Figure 43   Absorption Coefficient Vs. Incident Angle
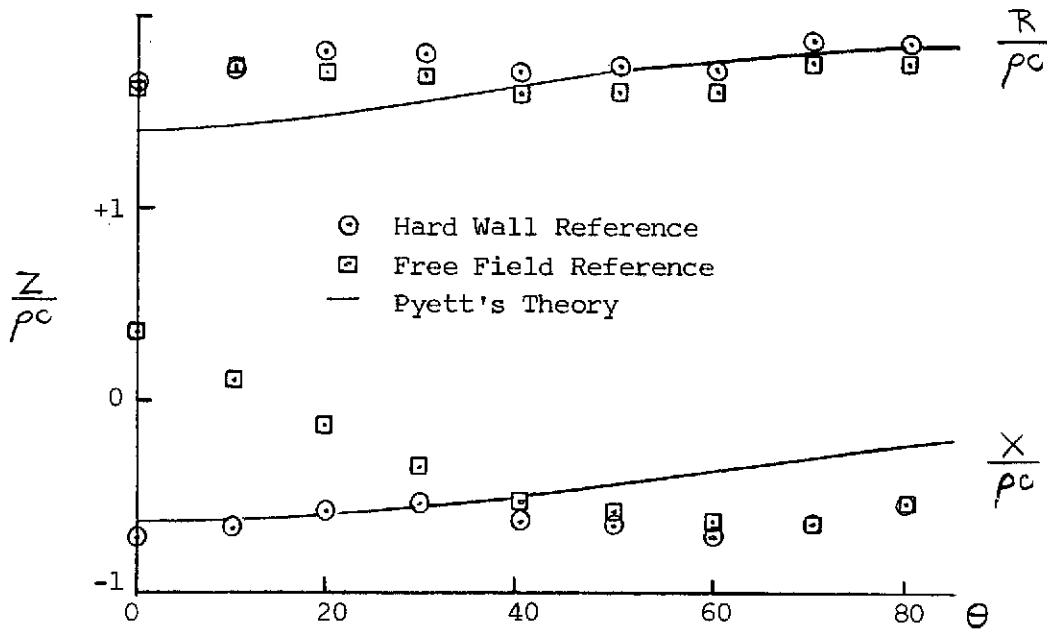for O.C. 705 Fiberglas -1.0", 3000 Hz
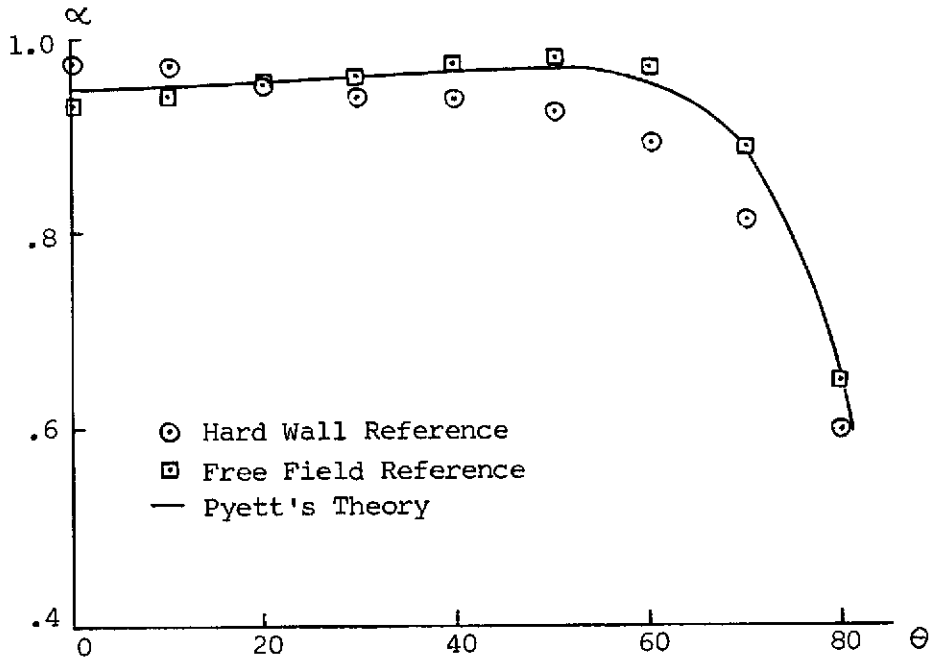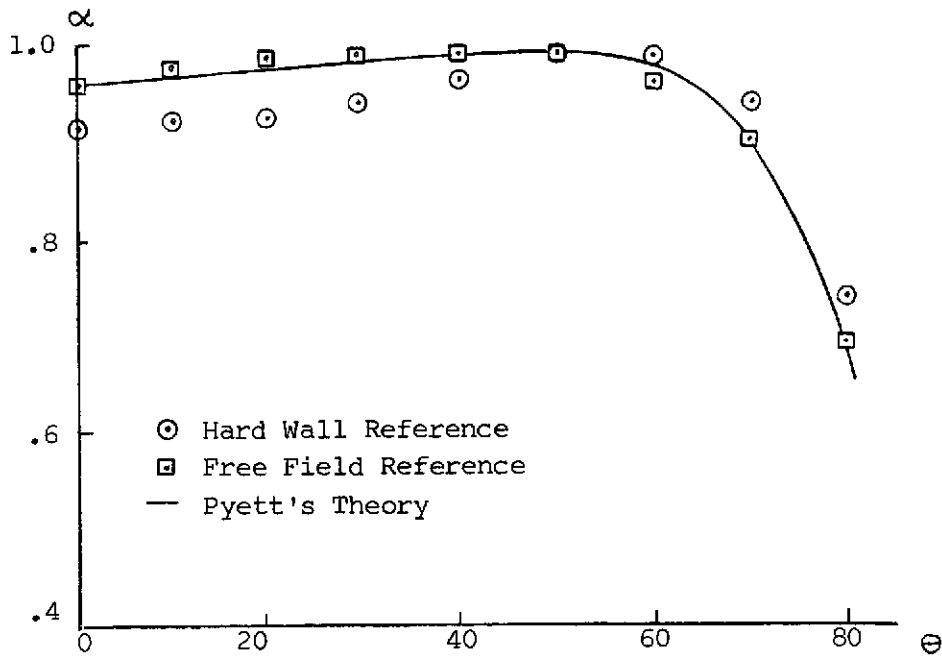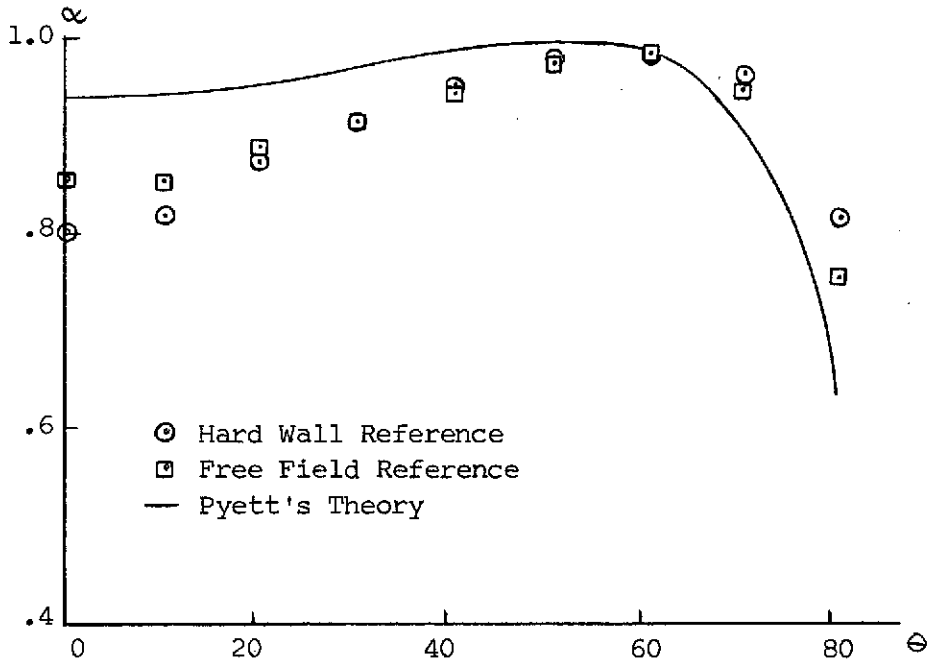
Figure 44   Absorption Coefficient Vs. Incident Angle
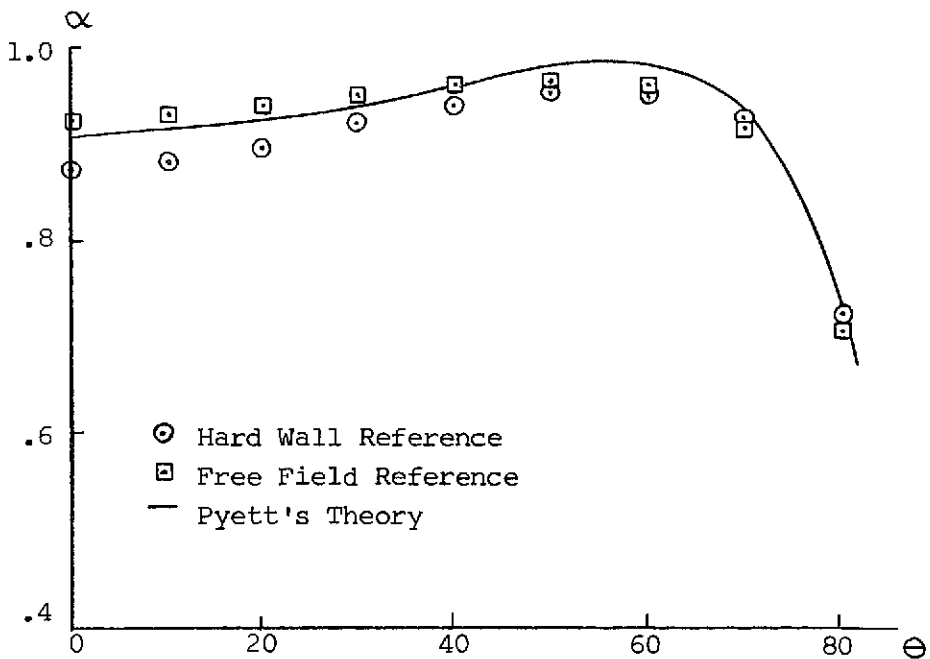for O.C. 705 Fiberglas -1.0", 4000 Hz

Figure 45   Abosrption Coefficient Vs. Incident Angle
for O.C. 705 Fiberglas -1.0", 5000 Hz

Therefore, since P_2 approaches zero as Θ approaches 90 degrees, α_Θ will approach zero at grazing incidence.

Similar results for the absorption coefficient and specific normal impedance as a function of incident angle were obtained for other samples of Owens Corning Fiberglass but were not included since their behavior did not differ markedly from that for the Owens Corning 705 Fiberglas.

5.4 Theoretical Results

The expressions for the specific normal impedance of a porous material as derived by Beranek and Ford are quite similar as seen by Equations 3.50 and 3.84 respectively. Obviously, the main difference arises from Beranek's assumption of isothermal conditions for wave propagation within the material. Another difference between these two expressions is that the porosity Ω does not appear as a part of the argument of the hyperbolic cotangent function in Ford's equation. This is because the continuity equation used by Beranek and Ford respectively differ as shown below.

$$\frac{\partial u}{\partial x} = \Omega K \frac{\partial p}{\partial t} \tag{5.5}$$

$$\frac{\partial v}{\partial x} = K \frac{\partial p}{\partial t} \tag{5.6}$$

As would be expected, the phase velocities for propagation within the material also differ and are given by the following expressions

$$C_2 = \frac{c\left(\frac{1}{1.4}\right)^{\frac{1}{2}}}{\Omega^{\frac{1}{2}}\left(1 - \frac{iR_s}{\rho\omega}\right)^{\frac{1}{2}}} \tag{5.7}$$

$$C_2 = \frac{c\left(\frac{\gamma}{1.4}\right)}{\left(1 - \frac{j R_s}{\rho \omega}\right)^{\frac{1}{2}}} \quad , \gamma = 1.0, 1.2, 1.4 \quad (5.8)$$

However, for the materials we will consider, the porosity has a value

of .96 to .99 so that the difference in propagation velocities should

have a minimal effect on the results. Since the glass fiber materials

of interest in this study resemble the mathematical model for a porous

sound absorbing material as used in both Beranek's and Ford's theories,

one should be able to use these theories to calculate their absorption

properties. The results for each of these theories will be presented

separately and compared with a standing wave tube measurement.

Using Beranek's theory, the sound absorbing properties of a one-

inch thick sample of Owens Corning 705 Fiberglas can be calculated

in terms of its physical properties - namely, the porosity and flow

resistance. These parameters which appear in Equation 3.50 are chosen

to correspond to the properties of the material with both the nominal

flow resistance of 78 cgs rayls/inch and the measured flow resistance

of 26.3 cgs rayls/inch used in the calculations. The agreement be-

tween measurement and theory for the impedance and absorption

coefficient at normal incidence for this sample is shown in Figures

46 and 47. As seen by the curves, the theory underpredicts the real

component of the impedance and also the absorption coefficient. Since

only two physical parameters, the porosity and flow resistance,

determine the acoustic behavior of the material, it would seem that

this discrepancy is due to the value of one or both of these proper-

ties. To determine the effect each of these parameters has on the

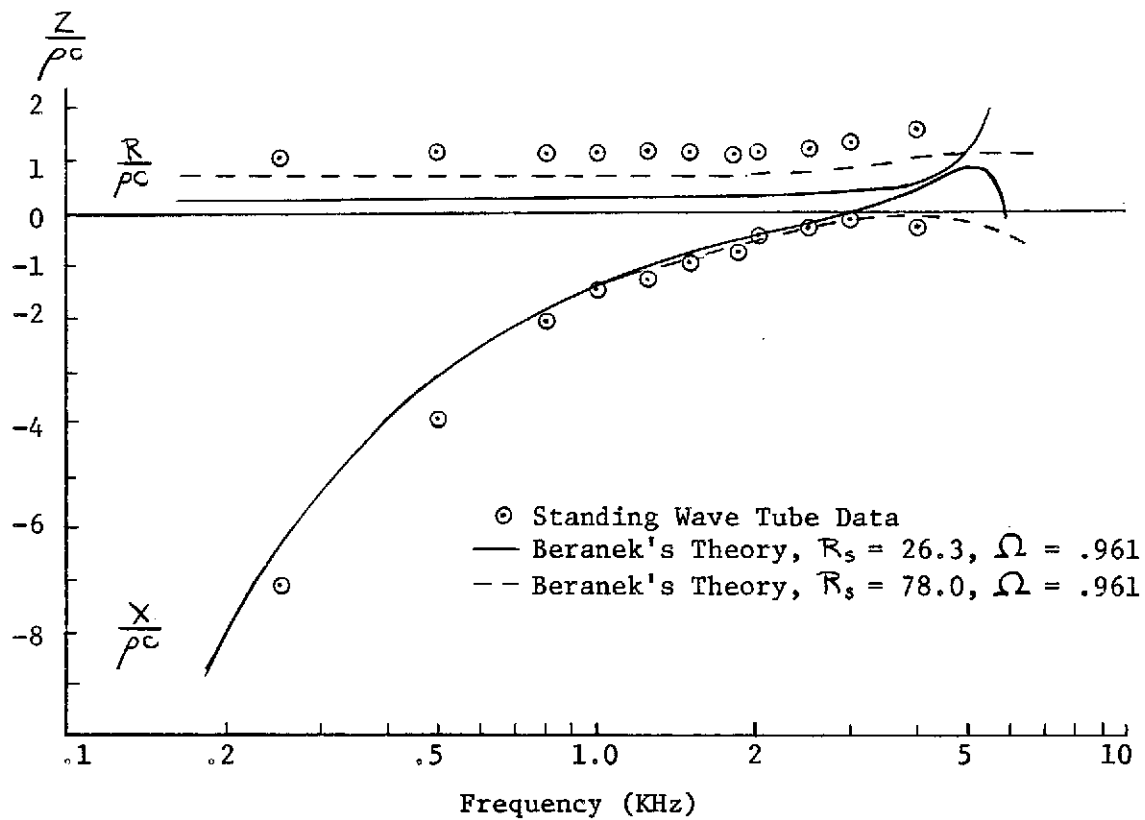impedance, calculations were made for a range of values in both

Figure 46   Impedance Measured with Standing Wave Tube and Calculated from Beranek's Theory for O.C. 705 Fiberglas -1.0"
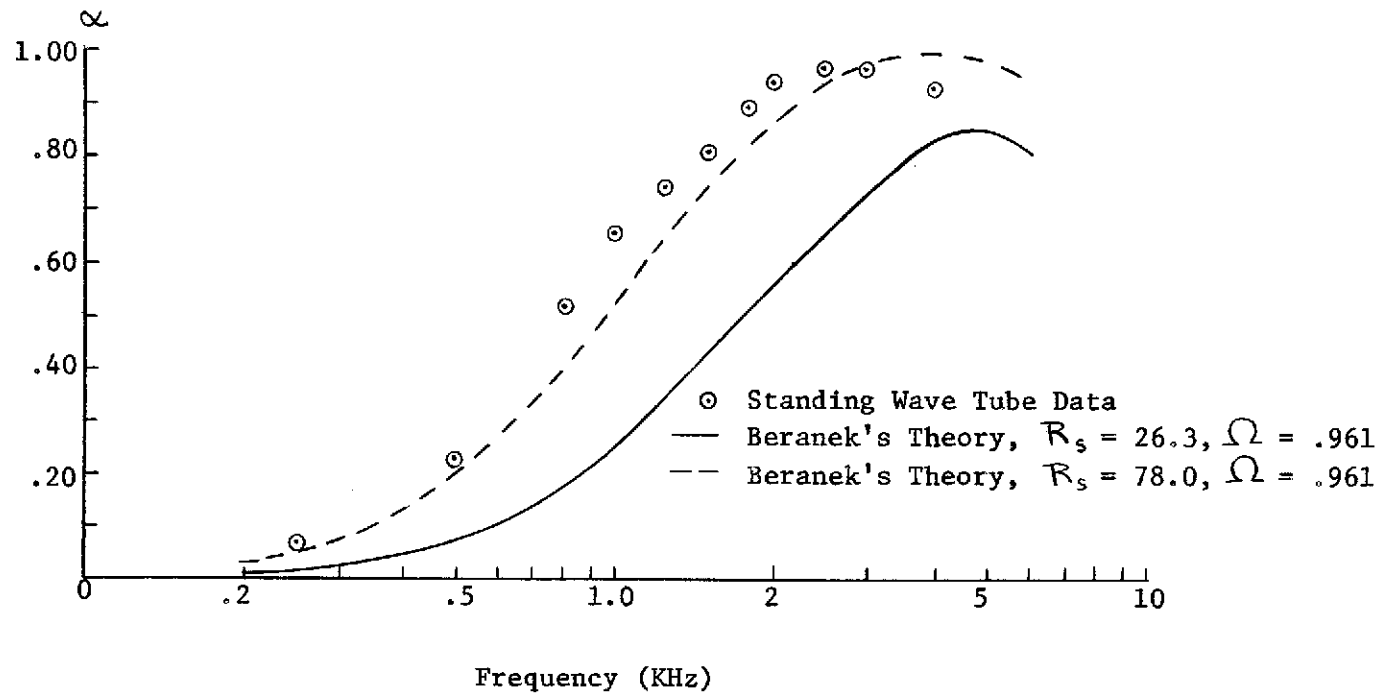
Figure 47 Absorption Coefficient Measured with Standing Wave Tube and Calculated from
Beranek's Theory for O.C. 705 Fiberglas -1.0"

porosity and flow resistance that would be representative of the manufacturing tolerances for these materials. The impedance calculated from Beranek's theory for a material with limiting values of .94 and .99 for porosity and a flow resistance of 26.3 cgs rayls/inch is shown in Figure 48. Similarly, for the same range of porosity, the impedance calculated for a flow resistance of 78 cgs rayls/inch is shown in Figure 49. These results indicate that a variation in porosity from .94 to .99 will have a negligible effect on the normal impedance of this material below 5000 Hz. For a constant porosity of .961, the impedance and absorption coefficient of this material calculated for several flow resistance values are shown in Figures 50 and 51. The variation in flow resistance affects only the real component of the impedance, and leaves the imaginary component relatively unchanged for frequencies below 2000 Hz. Considering the experimental results in Figure 21, a flow resistance of nearly 140 cgs rayls/inch would be necessary to calculate impedance values corresponding to those measured with the standing wave tube apparatus for a one-inch thick sample of Owens Corning 705 Fiberglas. Since the range of flow resistance values for this material due to manufacturing specifications is 60 to 99 cgs rayls/inch, the value of 140 cgs rayls/ inch is completely outside of this range. Therefore, the flow resistance as used in this theory does not account for the total dissipation within the material and other dissipation mechanisms must be present. Beranek has remedied this problem by introducing a "dynamic" flow resistance to compensate for this factor. This parameter is determined from standing wave tube measurements by fitting curves for the impedance calculated at different flow

Figure 48   Specific Normal Impedance Calculated from Beranek's Theory
for $R_s = 26.3$, $\Omega = .94$ and $\Omega = .94$
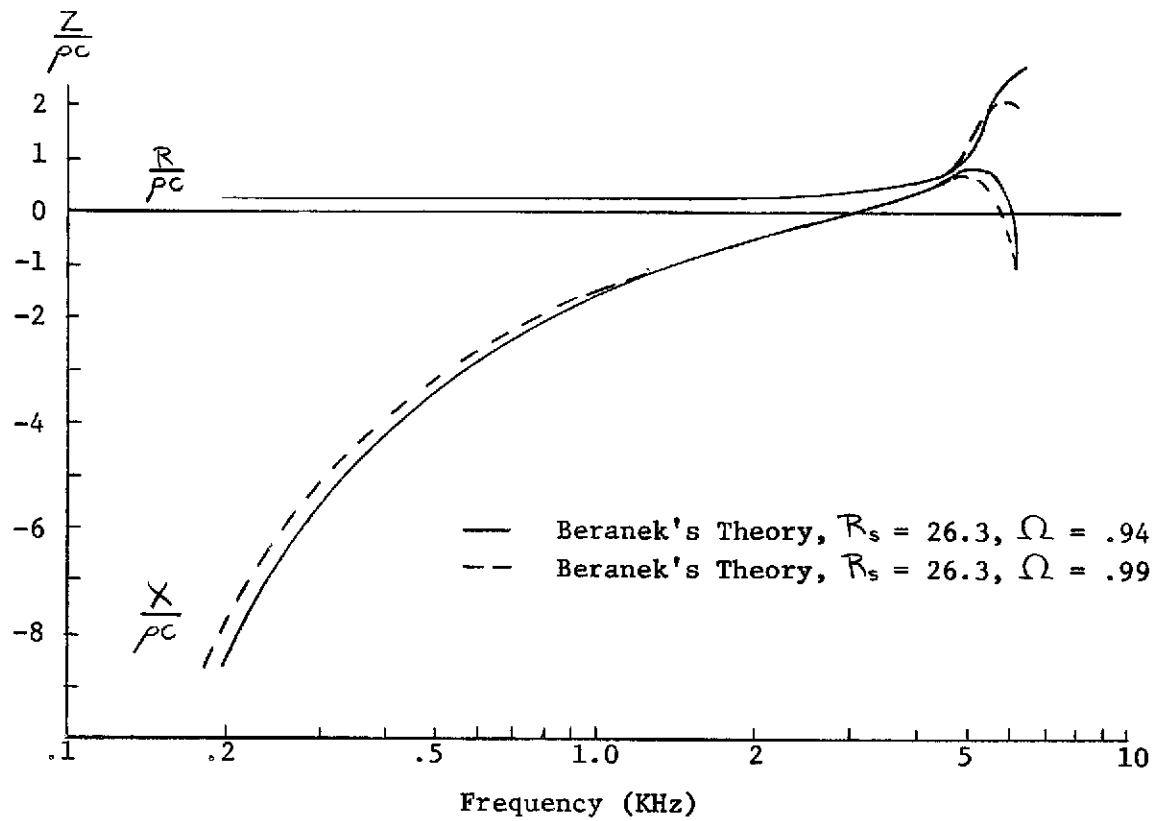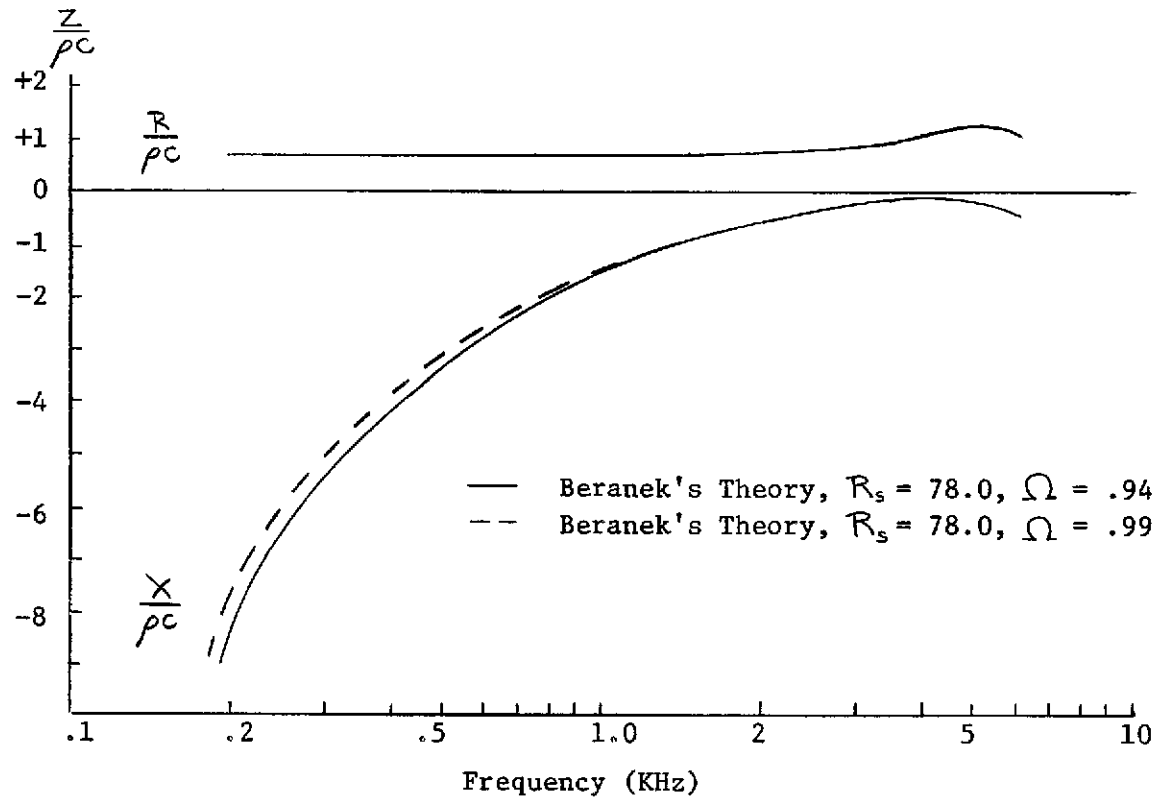
Figure 49   Specific Normal Impedance Calculated from Beranek's Theory
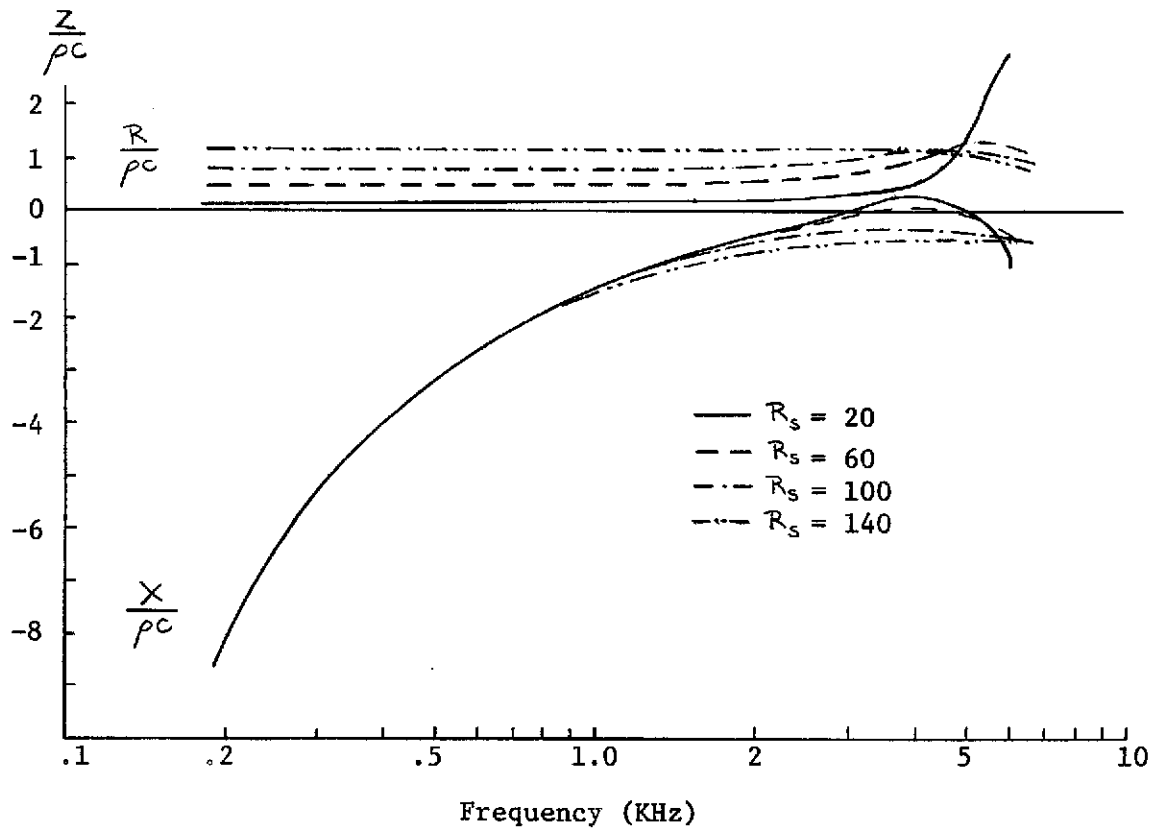for $\mathcal{R}_s = 78.0$, $\Omega = .94$ and $\Omega = .99$

Figure 50   Specific Normal Impedance Calculated from Beranek's Theory
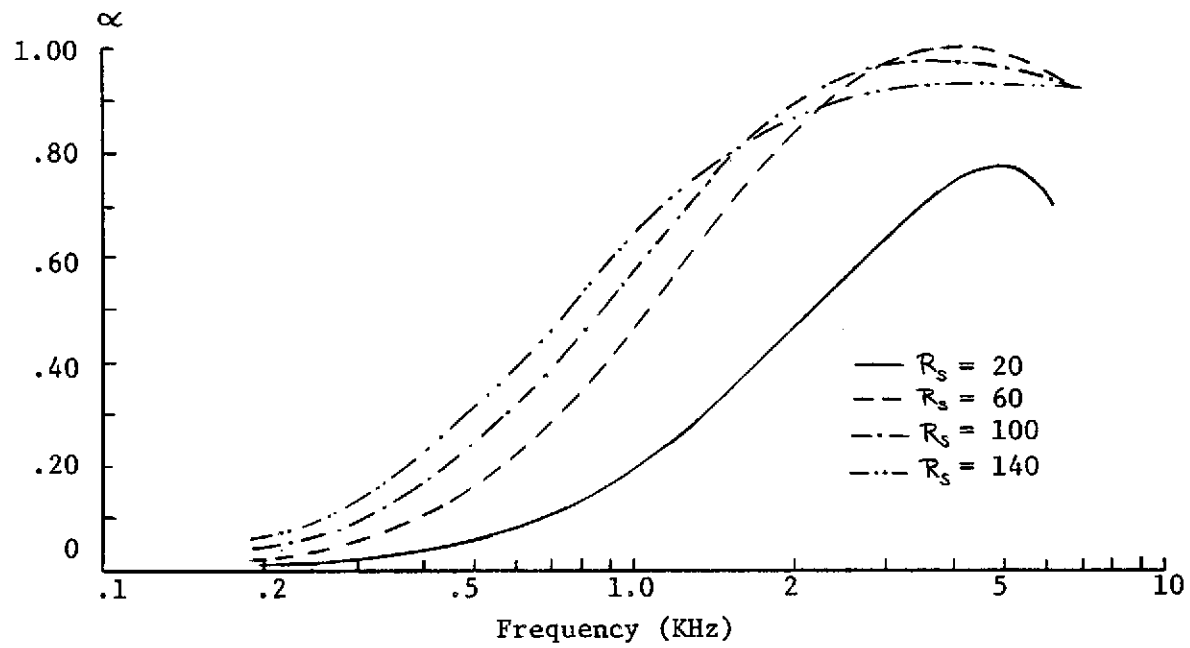for Ω = .961 and $\mathcal{R}_s$= 20, 60, 100, 140

Figure 51   Absorption Coefficient Calculated from Beranek's Theory
for $\Omega = .961$, $\mathcal{R}_s = 20$, 60, 100, 140

resistance values to the experimental results. The dynamic flow re-sistance is different from the measured static flow resistance and is partially explained by Beranek as being due to the nonisotropic nature of the materials. However, this new parameter does not really solve the problem since it bears no direct relationship to the static flow resistance and can only be determined from impedance measurements. In Table 10, the variations between these values as presented by Beranek are listed, with "dynamic" values being both above and below the measured static values for different materials. In short, the use of this new parameter does not seem to logically account for the dissipation within the materials.

Ford's theory for sound absorption by a porous material is also dependent on the flow resistance and porosity of the material, but introduces a new parameter Υ to account for wave propagation within the material under isothermal or adiabatic conditions or any condition between these two extremes. To determine what effect this parameter has on the acoustic properties of the material, the value of Υ will be chosen as 1.0 and 1.4 for isothermal and adiabatic conditions respectively and as 1.2 as an average between these two extremes. The values of porosity and flow resistance corresponding to the properties of a one-inch thick sample of Owens Corning 705 Fiberglas were used to calculate the impedance and absorption coefficient at normal incidence from Ford's theory. Using the measured flow resist-ance of 26.3 cgs rayls/inch, the calculated results for the sample are shown by the curves in Figures 52 and 53. The calculated results for the same sample using the nominal flow resistance of 78 cgs rayls/ inch are shown in Figures 54 and 55. As seen by these curves, the

TABLE 10

Beranek's Flow Resistance Data

Flow Resistance $(R_s/\rho c)$

Static	Dynamic
17.6	10.0
1.7	4.5
5.4	6.0
13.9	10.0
4.5	6.0

Figure 52 Impedance Calculated from Ford's Theory for
O.C. 705 Fiberglas –1.0", R_s = 26.3, Ω = .961

Figure 53   Absorption Coefficient Calculated from Ford's Theory for
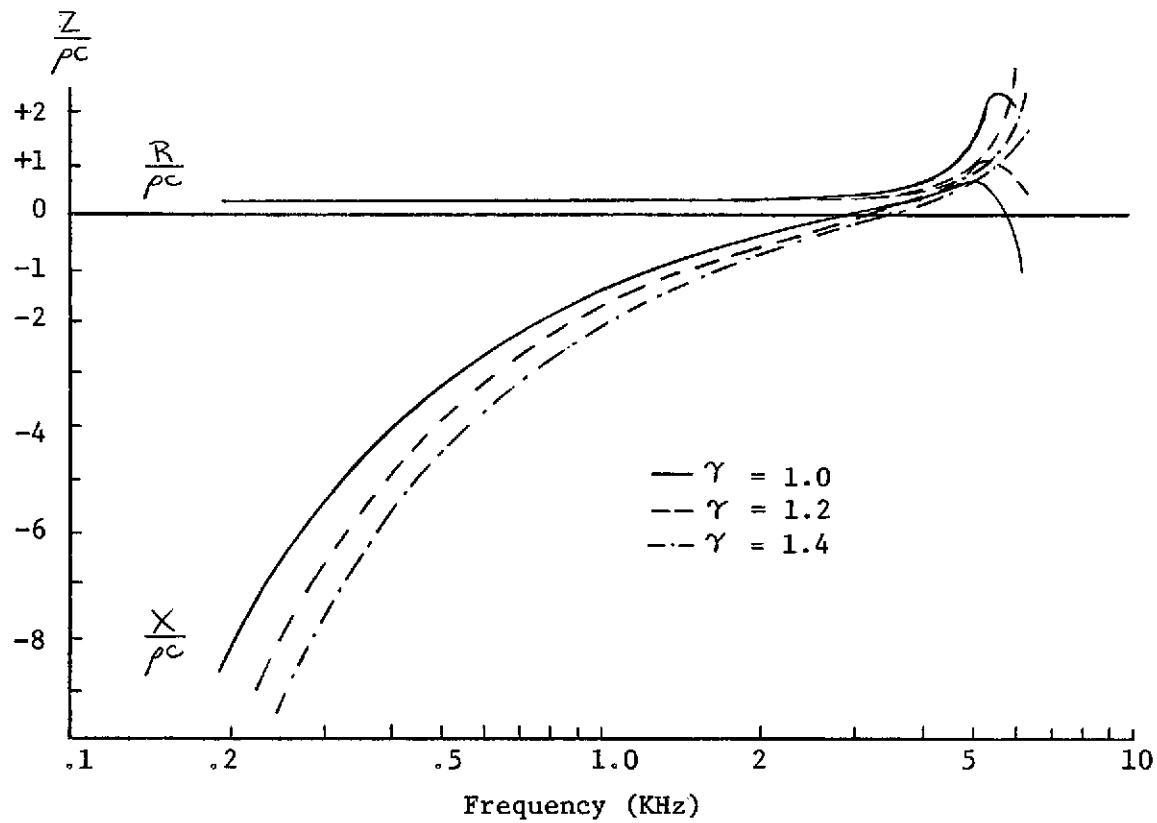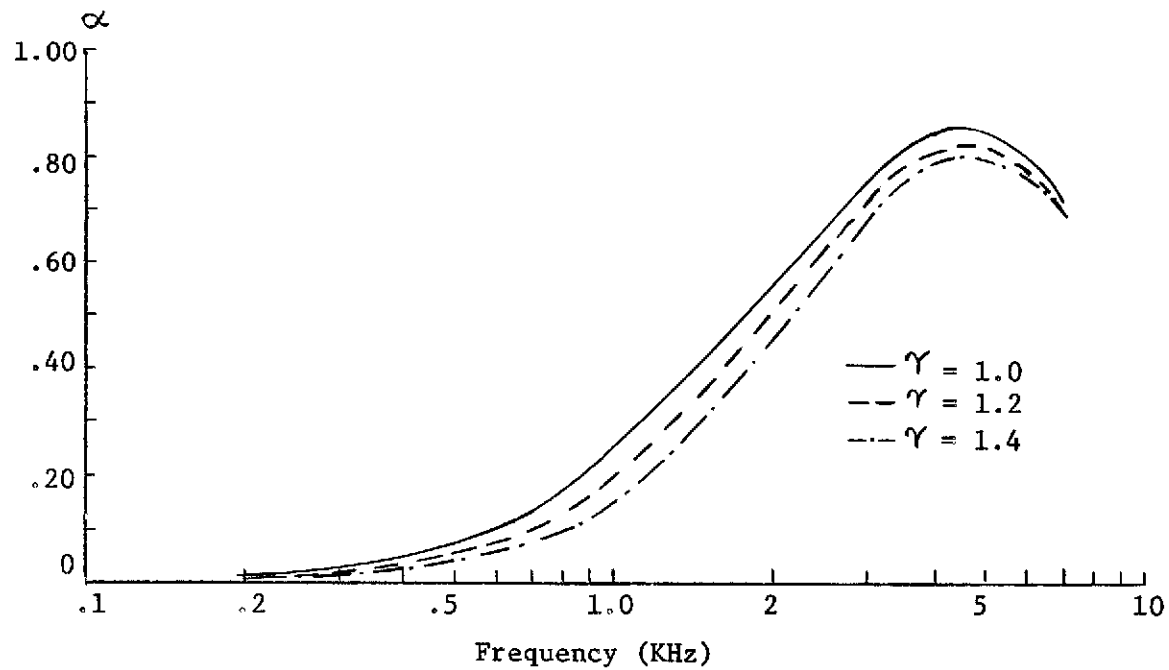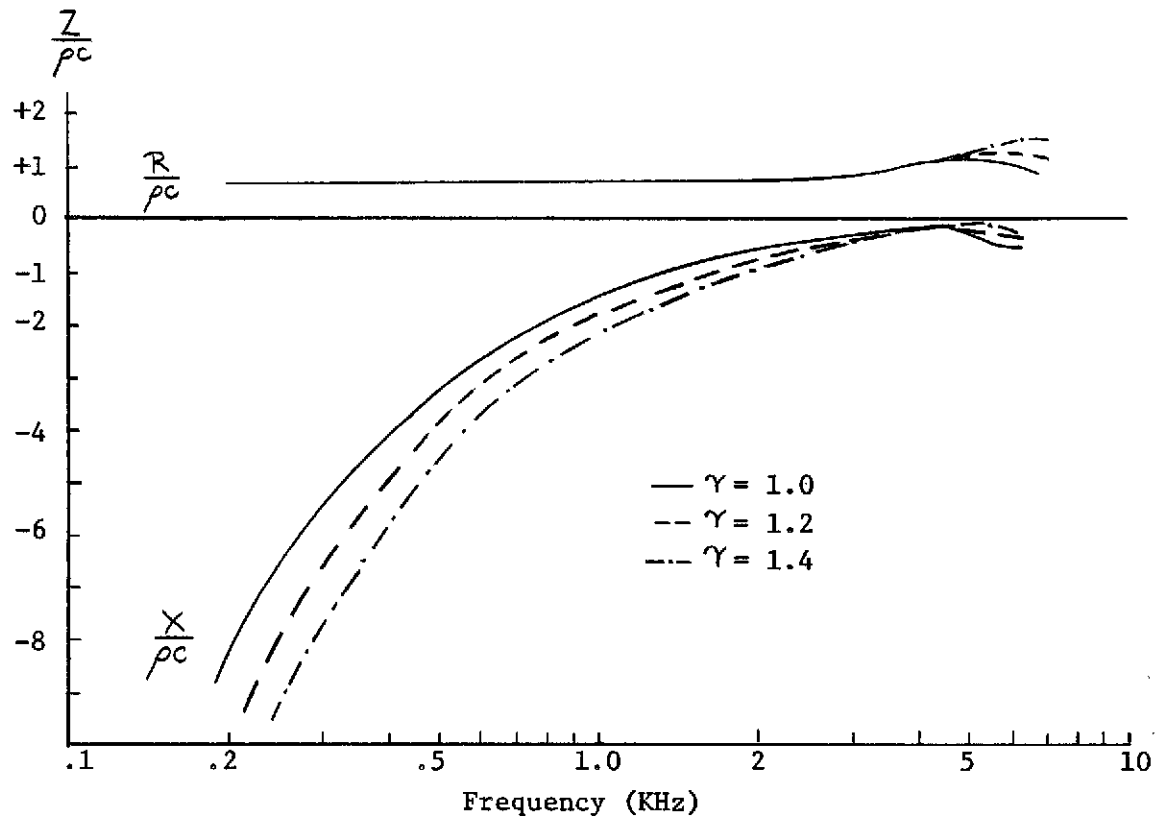O.C. 705 Fiberglas -1.0", $\mathcal{R}_s = 26.3, \Omega = .961$

Figure 54   Impedance Calculated from Ford's Theory for
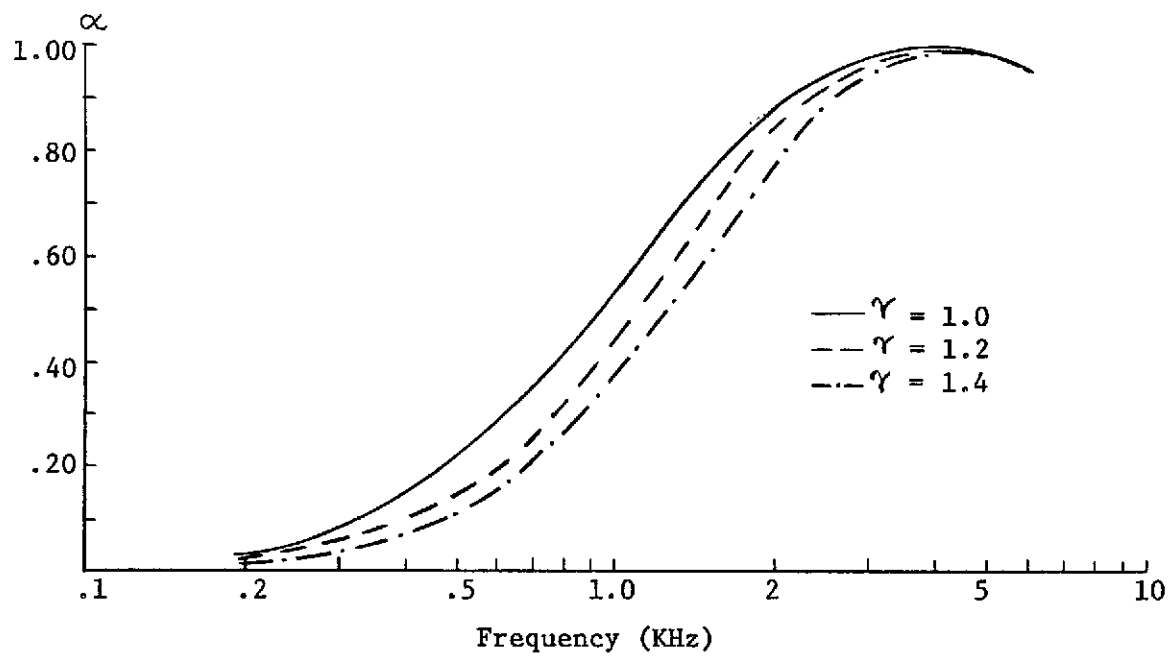O.C. 705 Fiberglas -1.0", R_s = 78.0, Ω = .961

Figure 55   Absorption Coefficient Calculated from Ford's Theory for
O.C. 705 Fiberglas -1.0", R_s = 78.0, Ω = .961

value of Υ affects only the imaginary component of the impedance and
leaves the real component unchanged for frequencies below 4000 Hz.
However, comparing these results with Figures 21 and 22, the values
calculated from Ford's theory also underpredict the real component
of the impedance and also the absorption coefficient. A change in
the flow resistance would affect the absorption characteristics in
the same manner as shown in Figures 50 and 51. This is obvious
since both Equation 3.50 of Beranek's theory and Equation 3.84 of
Ford's theory have the same dependence on the flow resistance. Thus,
a flow resistance of 140 cgs rayls/inch would be required for the
real componenent of the impedance to coincide with standing wave
measurements for this material, and as noted previously, this value
would not be consistent with the manufacturer's quoted properties of
the material. For the value of Υ chosen as 1.0, i.e., isothermal
conditions, the values calculated from Ford's theory are in close
agreement with results from Beranek's theory. This would be expected
since Beranek's theory limits wave propagation within the porous
material to isothermal conditions only.

The investigation of these theories for normal incidence acoustic
absorption has revealed several important results in terms of the
properties of a glass fiber material. These results will be stated
in terms of their effect on the real and imaginary components of
the impedance since the absorption coefficient is dependent on both
of these parameters. The value of flow resistance will affect only
the real component of the impedance, leaving the imaginary component
unchanged. For conditions of wave propagation within the material,
the value of Υ will alter only the imaginary component of the

impedance. Furthermore, the use of a flow resistance also does not account for the total dissipation in glass fiber materials and further dissipation due to viscous or thermal effects may be prominent for these materials. Due to the discrepancy between measurement and theory for normal incidence acoustic absorption, the extension of these theories to oblique incidence behavior was not included. This subject will be covered by Pyett's theory.

The oblique incidence acoustic behavior of a material can be calculated from Pyett's theory in terms of two propagation parameters. These parameters are determined from normal impedance measurements with a standing wave tube for samples of different thicknesses. Figures 56 and 58 show the attenuation constant and phase constant for samples of Owens Corning 703, 704, and 705 Fiberglas, as compared to the phase constant k for wave propagation in air. The impedance and absorption coefficient calculated at oblique incidence for a one-inch thick sample of Owens Corning 705 Fiberglas are shown in Figures 38 to 45 together with experimental results. The calculated impedance increases from its value at normal incidence as the incident angle increases from zero to 90 degrees. Hence, the glass fiber material behaves as an extended reacting material. The absorption coefficient has a maximum value at an oblique angle of incidence of approximately 60 degrees. This agrees favorably with experimental results for this material. Although the agreement between measurement and theory is fairly good, there are two disadvantages with this approach. First, several normal impedance measurements must be made in order to determine the bulk acoustic parameters for the material; and second, due to the non-homogeneous nature of the material, it is possible
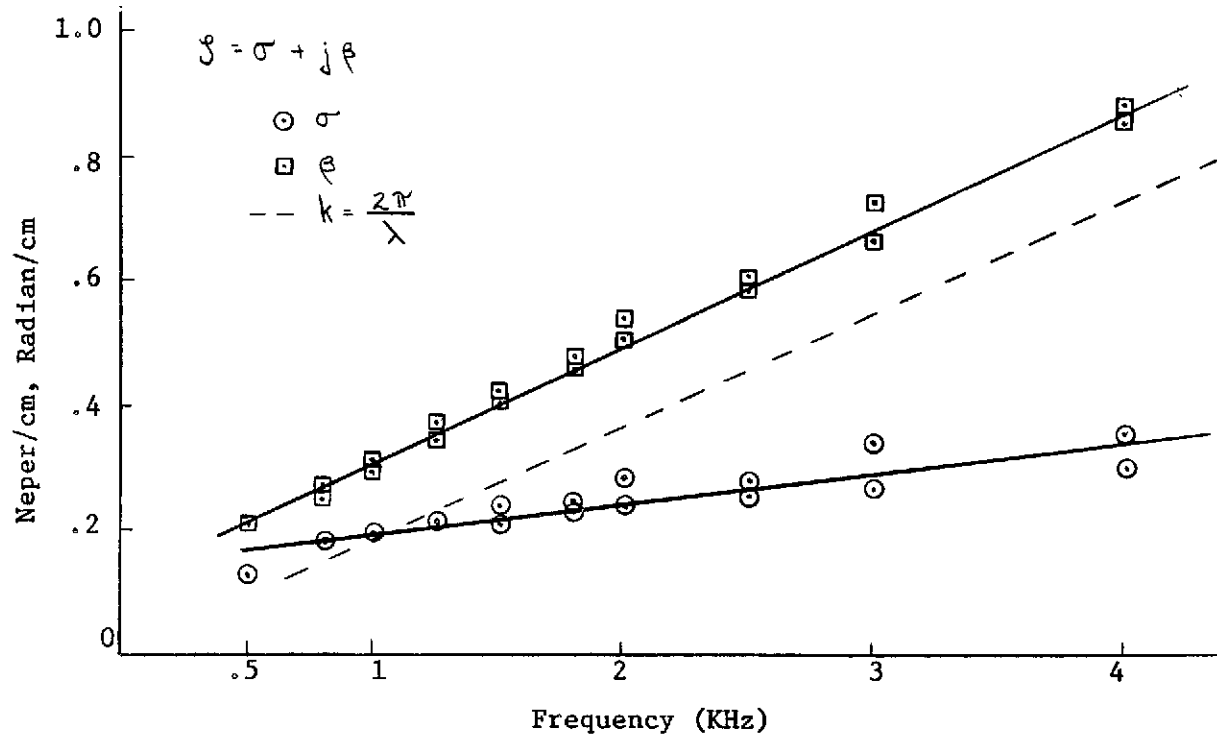
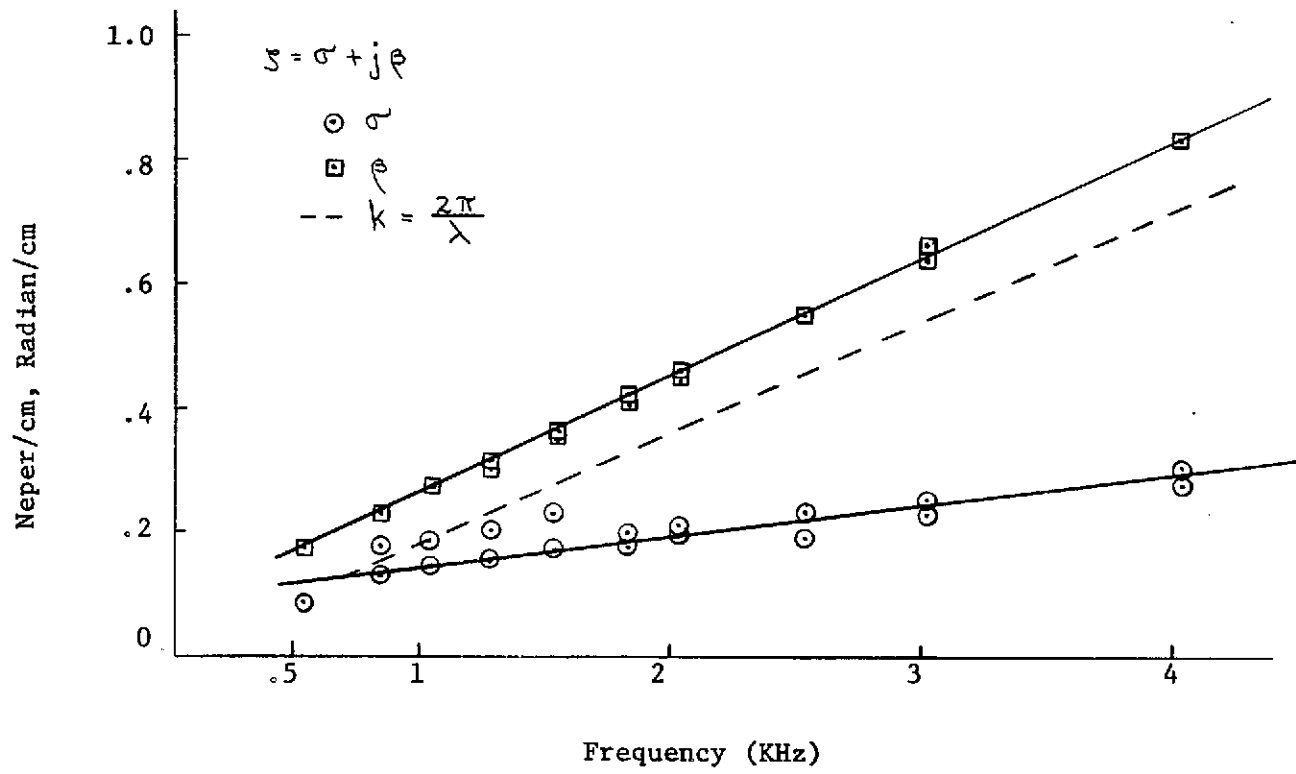Figure 56   Attenuation Constant and Phase Constant for O.C. 703 Fiberglas

Figure 57   Attenuation Constant and Phase Constant for O.C. 704 Fiberglas
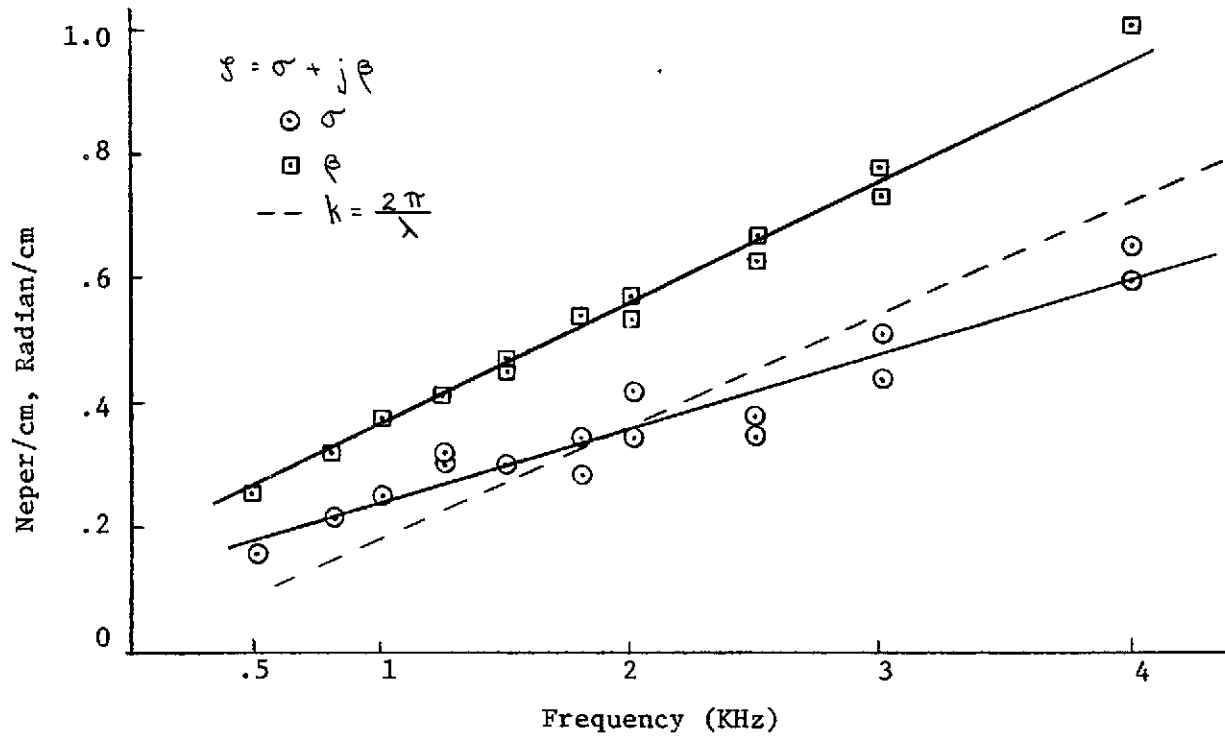
Figure 58   Attenuation Constant and Phase Constant for O.C. 705 Fiberglas

that the bulk acoustic parameters measured for a single sample may not

be representative of the acoustic parameters for the entire material.

CHAPTER VI

CONCLUSIONS AND RECOMMENDATIONS

In summary, measurements of the absorption characteristics of a material at oblique incidence by the surface pressure methods are valid within a certain frequency range. The low frequency limit is determined by the size of the sample which must be large enough, relative to the wavelength, so that the surface behaves as an infinite boundary. The upper frequency limit is determined by the accuracy in measuring the phase angle upon which this method depends strongly. However, due to the limitations of temperature variation and diffraction, the accurate measurement of the phase angle makes this method very difficult to perform.

The following recommendations can be made for future measurements using the surface pressure method.

1. The sample should be as large as possible to insure that the surface behaves as an infinite boundary. The ratio of the length of the horizontal dimension of the sample to the wavelength at the lowest frequency of interest should be at least 15.

2. The sample should be either square or rectangular in shape so that the geometry of the finite surface does not reinforce the effect of diffraction.

3. The vertical edges of the perfectly reflecting surface should be covered with a sound absorbing material to reduce or eliminate diffraction from the edges.

4. Measurements at very oblique angles are not valid because of the rapid drop in surface pressure for incident angles greater than 80 degrees.

5. Adequate temperature stabilization between measurements must be assured and temperature gradients prevented so that no additional phase shift is introduced in the measurement of phase angle.

6. A theoretical analysis of the diffraction due to a finite sample would provide useful information on the limitations inherent with this method.

Additional oblique incidence measurements using techniques presented in Section 1.2 should be performed with the same samples to judge the validity of oblique incidence data obtained using the surface pressure method. The interference pattern method presented by Sides and Mulholland (4) would be preferred for future tests since it eliminates the problem of measuring the phase angle.

There was reasonably good agreement between oblique incidence absorption measurements with the surface pressure method and values calculated from Pyett's theory for the glass fiber materials. This indicates the oblique incidence acoustic behavior of a material can be calculated from experimentally determined bulk acoustic parameters. However, as stated previously, there are two disadvantages with this method. First, the bulk acoustic parameters for a material can be determined only from several normal impedance measurements with samples of different thickness; and second, if a material is in any way in-homogeneous, the bulk acoustic parameters measured for one sample may not be accurate representation of the parameters for the entire material.

It would be most advantageous to eliminate experimental measure-ments for an acoustic material and thus be able to predict its behavior for normal and oblique incidence from a knowledge of its physical

properties. The theories of Beranek and Ford have attempted to provide this type of analytical approach based on the parameters of porosity and flow resistance. However, considering the results for glass fiber materials, the agreement between measurement and theory is poor. Beranek has assumed that the compressions and rarefactions within the material occur for isothermal conditions rather than for adiabatic conditions which prevail for wave propagation in free air. This, he states, is true for many materials, especially below 2000 Hz. To modify this assumption, Ford has included a parameter γ in his theory which may have a value of 1.0 for isothermal conditions or 1.4 for adiabatic conditions or any value between these extremes. However, even for the variation in this parameter, the results calculated from theory do not predict the increased attenuation measured experimentally for these materials. Therefore, the effect of the porosity and flow resistance terms must be investigated. For glass fiber materials, the range in value for porosity has little effect on the calculated results as was previously shown. The total sound attenuation within these materials is accounted for by the flow resistance, which is assumed to be constant within the range of sound pressure levels generally encountered. The dependence of the impedance on flow resistance was presented in Section 5.4. In order that the impedance calculated for the glass fiber materials be in reasonable agreement with experimental values, the value of flow resistance must be greater than the upper limit of the range of values specified for manufacturing tolerances within the material. This would indicate other dissipation mechanisms involved within the material that are not included in the flow resistance term. Due to the internal structure of glass fiber materials,

the attenuation due to viscous and thermal effects for individual

fibers may have a pronounced effect on sound absorption. While the

frame of the material is assumed to remain rigid in these theories,

movement of individual fibers may also create increased attenuation.

In short, viscous and thermal interactions within the material on the

level of the microstructure have been neglected by these theories and

the total dissipation is accounted for only by the flow resistance,

a macroscopic property. Therefore, an investigation of the dependence

of sound absorption on the internal microstructure of these materials

would prove quite helpful in predicting their acoustic behavior.

Attenborough (25, 26) has modeled a fibrous absorbent as a collection

of cylindrical scatters and has developed a scattering theory approach

to determine the absorption characteristics in terms of fiber diameter

and fiber spacing. A scattering cross section, which includes viscous

and thermal effects, for a cylindrical obstacle is used in conjunction

with a single scattering theory to determine the sound absorption of

the glass fiber material. Further modifications include a multiple

scattering treatment to account for the interactions among scattered

waves. In this case, then, the dissipation mechanisms are due to:

1. Mode conversion to damped viscous and thermal waves in air
   at the fiber boundaries.

2. The energy loss due to formation of the internal incoherent
   field due to multiple scattering.

A logical continuation of this work should develop Attenborough's

scattering theory to include shear and thermal wave interactions.

Further consideration should include possible structure modifications

of the model to give a more accurate representation of the actual

material. In addition, the inhomogeneous nature of these materials indicates that a statistical approach might also be used to treat variations within the microstructure for different samples of the same material. Beran (27) introduces flow through a porous media using Darcy's Law and statistics to determine the permeability of the medium. Such an analysis based on the microstructure would thus provide insight into the actual dissipation mechanisms involved within a material, and as an ultimate goal, would dictate which parameters are to be controlled in production in order to optimize results. These topics will be the subject of future research and study.

BIBLIOGRAPHY

1. "Impedance and Absorption of Acoustical Materials by the Tube Method," 1970 Annual Book of ASTM Standards, Part 14, American Society for Testing and Materials, Philadelphia, pp. 126-138, (1970).

2. "Sound Absorption of Acoustical Materials in Reverberation Rooms," 1970 Annual Book of ASTM Standards, Part 14, American Society for Testing and Materials, Philadelphia, pp. 161-167, (1970).

3. Dubout, P. and Davern, W., "Calculation of the Statistical Absorption Coefficient from Acoustic Impedance Tube Measurements," Acustica, 9, No. 1, pp. 15-16, (1959).

4. Sides, D. J. and Mulholland, K. A., "The Variation of Normal Layer Impedance with Angle of Incidence," Journal of Sound and Vibration, 14, pp. 139-142, (1971).

5. Tocci, G. C., "Noise Propagation in Corridors," M.S. Thesis, Massachusetts Institute of Technology, (1973).

6. Velizhanina, K. A., Voronina, N. N., and Kodymskaya, E. S., "Impedance Investigation of Sound-Absorbing Systems in Oblique Sound Incidence," Soviet Physics - Acoustics, 17, No. 2, pp. 193-197, (1971).

7. Pyett, J. S., "The Acoustic Impedance of a Porous Layer at Oblique Incidence," Acustica, 3, pp. 375-382, (1953).

8. Shaw, E. A. G., "The Acoustic Wave Guide, I and II," Journal of the Acoustical Society of America, 25, p. 224, (1953).

9. West, M., "Acoustic Waveguide Having a Variable Section," Journal of the Acoustical Society of America, 47, p. 12 (1970).

10. Ingard, U., and Bolt, R. H., "A Free Field Method of Measuring the Absorption Coefficient of Acoustic Materials," Journal of the Acoustical Society of America, 23, No. 5, pp. 509-516, (1951).

11. Beranek, Leo L., Noise and Vibration Control, McGraw Hill Book Company, New York, pp. 245-269, (1971).

12. Industrial Insulation 700 Series, Owens Corning Fiberglass Corporation.

13. Sabine, H. J., personal communication, November 16, 1972.

14. Sabine, H. J., personal communication, January 26, 1967.

15. Zwikker, C., and Kosten, C. W., Sound Absorbing Materials, Elsevier Publishing Company, Inc., New York, (1949).

16. Beranek, Leo L., "Acoustic Impedance of Porous Materials," Journal of the Acoustical Society of America, 13, pp. 248-260, (1942).

17. Ford, R. D., Landau, B. V., and West, M., "Reflection of Plane Oblique Air Waves from Absorbents," Journal of the Acoustical Society of America, 44, No. 2, pp. 531-536, (1968).

18. Morse, Philip M., and Ingard, K. Uno, Theoretical Acoustics, McGraw Hill Book Company, New York, pp. 227-270, (1968).

19. Rybner, J., Nomograms of Complex Hyperbolic Functions, Jul. Gjellerups Forlag, Copenhagen, (1955).

20. McCracken, Daniel D., A Guide to Fortran IV Programming, John Wiley and Sons, Inc., New York, pp. 31-35, (1965).

21. Kinsler, L. E., and Frey, A. R., Fundamentals of Acoustics, John Wiley and Sons, Inc., New York, pp. 130-136, (1962).

22. Standing Wave Apparatus Type 4002 - Instructions and Applications, Bruel and Kjaer, Copenhagen, (1955).

23. "Airflow Resistance of Acoustical Materials," 1970 Annual Book of ASTM Standards, Part 14, American Society for Testing and Materials, Philadelphia, pp. 223-229, (1970).

24. Hughes, W. J., personal communication, April 18, 1973.

25. Attenborough, K., and Walker, L. A., "Scattering Theory for Sound Absorption in Fibrous Media," Journal of the Acoustical Society of America, 49, pp. 1331, (1971).

26. Sides, D. J., Attenborough, K., and Mulholland, K. A., "Application of a Generalized Acoustic Propagation Theory to Fibrous Absorbents," Journal of Sound and Vibration, 19, pp. 49, (1971).

27. Beran, M. J., Statistical Continuum Theories, Chapter 6 - Flow Through Porous Media, Interscience Publishers, (1968).

APPENDIX - A

NEWTON-RAPHSON ITERATION METHOD

The solution to an equation may be found using an iteration technique such as the Newton-Raphson method. According to this method, if x_i is an approximation to a root of the function,

$$F(x) = 0 \tag{A.1}$$

then a better approximation is given by x_{i+1} where

$$x_{i+1} = x_i - \frac{F(x_i)}{F'(x_i)} \tag{A.2}$$

$F'(x_i)$ denotes the derivative of $F(x)$ with respect to x evaluated at x_i. The root of Equation A.1 can be obtained to the desired accuracy by iterating successive approximations. The use of an electronic computer renders this method very simple to perform.

In our case we are interested in solving the equation

$$\cosh(2\zeta_x d) = U + jV \tag{A.3}$$

for values of $2\zeta_x d$ where U and V are known. Since ζ_x is complex, this involves finding solutions for the complex argument of a hyperbolic cosine function. If we introduce the complex numbers A and B such that

$$A = U + jV \tag{A.4}$$

$$B = 2 \S_x d = 2d(\sigma_x + j\beta_x) \qquad (A.5)$$

$$B = b_1 + j b_2 \qquad (A.6)$$

Equation A.3 may be rewritten as a function of B

$$F(B) = \cosh B - A = 0 \qquad (A.7)$$

The derivative of $F(B)$ with respect to B is

$$F'(B) = \sinh B \qquad (A.8)$$

Therefore, if B_1 is an approximation to the root of Equation A.7, then a better approximation is given by

$$B_{i+1} = B_i - \frac{\cosh B_i - A}{\sinh B_i} \qquad (A.9)$$

The root of $F(B)$ is obtained by taking successive approximations with the iteration formula of Equation A.9. It must be noted that there are two solutions to Equation A.7 since the hyperbolic cosine is an even function.

$$B_1 = b_1 + j b_2 \qquad (A.10)$$

$$B_2 = -B_1 = -b_1 - j b_2 \qquad (A.11)$$

Furthermore, the hyperbolic cosine of a complex argument is invariant for multiples of 2π added to or subtracted from the imaginary

component. Therefore,

$$B_1 = b_1 + j \left(b_2 \pm 2\pi m \right)$$

(A.12)

$$B_2 = -b_1 - j \left(b_2 \pm 2\pi m \right)$$

(A.13)

are the set of all solutions. However, considering the physical aspects of the problem, we are interested only in roots with a positive real component. This corresponds to the attenuation constant of the appropriate wave propagation parameters.

APPENDIX - B

INTERFERENCE PATTERN CALCULATION

To predict the location of the pressure maxima and minima, an incident plane wave is assumed diffracted at the edges of a finite-sized panel. Three pressures - p_1 and p_3, the pressures diffracted from the edges, and p_2, the pressure from the incident wave - will be measured by the microphone located at the center of the panel. The important consideration is the phase relationships between these pressures as determined by the angle of incidence. Referring to Figure 59, the phase component of each pressure will be taken relative to the line $X_1 X_2$. Therefore,

$$p_2 = A e^{j(\omega t + k \frac{a}{2} \sin\theta)} \tag{B.1}$$

$$p_1 = B e^{j(\omega t + k \frac{a}{2})} \tag{B.2}$$

$$p_3 = C e^{j(\omega t + k \frac{a}{2} + ka\sin\theta)} \tag{B.3}$$

The pressure at O is the sum of these three pressures. Omitting the time factor $e^{j\omega t}$, we have

$$p_0 = B e^{jk\frac{a}{2}} + A e^{jk\frac{a}{2}\sin\theta} + C e^{j(k\frac{a}{2} + ka\sin\theta)} \tag{B.4}$$

Furthermore, we will assume that the amplitude of the pressure at each edge is the same so that $B = C$. Multiplying p_0 by its complex conjugate, we obtain

$$|p_0|^2 = A^2 + 4B^2 \cos^2\left(k\frac{a}{2}\sin\theta\right) + 4AB\cos\left(k\frac{a}{2}\sin\theta\right)\cos\left(k\frac{a}{2}\right) \quad \text{(B.5)}$$

The pressure fluctuations will have maximum and minimum values where the derivative with respect to θ is zero.

$$\frac{\partial|p|^2}{\partial\theta} = 4Bka\cos\theta\sin\left(k\frac{a}{2}\sin\theta\right)\left[B\cos\left(k\frac{a}{2}\sin\theta\right) + \frac{A}{2}\cos\left(k\frac{a}{2}\right)\right] \quad \text{(B.6)}$$

For the derivative to be zero for some angle θ, the following conditions are found:

1. $\cos\theta = 0$ (B.7)

$$\theta = \frac{\pi}{2}, \frac{3\pi}{2}$$

2. $\sin\left(k\frac{a}{2}\sin\theta\right) = 0$ (B.8)
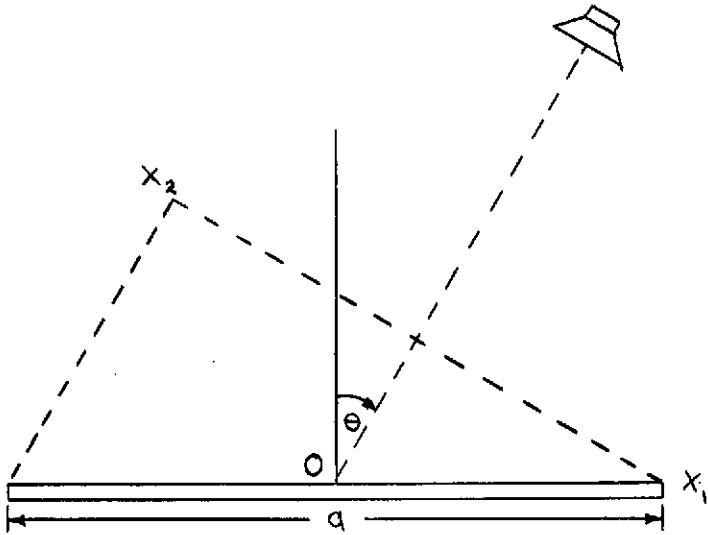
$$\sin\theta = n\frac{\lambda}{a} \qquad n = 0, 1, 2, \ldots$$

Figure 59   Geometry for Surface Pressure Method Tests